Entrance length of suspension pipe flows

An experimental study

Gokul Chirukandath Satish

Delft University of Technolog

TU Delft

Entrance length of suspension pipe flows

An experimental study

by

Gokul Chirukandath Satish

to obtain the degree of Master of Science
at the Delft University of Technology.
to be defended publicly on Wednesday, December 6, 2023 at 13:00.

Student number:	5479630	
Project duration:	January 19, 2023 - December 6, 2023	
Thesis committee:	Prof.Dr.Ir. Chrsitian Poelma	TU Delft, Supervisor, Chair
	Dr.Ir. Willian Hogendoorn	TU Delft, Supervisor
	Dr.Ir. Tim Nijssen	TU Delft, Examiner
	Dr. Dhruv Mehta	TU Delft, Examiner

TU Delft

Acknowledgement

I want to express my deepest gratitude to my supervisors, Prof.Dr.Ir. Christian Poelma and Dr.Ir. Willian Hogendoorn, for their consistent support and guidance throughout the completion of this thesis. Their expertise and active involvement at every stage were instrumental in bringing this work to fruition. I am particularly thankful for their invaluable help in setting up the experiments and helping me understand the functioning of the components of the setup, a task that proved crucial given my limited prior experience in experimental techniques. Additionally, their meticulous feedback on the results, especially in terms of displaying and intepreting results, significantly contributed to improving my master thesis. I would also like to extend my thanks to Dr.Ir. Tim Nijssen and Dr. Dhruv Mehta for agreeing to be a part of my thesis committee.

The assistance of the Process and Energy employees was indispensable in the completion of this thesis. I extend my gratitude to Bart Hoek, Michel van den Brink, and Gertjan Mulder for supplying the mechanical components and tools essential for building my experimental setup. Additionally, I would like to thank Udhav for taking his time and helping me out in conducting pressure drop measurements when faced with obstacles.

Embarking on my masters journey at TU Delft has proven to be an exhilarating roller coaster ride, filled with a myriad of highs and lows that have collectively shaped my academic and personal growth. Throughout this period, I've been exceptionally fortunate to be surrounded by a group of good friends whose unwavering support has been a source of encouragement during both the triumphs and challenges. I extend my heartfelt gratitude to my friends in Delft, who have stood by me creating a sense of belonging that has made my time at TU Delft truly memorable. I would also like to extend my gratitude to my friends in India, who, despite the physical distance, have been a constant source of motivation and support during moments of academic rigor. Lastly, but most importantly, I would like to extend my profound gratitude towards my parents and my sister without which all of this would not have been possible.

Gokul
Delft, December 2023

Abstract

Particle-laden pipe flows are ubiquitous in industrial applications. Examples are industries like dredging, slurry transport, and the transport of reactants and products in chemical industries. One of the most important factors in these transport processes is the friction coefficient which relates directly to the pumping power which is a significant parameter for industries when viewed from an economic standpoint. The migration of particles in dense suspensions can significantly impact the friction coefficient in pipe flow. The clustering of particles in the core can lead to a reduction in the friction factor compared to a well-mixed particle suspension. This reduction is attributed to the decreased effective viscosity near the pipe wall. While the development lengths of single-phase flows are well known, limited knowledge exists regarding the development of velocity and concentration profiles in suspension flows.

The goal of this thesis is to study the development of neutrally buoyant suspension pipe flows. The experimental setup was validated using pressure drop measurements and the entrance length for single-phase pipe flow was obtained. The experiments for suspension flows involved varying the suspension Reynolds number and volume fractions keeping the particle size constant. Ultrasound imaging technique is used to circumvent the opacity of the suspension to study the development of suspension pipe flow. The inlet conditions for concentration were characterized, obtaining a uniform distribution at the inlet. Measurements are conducted at various locations downstream of the pipe and the velocity of the dispersed phase is obtained using ultrasound imaging velocimetry. Additionally, insights into the development of the concentration profile are obtained by checking the convergence towards a fully developed intensity profile, despite the fact that the image intensity doesn't directly correlate to concentration profiles. The velocity profiles and intensity profiles were analysed to understand the effect of radial migration on both concentration and velocity profiles. The entrance lengths for concentration and velocity were obtained for volume fractions ranging from 0.17 to 0.25 and suspension Reynolds numbers ranging from 500-2000. The results obtained revealed that the entrance length for concentration was greater than the entrance length for velocity. Scaling of the concentration entrance length with suspension Reynolds number and volume fractions were determined, and suspension Reynolds number scaled with an exponent of -1.62 and volume fraction scaled with an exponent of -2.1. This implies that the entrance length decreases with an increase in suspension Reynolds number and volume fraction. However, no definite trend was observed for the velocity entrance length.

Contents

List of Figures

List of Tables

Nomenclature

Abbreviations

Symbol	Definition	Unit
Re	Reynolds number	-
Re_p	Particle Reynolds number	-
Re_s	Suspension Reynolds number	-
D	Diameter of the pipe	[m]
H	Half width of the channel	[m]
R	Radius of the pipe	[m]
f	Darcy friction factor	-
L_v	Velocity entrance length	[m]
L_ϕ	Concentration entrance length	[m]
L	Length of pipe	[m]
E_p	Evolution parameter	-
a	Particle radius	[m]
d	Particle diameter	[m]
St	Stokes number	-
τ_p	Particle response time	[s]
τ_f	Time scale of flow	[s]
c_s	Speed of sound in suspension	[m/s]
c_f	Speed of sound in fluid	[m/s]
k_f	Compressibility of fluid	[N/m^2]
k_p	Compressibility of particle	[N/m^2]
Q	Volume flow rate	[m^3/s]
u_z	Streamwise velocity	[m/s]
u_b	Bulk velocity	[m/s]

Symbol	Definition	Unit
u_p	Particle velocity	[m/s]
u_c	Centerline velocity	[m/s]
ρ	Density of the fluid	[kg/m^3]
ρ_p	Density of the particle	[kg/m^3]
ϕ	volume fraction	-
ϕ_b	bulk volume fraction	-
ϕ_m	jamming volume fraction	-
μ_0	Dynamic viscosity of the fluid	[Pa·s]
μ	Dynamic viscosity of the suspension	[Pa·s]

1

Introduction

Multiphase flow in fluid mechanics refers to the movement of two or more thermodynamic phases of materials occurring simultaneously. This can involve either a single chemical component with different thermodynamic phases, such as water and water vapor or multiple chemical components, like oil and water, flowing together. In general, the flow has two distinct phases: a dispersed phase and a continuous phase. A suspension is a type of mixture where the solid particles are dispersed throughout a fluid, which acts as the continuous phase. Suspension flows are extremely common in our everyday life, for instance, the fabrication of cement or the painting of walls, paint being a suspension. Other applications include fluidized bed reactors used in process industries. In addition to this, multiphase flows can be observed in various natural phenomena. For example, sediment transport in rivers and volcanic ash clouds are examples where multiple phases are present. Another example is the flow of blood through arteries (See figure 1.1).

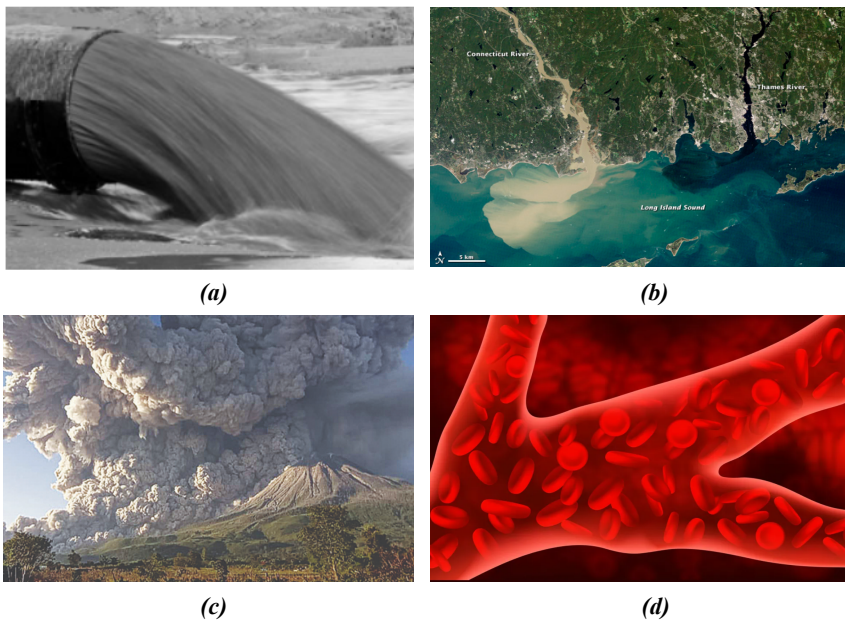

Figure 1.1: Examples of particle-laden flow: (a) Slurry transport [15] (b) Sediment transported by the Connecticut river into Long Island Sound [58] (c) Volcano ash cloud from a volcano eruption in Indonesia [54] (d) Blood flow through arteries [55].

The behavior of suspensions has a significant impact on various aspects of human life, including the environment, medicine, and the economy. From an economic standpoint, the efficiency of pipeline transport in industries such as oil and gas is closely linked to the cost of operating pumps. The flow regime plays an important role in the transport of suspensions, with turbulent flow being preferred for slurry transport in pipelines to keep particles suspended. On the other hand, laminar flow is preferred

for the transport of suspensions in sewer systems depending on the properties of the suspension and the flow rate. From an environmental perspective, the disposal of suspension wastes from industries can have adverse effects on aquatic plants and animals [40]. Additionally, suspensions can negatively impact air quality in both industrial and urban areas, particularly if they contain particulate matter, leading to respiratory health issues for humans [4] and animals. In the medical field, suspensions are used as contrast agents to improve the results of MRI [36] or CT scans.

Single-phase pipe flow is characterized by an important parameter, the Reynolds number [6]. This parameter characterizes the flow regime, which can be either laminar or turbulent. For example, the friction factor is a function of Reynolds number and is different for laminar and turbulent regime and this has a direct impact on pressure drop. When particles are present in the system, they can affect the viscosity of the suspension [22], which alters the Reynolds number. This, in turn, has an impact on the friction factor, which affects the pressure drop. In the industrial applications aforementioned (especially transport in pipelines), this pressure drop is a critical parameter as it directly affects the efficiency and cost of the process. An important parameter that has a significant effect on the pressure drop in pipe flow is the entrance length. Apart from transport in pipelines, entrance length is important for many flow measurement devices as they need fully developed flow to function properly.

The study of entrance length in a pipe is an age-old problem. Numerous attempts have been made to study the entrance length in pipe flows. The research towards the understanding of entrance length in laminar [14] and turbulent regimes for single-phase flows are well documented using theoretical and empirical relations. However, the entrance length in suspension pipe flows needs a deeper inspection due to their applications in industries like dredging, chemical processing industries, etc. The influence of the dispersed phase on the flow makes the study more complex and interesting.

1.1. Outline

The outline of this thesis is as follows. Chapter 2 introduces the concept of entrance length and presents an extensive literature review on entrance length on suspension pipe flows. Furthermore, it also presents the research objectives of the present thesis that can be arrived at from the literature review. This is followed by Chapter 3 which describes the experimental setup in detail. The methodology is also presented which was used to carry out the thesis. This is followed by Chapter 4 which discusses the results obtained from the experimental campaign. Finally, in Chapter 5, conclusions from this study and recommendations to improve the current research and interesting areas for future work are presented.

2

Literature review

The literature review focuses on the physics and background literature behind the problem. This section begins by discussing single-phase pipe flows and the entrance length of single-phase pipe flows. It then moves to examine suspension pipe flows and investigates the migration phenomenon that occurs within them. Finally, the discussion focuses on the entrance length of suspension flows. The chapter concludes with summary of the literature study and finally the research questions to be addressed in this study are formulated.

2.1. Single phase pipe flow

Poiseuille conducted experiments on capillary tubes, which led to the development of the Hagen-Poiseuille equation, one of the earliest and most influential works on pipe flow [53]. This equation connects the pressure drop per unit length, volumetric flow rate, viscosity, and pipe diameter in laminar flows. Hagen also had similar results to that of Poiseuille. However, he also had results observing laminar to turbulent transition [53].

All these results paved the way for the experiments of Osborne Reynolds, who defined the main governing parameter for single-phase pipe flow, the 'Reynolds number'. He studied the effect of flow velocity on the flow state by injecting dye and observing the flow. The Reynolds number is defined as:

$$Re = \frac{\rho u D}{\mu_0}, \tag{2.1}$$

where ρ is the density of the fluid, u is the bulk velocity, D is the diameter of the pipe and μ_0 is the dynamic viscosity of the fluid (a subscript is used to differentiate from suspension viscosity μ which will be used later). Based on the Reynolds number, the flow can be characterized into laminar and turbulent regime.

2.1.1. Laminar flows

At low Reynolds numbers, the flow is in the laminar regime and it is characterized by an orderly flow of fluid layers and those layers do not mix with each other. In the case of pipe flow, the fluid layers move in the direction parallel to the pipe and the flow does not have swirls or eddies. The pressure drop (Δp) is one of the main parameters in a pipe flow, and it is given by the Darcy-Weisbach equation,

$$\Delta p = f \cdot \frac{\rho}{2} \cdot u^2 \cdot \frac{L}{D}, \tag{2.2}$$

where f is the Darcy friction factor and L is the length of the pipe. For fully developed laminar flows, the Darcy friction factor is given as $f = 64/Re$ [38].

2.1.2. Turbulent flows

For higher Reynolds numbers, the flow is in the turbulent regime and it is characterized by chaotic fluctuations and the presence of eddies. Unlike the laminar regime, the fluid layers keep on mixing.

The transition from a laminar regime to a turbulent regime is characterized by the presence of transient turbulent structures that either decay or split after a characteristic time. For turbulent pipe flow, the Darcy friction factor was approximated by Blasius (for a smooth pipe). Unlike laminar flows, it is not exact and is given by

$$f = \frac{0.316}{Re^{0.25}}.$$

This relation is valid for $2100 < Re < 10^5$.

In industrial applications, the pressure drop is an important parameter in pipe flows. Pipe diameter, pipe roughness, pipe length, and flow rate affect the pressure drop significantly. The phenomenon of entrance length also affects the pressure drop and cannot be neglected in practical applications.

2.1.3. Entrance length

In fluid mechanics, the entrance length in pipe flow refers to the length from the inlet of the pipe to the point where the flow becomes fully developed. During the entrance length, the flow undergoes changes due to the presence of walls which impose a no-slip condition. Figure 2.5 shows the velocity profile development of a fluid entering a pipe.

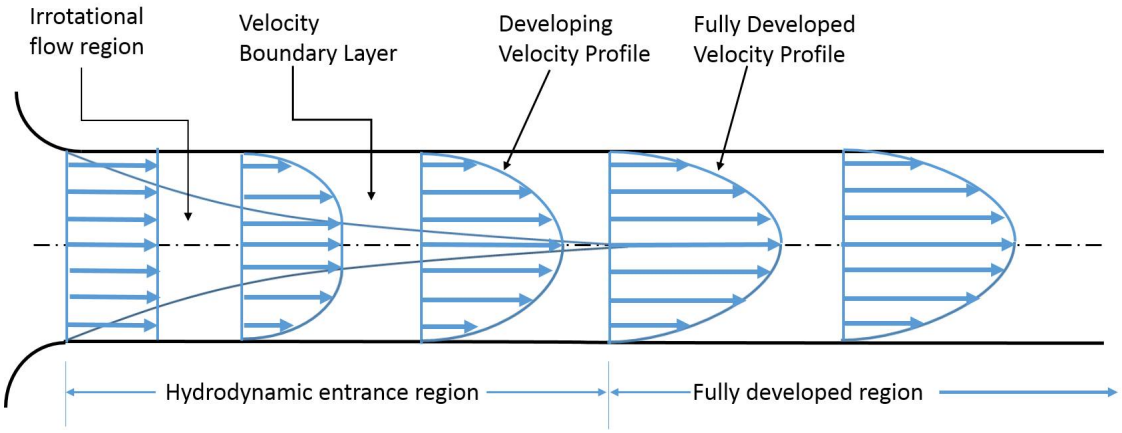

Figure 2.1: Development of fluid flow in a pipe, reproduced from [12].

From figure 2.5, it can be seen that the velocity profile does not change in the direction of flow once it is fully developed. The region which gets affected by the shearing of fluid layers is defined as the boundary layer. The hydrodynamic entry length is usually taken to be the distance from the pipe entrance to where the center line velocity reaches within about 1 percent of the fully developed value (Hornbeck [28]).

One of the first to study the development length in pipe flows was Schiller [47]. He used an integral approach, assuming a parabolic velocity profile in the boundary layer. He ignored the viscous dissipation in the boundary layer and only applied the mechanical energy balance into the inviscid core. This led to inaccuracy in his result. He found that

$$\frac{L_v}{D} = 0.0288 \cdot Re, \tag{2.3}$$

where L_v is the entrance length for velocity.

A similar approach was used by Bogue [8] to study the development length in pipe flows for nonelastic, non-newtonian fluids, except for a quartic velocity profile assumption in the boundary layer. He also obtained the exact same results as that of Schiller. Langhaar [31] linearized the momentum equation to derive an approximate solution for the development length. He found that

$$\frac{L_v}{D} = 0.0575 \cdot Re. \tag{2.4}$$

A similar approach was used by Sparrow et al. [51] used a stretched axial co-ordinate method and improved the analytical method of Langhaar to obtain

$$\frac{L_v}{D} = 0.056 \cdot Re. \tag{2.5}$$

Hornbeck [28], Christiansen and Lemmon [11], Vrentas et al. [57], Friedmann et al. [20], Atkinson et al. [5], Fargie and Martin [17], Gupta [23] and Durst et al. [14] conducted numerical studies to find the development length in laminar pipe flows. The non-dimensional entrance length (L/D) as a function of Reynolds numbers were found out in the aforementioned studies and these are summarised in the table below.

Author	**Year**	**Method**	$L_v/D = f(Re)$
Schiller [47]	1922	Analytical study	$0.0288Re$
Langhaar [31]	1942	Analytical study	$0.0575Re$
Bogue [8]	1959	Analytical study	$0.0288Re$
Sparrow et al. [51]	1964	Analytical study	$0.056Re$
Hornbeck [28]	1964	Numerical study	$0.057Re$
Christiansen and Lemmon [11]	1965	Numerical study	$0.055Re$
Vrentas et al. [57]	1966	Numerical study	$0.056Re$
Friedmann et al. [20]	1968	Numerical study	$0.056Re$
Atkinson et al. [5]	1969	Numerical study	$0.59 + 0.056Re$
Fargie and Martin [17]	1971	Numerical study	$(0.049 - 0.068)Re$
Gupta [23]	1977	Numerical study	$0.0675Re$
Durst et al. [14]	2005	Numerical study	$[0.619^{1.6} + (0.0567Re)^{1.6}]^{1/1.6}$

For turbulent pipe flows, the most commonly used relation in literature for the development length is given by (Anselmet et al. [2]),

$$\frac{L_v}{D} = 1.6 \cdot Re^{0.25}. \tag{2.6}$$

For industrial applications, the non-dimensional entrance length is often approximated as 10 (Y.A. Cengel [12]).

In summary, there has been extensive research conducted on the entrance length of single-phase pipe flows, and a significant amount of knowledge has been accumulated on the subject over the years. This is evident from past studies, which are summarized in theoretical and empirical relations. In the next section, we will look into suspension flows.

2.2. Suspension pipe flows

Research on suspension flows was motivated by its applications in the daily life of humans. Spherical particles will be used in this study. Suspension flows are characterized by a few parameters and those are

- Suspension Reynolds number (Re_s) :
  It is defined as the ratio of inertial to viscous forces and is given by

$$Re_s = \frac{\rho u_s D}{\mu}, \tag{2.7}$$

  where u_s is the suspension bulk velocity and μ is the corrected viscosity of the suspension.

- Particle Reynolds number (Re_p) :
  It is similar to that of the Reynolds number, but it to characterize the flow regime around particles. It is given by

$$Re_p = \frac{\rho u_s a}{\mu_0}, \tag{2.8}$$

  where a is the radius of the particle and μ_0 is the dynamic viscosity of the fluid.

- Particle size:
  It is denoted by a non-dimensional parameter d/D, where d is the particle diameter.

- Density ratio:
  It is denoted by a non-dimensional parameter ρ_p/ρ, where ρ_p is the density of the particle. This parameter accounts for the buoyancy effects. For heavier particles, this ratio will be greater than 1.

When suspended particles are added to a fluid, the resulting mixture will have a higher effective viscosity than the pure fluid. The increase in viscosity is due to the resistance created by particles to the flow thereby making it difficult for the suspension to flow. This increase in viscosity can be described using a correction proposed by Einstein for a suspension with rigid spheres, which takes into account the volume fraction of the particles in the mixture [22]. It is given by,

$$\frac{\mu}{\mu_0} = 1 + \frac{5\phi}{2}, \tag{2.9}$$

where ϕ is the volume fraction. However, this correction is only valid for low-volume fractions (less than 0.05) and does not account for the interactions between particles at higher-volume fractions. To address this, Eiler proposed a semi-empirical viscosity model that considers both the hydrodynamic contribution at low-volume fractions and the contact contribution at high-volume fractions (Stickel and Powell [52]). This model will be used in this thesis and is given by,

$$\frac{\mu}{\mu_0} = \left(1 + 1.25\frac{\phi}{1-\phi/\phi_m}\right)^2, \tag{2.10}$$

where ϕ_m is the maximum packing particle volume fraction. $\phi_m = 0.64$ (Stickel and Powell [52]).

Before moving on to the entrance length of suspension flows, the migration of particles in particle-laden flow should be understood as it affects the entrance length. The migration causes viscosity gradients in the flows. For example, in shear induced migration (discussed in section 2.2.2) in pipe flow, particles migrate to the center and the viscosity will be higher near the axis of the pipe compared to a position intermediate to the wall and the axis of the pipe. Equation 2.10 is an empirical relation for a homogeneous suspension. But migration creates a non homogeneous concentration distribution. Suspension viscosity depends on the local concentration and it varies along the radial positions of the pipe due to migration. A detailed assessment of suspension rheology is not the scope of this project and the viscosity model proposed by Eiler will be used in this thesis.

The migration of particles must be complete for the flow to be fully developed. The upcoming section will look into the migration of particles in suspension flows.

2.2.1. Migration

One of the first studies observing lateral migration in dilute suspension pipe flows was done by Segre and Silberberg [48]. The work found the migration of particles to an intermediate location between the pipe wall and the pipe axis. This radial location is approximately at a distance of approximately 0.6 times the tube radius from the tube axis (Segre-Silberberg annulus). This phenomenon is also known as the tubular pinch effect or the Segre-Silberberg effect. Nakayama et al. [39] conducted an experimental and numerical study of neutrally buoyant spherical particles suspended in laminar flow in a circular tube. They varied the Re from 100 to 1000 for a particle to tube diameter (d/D) of 0.1. For $Re = 100$, they observed that the particles were in the Segre-Silberberg annulus.

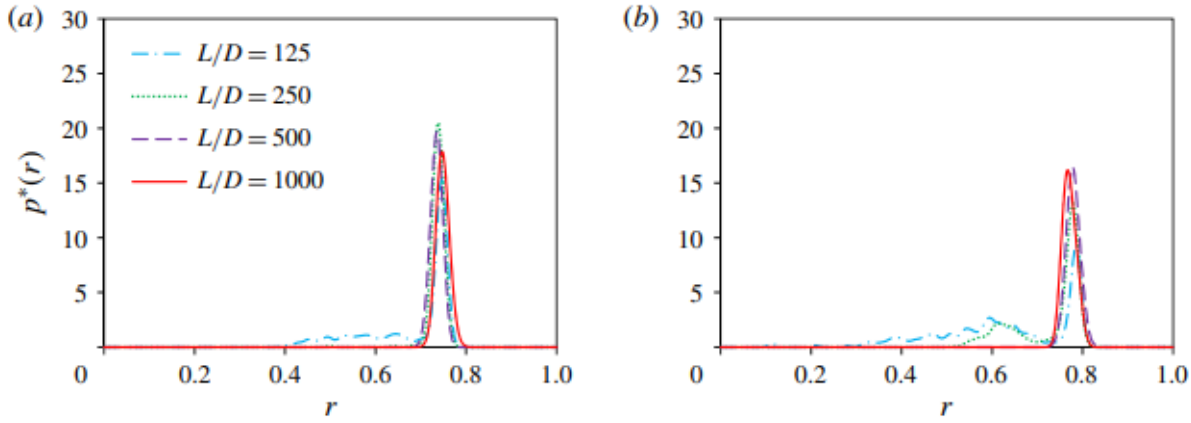

Figure 2.2: Probability distribution function of particles for (a) $Re = 300$ (b) $Re = 600$ at various locations of the pipe, reproduced from Nakayama et al. [39]

The authors found that increasing the Reynolds number to 300 and 600 (see figure 2.2) leads to a shift in the probability distribution function towards the right, suggesting that the particles accumulate at an outer annulus.

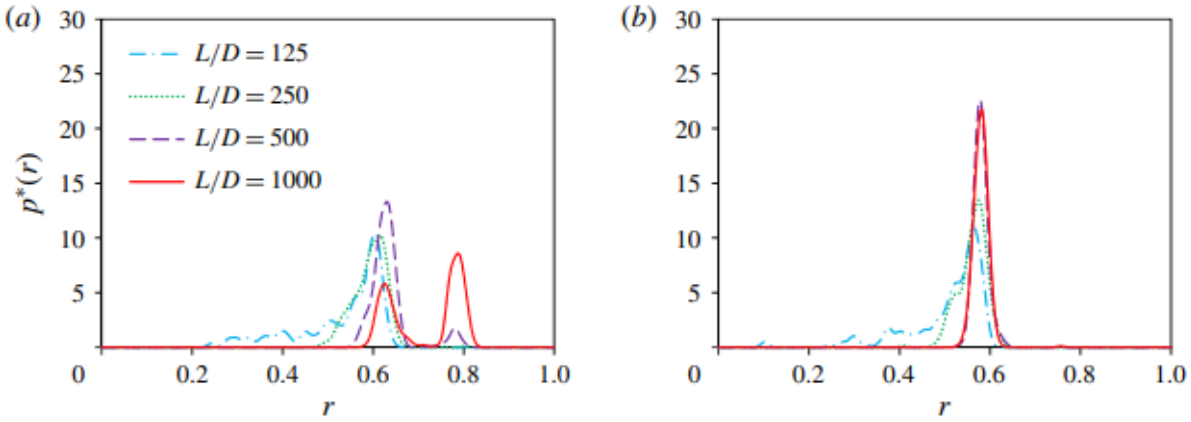

Figure 2.3: Probability distribution function of particles for (a) $Re = 790$ (b) $Re = 900$ at various locations of the pipe, reproduced from Nakayama et al. [39]

At a Reynolds number of 790 (see figure 2.3), the probability distribution curve shown in Figure 2.3 showed the presence of two peaks at length of 1000 pipe diameters, suggesting that particles accumulate at two distinct locations, with one being the Segre-Silberberg annulus. As the Reynolds number was increased to 900, the particles accumulated at the Segre-Silberberg annulus. It is possible that the second annulus is only temporary, and if the flow is allowed for 1000 times the diameter more, the particles could end up moving into the SS annulus. This might require a very long entrance length making it irrelevant in practical applications.

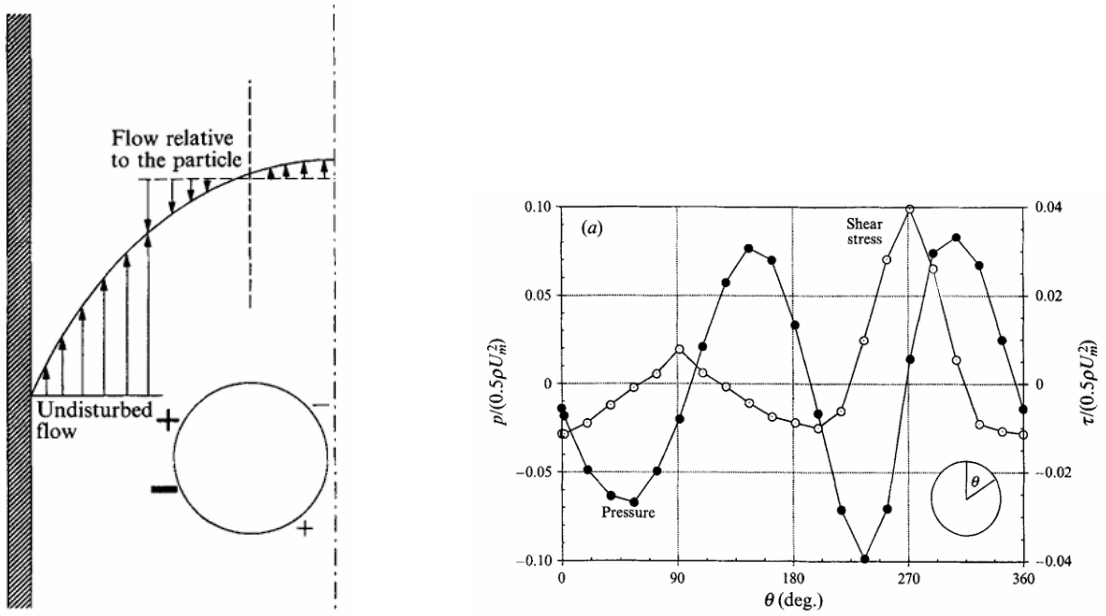

Figure 2.4: (a) Lift force concept due to parabolic velocity profile on a spherical particle. (b) The non-dimensional pressure and shear stress distribution around the sphere. Reproduced from Feng et al. [18]

The physics behind the lateral migration of particle to the Segre-Silberberg annulus can be explained using the Direct numerical simulation results of Feng et al [18]. Figure 2.4(a) illustrates the concept of lift force which causes the migration. Due to the parabolic velocity profile inside the pipe, the relative velocity of the particle closer to the wall is greater than the relative velocity of the particle closer to the pipe axis. This creates a lower pressure region on the surface of the sphere closer to the wall compared to the surface of the sphere closer to the pipe axis. This difference in pressure creates a lift force which helps the particle migrate towards the wall. This theory was validated with pressure distribution results of Feng et al [18]. The '-' and '+' in Figure 2.4(a) corresponds to the minimum and maximum non dimensional pressures respectively in Figure 2.4(b). The authors observed that the negative pressure in quadrant 3 is greater in magnitude compared to that of positive pressure in quadrant 4 which gives rise to a lateral thrust force towards the wall. The lateral drift of the particle stops when the repulsive effects arising from the wall in the direction of the tube axis causes an equilibrium of the forces in the lateral direction. The above studies were conducted using dilute suspensions.

Upon investigating concentrated suspension flows, scientists discovered another phenomenon known as shear-induced migration. It is essential first to have an understanding of shear-induced migration in order to understand the concept of entrance length in suspension pipe flows because this phenomenon affects the entrance length in concentrated suspension flows.

2.2.2. Shear induced migration

Shear induced migration is a phenomenon in which an initial homogenous suspension in a shear flow rearranges to a non-homogenous suspension due to the migration of particles from regions of high shear rate to low shear rate causing concentration gradients which in turn causes viscosity gradients. Leighton and Acrivos [34] reported that the accumulation of the particles in the centre-line is due to the interaction between particles. It was observed that when there is an interaction between two particles, the dynamic of the flow around it will be changed significantly. The authors noted that the flow dynamics around particles are affected when they interact, and the introduction of a third particle can transform the hydrodynamic interaction into a more chaotic pattern in the surrounding flow field. Phillips et al. [44] build on this model and suggested that migration is not only due to the interaction between the particles but also due to the spatial variation of viscosity due to the addition of particles. Nott and Brady [42] proposed a model which solves mass and momentum equations for both particle and fluid phases. The authors model made use of the physical concept that normal stress differences present

in the suspensions are the cause for migration of particles towards the center.

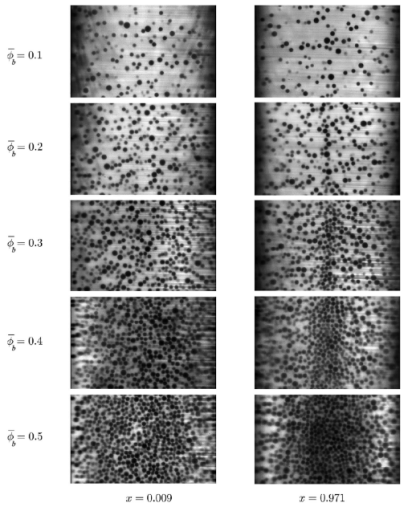

Figure 2.5: Shear induced migration for suspension channel flow at different bulk volume fractions, reproduced from [46]. The left panel corresponds to the inlet and the right panel corresponds to the exit of the channel.

One of the first studies observing shear induced migration in pipe flows was done by Karnis et al. [29]. He conducted optical measurements to study the effect of concentration and particle size using refractive indexed matched suspensions. It was found that as the concentration increased the velocity profile became blunt (as seen in Figure 2.6) due to the accumulation of particles in the center (partial plug flow). For the same concentration, a larger particle size produced more blunting in the velocity profile.

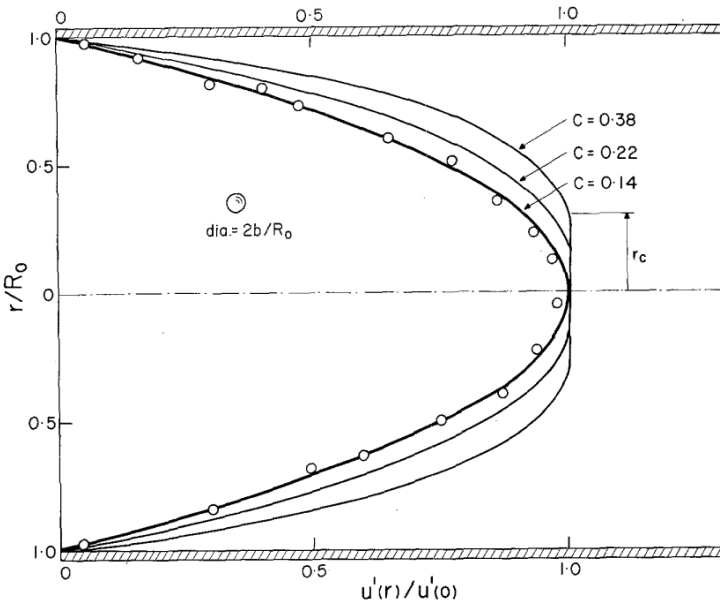

Figure 2.6: Velocity profiles for different bulk concentrations 0.14, 0.22 and 0.38, reproduced from Karnis et al. [29].

Hookham [27] utilized a laser-Doppler technique with modifications to investigate the velocity and concentration profiles of concentrated suspensions flowing through a rectangular channel. By analyzing the Doppler signals emitted by a trace fraction of fluorescent-dyed particles, the author observed that the velocity profiles were similar to that of Karnis et al.[29], displaying a blunted shape near the

center. Furthermore, Hookham discovered that the degree of blunting increased with higher bulk particle concentration or larger particle size-to-gap ratios. Koh et al. [30] used the same technique and observed the same as that of Hookham.

Gadala-Maria and Acrivos [21] observed a consistent viscosity decrease for volume fractions greater than 0.3 in a Couette viscometer suggesting a non-homogenous distribution of particles of the suspension. The experiments of Leighton and Acrivos [35] observed the migration of particles from a high shear region to a low shear region explaining the observations of Gadala-Maria and Acrivos [21].

Leighton and Acrivos [35] utilized scaling arguments to develop a universal expression for the "diffusive flux" of particles in a unidirectional shearing flow. Phillips et al. [44] later applied this model to predict the inhomogeneity of concentration in the pressure-driven flow of a tube. The model proposed that the overall flux is a combination of two contributions: the diffusive flux due to the gradient in the shear rate, and the diffusion resulting from the gradient in concentration. While this model was effective in predicting the occurrence of migration in unidirectional shearing flows, it was not able to accurately predict migration in curvilinear flows [10]. Nott and Brady [42] identified flaws in the model developed by Phillips and proposed an alternative approach, known as the suspension balance model. This model does not rely on diffusion but instead solves mass, momentum, and energy balance equations for both phases in order to obtain concentration and velocity profiles. Miller and Morris [37] modified the suspension balance model, which has now become a standard predictive model for volume fractions from 0.2 to 0.5 but still fails to predict the concentration near the walls (see figure 2.11).

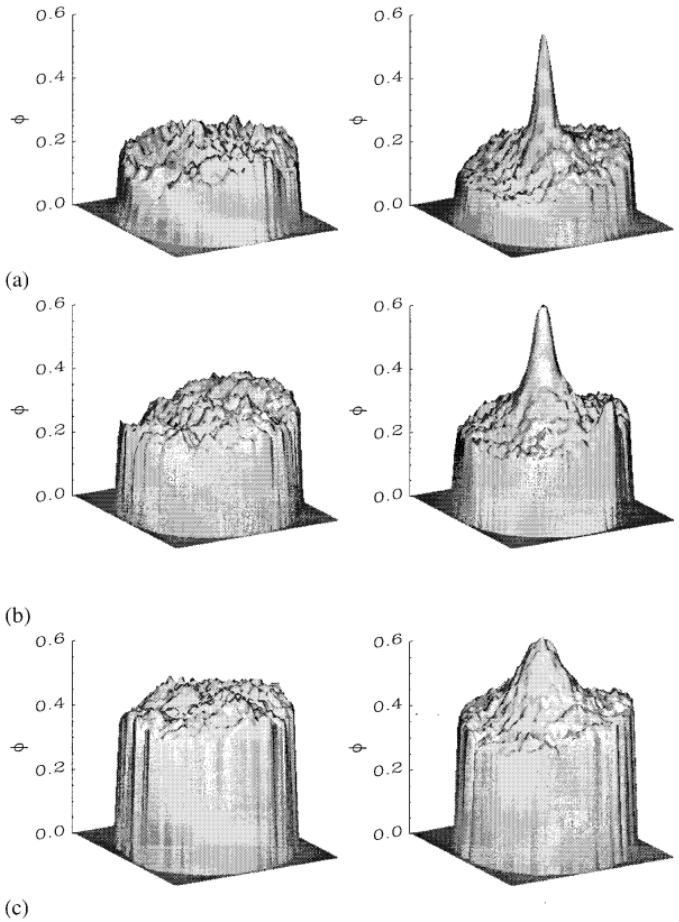

Figure 2.7: NMR images of concentration profiles at the initial state (left) and fully developed state (right) for a volume fraction of (a) 0.2 (b) 0.3 and (c) 0.45 with $d/D = 0.0256$, reproduced from Hampton et al. [24].

Sinton and Chow [49] conducted MRI experiments to study neutrally buoyant suspension flows in

pipes up to volume fractions 0.52. The studies were conducted in the viscous regime and they reported only a slight increase in volume fraction at the center of the flow which was opposite to that of Leighton and Acrivos [35]. Nott and Brady [42] showed that Sinton and Chow used an insufficient entrance length for their studies by using a scaling for the entrance length which is explained in section 2.2.3.

In an MRI study of pipe flow with neutrally buoyant particles, Hampton et al. [24] investigated the effects of particle size and volume fraction on velocity and concentration profiles. The Reynolds number was in the order of 1. Results showed a blunting in the velocity profile consistent with previous studies, and migration of particles towards the center at volume fractions above 0.2 (see Figure 2.7). However, for particles with a diameter-to-pipe-diameter ratio of 0.625 and a volume fraction of 0.1, no net radial migration was observed. The experimental results of the velocity profile and concentration profile at the fully developed state (explained in section 2.2.3) were compared to the analytical results of shear induced migration model and suspension balance model. For low-volume fractions, both models deviated from the experimental data. The authors concluded that the shear induced migration model predicts better results for smaller d/D and the suspension balance model for higher d/D. For small volume fractions, neither of these models had a good prediction. Butler and Bonnecaze [9] used electrical impedance tomography to study suspension flow through pipes and observed migration of the particles to the axis of the pipe. The results obtained by the authors were in good agreement with that of Hampton et al. [24]

Han et al. [25] studied the effect of particle Reynolds number (Re_p) on volume fractions ranging from 0.06 to 0.3 using MRI and suggested that for particle Reynolds numbers exceeding 0.1, inertial effects cannot be neglected for any volume fraction. As Re_p increases, the particles tend to migrate to an intermediate location between the pipe axis and the pipe wall due to the inertial effects as observed by Segre and Silberberg [48] (See Figure 2.8). This explains the reason for the surprising result of Hampton et al. [24] mentioned above. In Hampton's experiments, the particle Reynolds number was between 0.09-0.18, which indicates that the inertia effects were significant. The authors provide a unique example where inertial migration and shear induced migration occur concurrently.

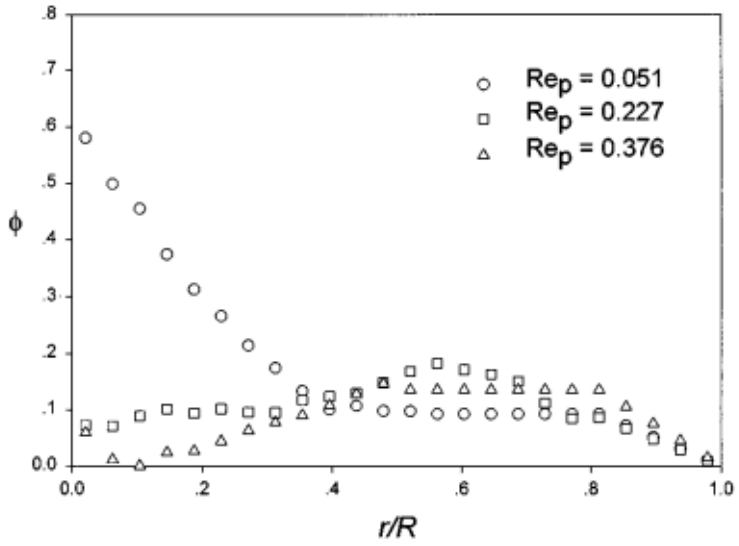

Figure 2.8: Concentration profiles for differing Re_p at volume fraction 0.1, reproduced from Han et al. [25]

Norman et al. [41] investigated the impact of buoyancy on low Reynolds number suspension pipe flows. They measured concentration profiles at various locations and observed that the entrance length for suspensions with neutrally buoyant particles was greater than for those with buoyant particles. This shows that buoyancy has a significant effect on the entrance length of suspension pipe flows at low Reynolds numbers.

In recent times, there has been a significant increase in research studies that focus on the behavior of suspended particles in channel or duct flows. These studies employ numerical simulations to investigate the physics behind the turbulent flow of particles within such confined environments. They study the transport of monodisperse particles [59] [60], polydisperse particles [32] [19] and non-spherical particles [16]. Recently, suspension pipe flows have been studied by Snook et al. [50], analyzing the effects of shear induced migration in oscillatory pipe flow through optical measurements. Their findings on concentration and velocity profiles were consistent with previous studies [24]. Ardekani et al. [3] conducted a numerical study on the impact of heat transfer in laminar and turbulent suspension flows. Their findings indicate that there is a significant enhancement in heat transfer in laminar suspension flows compared to laminar single-phase flows.

The works mentioned earlier predominantly focus on the laminar flow regime, within which the phenomenon of shear induced migration has been extensively investigated through various experimental and numerical studies. This migration phenomenon has a significant influence on the entrance length, as it must be complete for the flow to reach a fully developed state. In the next section, we look into the entrance length in suspension flows.

2.2.3. Entrance length in suspension flows

Using the shear induced migration hypothesis proposed by Leighton and Acrivos [35], Nott and Brady [42] were the first to give a scaling for the entrance length in suspension flows. According to the hypothesis, the average distance traveled by the particles perpendicular to the flow in time t is given by

$$y = 2(Dt)^{0.5}, \tag{2.11}$$

where D is the shear induced diffusivity. For a channel with half width H and particles with radii r, the time scale for reaching steady state (t_{SS}) is

$$t_{SS} \sim \frac{H^2}{4D}. \tag{2.12}$$

As the movement of the particles is solely influenced by hydrodynamics,

$$D = d(\phi)\dot{\gamma}a^2, \tag{2.13}$$

where $\dot{\gamma}$ is the shear rate and $d(\phi)$ is a non-dimensional function of the particle volume fraction. For dilute suspensions, $d(\phi) = 0.5\phi^2$ [34]. The average shear rate is estimated as $3\langle u\rangle/H$ where $\langle u\rangle$ is the average suspension velocity in the channel. On substituting these in equation 2.11, the time scale for reaching steady state is given by

$$t_{SS} \sim \Big(\frac{H}{a}\Big)^3 \frac{a}{12d(\phi)\langle u\rangle}, \tag{2.14}$$

which can be rewritten as

$$\frac{L}{H} \sim \Big(\frac{H}{a}\Big)^2 \frac{1}{12d(\phi)}. \tag{2.15}$$

where L is the entrance length.

For suspensions with $\phi > 0.3$, the value of $12d(\phi)$ is approximately 1 [42]. The entrance length scales as

$$L \sim \frac{H^3}{a^2}. \tag{2.16}$$

N. Phan-Thien and Z. Fang [43] investigated the entrance length of concentrated suspension in channel flows using a numerical study by using the model of Phillips et al. [44]. The authors observed that the velocity profile approaches a steady state much quicker than the concentration profile (see Figure 2.9).

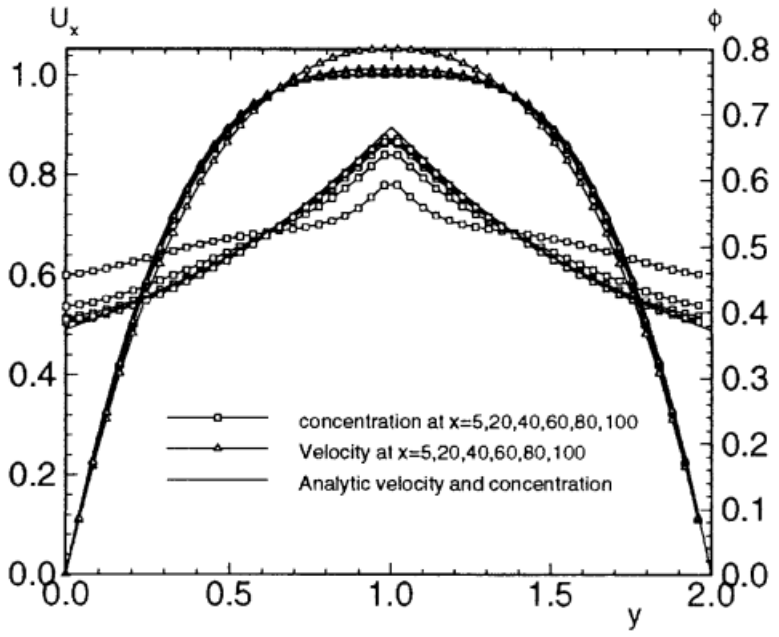

Figure 2.9: Development of the velocity profile and concentration profile along the channel for $r/H = 0.1$, reproduced from [43]

The authors defined the entrance length as the distance between the inlet and the location where there is a deviation less than 1% in the profile of the velocity and concentration at the center line from the well-established profile. They found that

$$L_v \approx 0.2H^3/a^2. \tag{2.17}$$

where L_v is development length of velocity.

$$L_\phi \approx 0.5H^3/a^2. \tag{2.18}$$

where L_ϕ is the development length of concentration. The obtained relations for the development length are independent of the concentration. They are also independent of the Reynolds number because the simulations were conducted in the stokes regime.

Hampton et al. [24] performed MRI experiments to study the entrance length of neutrally buoyant suspensions in pipe flow for different volume fractions and two different particle sizes ($d/D = 0.0256$ and $d/D = 0.0625$). To quantify the entrance length, the authors defined an evolution parameter, E_p which is a normalized concentration, for a generic profile Φ, which is given as

$$E_p = \frac{1}{A}\int \left|\frac{\Phi - \Phi_{\text{ref}}}{\Phi_{\text{avg}}}\right| dA, \tag{2.19}$$

where Φ_{ref} is the reference profile (velocity and concentration at the inlet) and Φ_{avg} is a scalar corresponding to the average value of Φ_{ref}. As the flow develops, the evolution parameter reaches an asymptotic value (see Figure 2.10). The authors defined the entrance length as the value where it reaches 95% of the fully developed value.

A function of the following form was fitted to the evolution parameter,

$$E_p = \alpha_1(1 - e^{\alpha_2 Z^{0.8}}) + \alpha_3 \tag{2.20}$$

where Z is the dimensionless axial distance from the inlet ($Z = L/r$), α_1, α_2 and α_3 are parameters of the fitted model. The form of this equation and coefficient for Z was obtained by fitting data obtained from numerical simulations of shear induced migration model by Phillips et al. [44]. This was the first experimental study on the entrance length of suspension pipe flows. The Reynolds number was in the order of 1. A coiled pipe setup was used by the authors for conducting experiments and this could lead to secondary flows and could cause inaccuracy in their results.

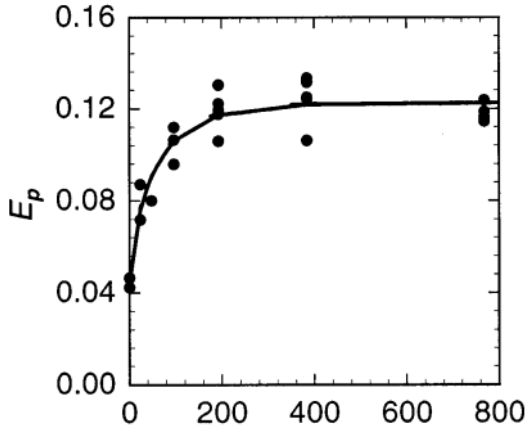

Figure 2.10: E_p plotted as function of Z by using the fitting function (Equation 2.20) for $\phi = 0.45$ and $d/D = 0.0256$, reproduced from [24]

The authors observed that the entrance length of both viscosity and concentration decreased with an increase in bulk volume fraction as well as an increase in particle size. The results obtained by the Hampton et al. are in fair agreement with that of N. Phan-Thien and Z. Fang [43] considering the different definitions of entrance length by the authors. The different definitions of the authors are not convertable to each other as N. Phan-Thien and Z. Fang [43] only focus on the centerline profile whereas the evolution parameter of Hampton et al. [24] considers the whole crossectional profile.

In a study conducted by Norman et al. [41], the entrance length of buoyant suspension flows in a pipe was investigated using Electrical Impedance Tomography. They proposed a scaling law for the entrance length of buoyant suspensions in a pipe flow and this was in good agreement with their experimental results. The scaling law is given by

$$L \sim \frac{R^3}{r^2 N_b f(\phi)} \tag{2.21}$$

where $f(\phi)$ is the hindered settling function and N_b accounts for the buoyancy effects and is in the order of 10 in many applications [41] implying that the entrance length of buoyant suspension flows is less compared to neutrally buoyant suspension flows.

Miller and Morris [37] conducted numerical studies using the suspension balance model to study neutrally buoyant suspension flows in 2D channel and pipe for volume fractions ranging from 0.2 to 0.5. The authors use a nonlocal stress contribution while modeling the normal particle stress and this contribution is a function of mean shear rate and a function of ϵ. ϵ is defined as r/L_{eff} (L_{eff} is the diameter for pipe and channel width for 2D channel). The nonlocal stress contribution (γ_{NL}) is given by,

$$\gamma_{NL} = f(\epsilon)\dot{\gamma}, \tag{2.22}$$

They tested the model for $f(\epsilon) = 0$, $f(\epsilon) = \epsilon$ and $f(\epsilon) = \epsilon^2$. The results of the simulations were compared to that of the experimental results of Hampton et al. [24] and $f(\epsilon) = \epsilon$ gave the best fit (see figure 2.11). The evolution parameter introduced by Hampton et al. was used by the authors to understand the axial development and to measure the entrance length.

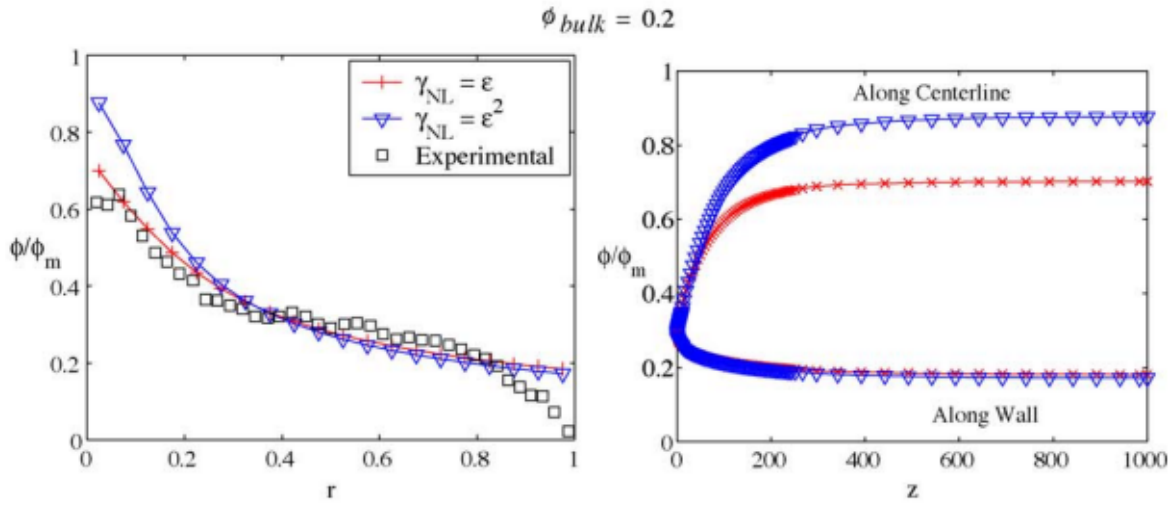

Figure 2.11: Fully developed cross-stream (at left) and axially developing (at right) ϕ/ϕ_m profiles comparing the effect of nonlocal stress contributions for pipe flows with $d/D = 0.0625$. Cross-stream profiles are compared to the experimental data of Hampton et al. [24], reproduced from Miller and Morris [37]

They found that for smaller particles, the predicted entrance length is much larger compared to that of the experimental result. However, for larger particles, the predicted entrance length was much closer to the experimental values. The authors also defined a new metric to measure the entrance length. This is defined as the length of pipe required for the pressure to reach 95% of its total drop from the inlet to the point where it becomes fully developed. The entrance lengths obtained from the pressure drop values were smaller when compared to the entrance length obtained using the evolution parameter. The pressure drop scales proportionally with the shear stress at the wall, which scales with the viscosity. Shear induced migration decreases the volume fraction near the wall and this decreases the viscosity adjacent to the wall with the velocity not being altered that much. As we approach the fully developed state majority of the particles would have migrated to the center and the pressure drop won't have much effect whereas the other measurement is based on the concentration profiles. This could be the reason that the length obtained through pressure drop is slightly smaller compared to that obtained through the evolution parameter for concentrations.

Lecampion and Garagash [33] pointed out that the suspension balance model used by Miller and Morris to study the entrance length had used exaggerated values for their parameters to fit with the experimental data. Miller and Morris [37] used a value of 0.68 for the maximum particle volume fraction. The permeability for a volume fraction of 0.45 is taken to be 6 times the experimental value in their model. Lecampion and Garagash proposed a model which does not have any fitting parameters to study the entrance length using frictional rheology. Their model had good agreement with the experimental results of Hampton et al. [24]. For a neutrally buoyant suspension flowing through a pipe, the authors found a relation between the entrance length of concentration and entrance length of velocity using the same metric proposed by that of Hampton et al. [24]. It is given by

$$L_\phi \approx 1.136 L_v. \tag{2.23}$$

The authors also studied the entrance length with the metric of pressure drop defined by Miller and Morris [37]. The results obtained were similar in trend to that of Miller and Morris. The table below summarises all the results that were discussed above. All these studies were conducted in the Stokes regime.

Author	Year	Method	Entrance length	Configuration
Nott and Brady [42]	1994	Analytical	$L_\phi \sim H^3/a^2$	Channel
Nott and Brady [42]	1994	Analytical	$L_\phi \sim R^3/a^2$	Pipe
N. Phan-Thien and Z. Fang [43]	1996	Numerical study	$L_v \approx 0.2H^3/a^2$	Channel
N. Phan-Thien and Z. Fang [43]	1996	Numerical study	$L_\phi \approx 0.5H^3/a^2$	Channel
Hampton et al. [24]	1997	Experimental study	-	Pipe
Norman et al. [41]	2005	Experimental study	$L_v \sim R^3/(r^2 N_b f(\phi))$	Pipe
Miller and Morris [37]	2006	Numerical study	-	Pipe/Channel
Lecampion and Garagash [33]	2014	Numerical study	$L_\phi \approx 1.136 L_v$	Pipe

2.3. Summary of previous works and current objectives

The preceding sections have provided an outline of the relevant research studies related to the present research topic. A summary of these studies will help in defining the scope and the research objectives of this thesis.

2.3.1. Observations from previous studies

The literature review provided an overview of the thesis problem statement, highlighting the abundance of studies on single-phase pipe flows that have led to a significant amount of knowledge being acquired in entrance length for both laminar and turbulent regimes over the years. However, there is a noticeable scarcity of research on the entrance length of suspension pipe flows, with most studies relying on numerical simulations and only one experiment conducted in 1997 by Hampton et al. [24].

The scaling provided by Nott and Brady [42] is valid only in the Stokes regime and doesn't have a dependence on the Reynolds number. N. Phan-Thien and Z. Fang [43] using numerical simulations studied the entrance lengths of suspension flows and observed that the development length of velocity and concentration are different. These were also independent of the Reynolds number. An experimental study conducted by Hampton et al [24] used a coiled tube which could lead to secondary flows and the Reynolds number for the study was in the order 1. Compared to single-phase pipe flows, no relation with respect to the Reynolds number has been figured out to date for the entrance length of suspension pipe flows. This is the only experiment which has been conducted in studying the entrance length of suspension pipe flows. There is a lack of experimental data on the entrance length of suspension pipe flows in both laminar and turbulent flows. However, numerical techniques have been utilized to make progress in studying the entrance length of suspension flows [37], [33]. The scope of these studies are limited to the Stokes regime as there is a lack of experimental data available for comparison purposes. However, for natural and industrial processes the inertial effects cannot be neglected. To sum up, a better understanding of the entrance length of suspension flows is needed.

2.3.2. Objectives

The preceding sections have pointed out the relevant research areas with respect to the problem at hand. The objective of this project is to address specific gaps identified in existing literature in order to enhance our understanding to improve the design of industrial process which make use of the entrance length.

The project focuses on particle-laden pipe flow with the dispersed phase being non-colloidal neutrally buoyant spherical particles so that the effects of Brownian motion, buoyancy, and Van der Waals forces can be neglected. The volume fractions will be varied from 0.17 to 0.25 and spherical particles with a d/D ratio of $1/17$ will be used in this study. The study will be conducted using experimental techniques. Ultrasound image velocimetry will be used to measure the velocity profiles of the dispersed phase and concentration profiles (by measuring the intensity) at various locations downstream of the pipe. The research theme can be formulated as

'Entrance length of suspension pipe flows - An experimental study.'

with the following open questions to be addressed in this project.

- Study the entrance length for velocity and concentration of suspension pipe flows for Reynolds numbers in the range 500 - 2000 for volume fractions ranging from 0.17-0.25.
- To study how the development length scales with suspension Reynolds number and volume fraction.

3

Experimental setup and Data acquisition

This chapter discusses the basic principle of Ultrasound imaging and velocimetry which was used to study the entrance length of suspension pipe flows. The experimental setup, its components of the setup and specifications used to acquire data are described in detail.

3.1. Ultrasound Imaging and Velocimetry

One of the main complications faced while experimentally studying dispersed multiphase flows is the lack of optical access due to the presence of multiple scattering surfaces which makes optical experimental techniques ineffective. To investigate dispersed multiphase flows, non-optical measurement techniques are used or the opacity of the flows are circumvented by matching the refractive indices of both the phases. Ultrasound imaging is one of the techniques which is used circumvent opacity in dispersed multiphase flows. The significant advantages of using ultrasound over other measurement techniques like Magnetic Resonance Imaging (MRI), Electrical Impedance Tomography (EIT), etc. for dispersed multiphase flows, is that ultrasound is safe, easy to use, versatile and comparatively economical.

3.1.1. Basics of ultrasound imaging

Ultrasound is characterized by sound with frequencies higher than 20 KHz and the imaging techniques are based on the use of acoustic waves. The elements of the ultrasound transducer are made of piezoelectric material which when deformed by an alternative signal produces pressure waves which travels through the medium. The presence of another medium whose acoustic properties are different from that of the surrounding medium generates echoes which are received by the transducer elements which convert the acoustic waves back into electronic signals.

Figure 3.1 explains the working of ultrasound imaging. The acoustic waves from the transducer element on encountering a medium whose acoustic properties are different from that of the surrounding medium generate echoes which are received by the transducer elements which convert the acoustic waves back into electronic signals which is shown in figure 3.1(b). These initial electronic waves received are referred to as Radio Frequency (RF) data. By using the speed of sound, time axis data, and signal processing steps the RF data is converted to the spatial domain and this is referred to as A-mode image ('A' for amplitude). This is done for every element in the transducer and results in a 2D image which is referred to as B-mode image ('B' for brightness) as shown in figure 3.1(d).

On measuring suspension flows, due to multiple scattering surfaces of the dispersed phase, the signal attenuates. The signal intensity is compensated as the signal travels deeper into the medium and this is called time gain compensation.

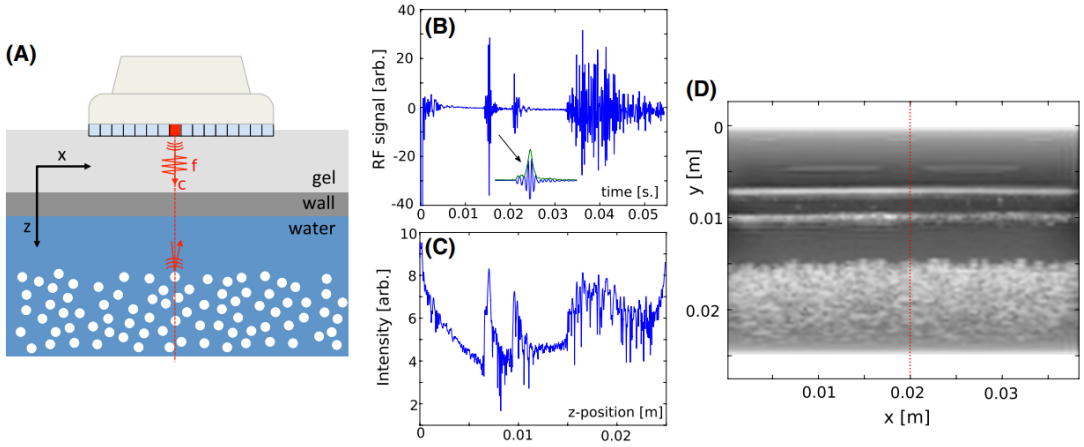

Figure 3.1: Ultrasound imaging (a) Geometry(b) RF signal (c)A-mode image (d) B-mode image. Reproduced from Poelma [45].

3.1.2. Ultrasound image velocimetry

Ultrasound image velocimetry (UIV) is an ultrasound version of Particle image velocimetry (PIV). UIV is a valuable alternative to obtain velocity fields where optical access is limited. The basic principles are similar to that of PIV. The flow is seeded with particles with the expectation that the seeded particles follow the flow. Images are captured using the ultrasound sensor at two different time instances based on the flow conditions and this helps to evaluate the particle displacements. To calculate the particle displacements, the image pairs are divided into interrogation windows such that each window has sufficient number of particles. A cross-correlation algorithm between the image pairs is used to obtain the displacement of particles. Since the seeded particles follow the flow, the displacement of the particle is the same as the displacement of fluid surrounding this particle. For UIV, the seeded particles should not only follow the flow but should also have the right acoustic properties. For a detailed review, the reader is referred to Poelma [45].

One of the non-dimensional number that governs the behavior of suspended particles in fluid flow is referred to as the Stokes number (St). It is defined as the ratio of the characteristic time of the particle (τ_p) to the characteristic time of the flow (τ_f).

$$St = \frac{\tau_p}{\tau_f}. \tag{3.1}$$

Stokes drag predominantly governs particle dynamics, especially in a fluid undergoing acceleration. The difference between the fluid velocity (u) and particle velocity (u_p) can be calculated as:

$$u_p - u = \frac{d^2(\rho_p - \rho)}{18\mu_0}\frac{du_p}{dt}. \tag{3.2}$$

This difference in velocities represents the velocity lag or this can be defined in the form of particle response time (τ_p), which is the amount of time the particle takes to adjust to the changes in flow. The particle response time is given by

$$\tau_p = \frac{d^2(\rho_p - \rho)}{18\mu_0}. \tag{3.3}$$

For velocity measurements, the lower the Stokes number the better the tracing accuracy due to the fact that the response time of the particle is much less compared to that of the flow, and the particle would follow the flow. Stokes number less than 0.1 ensures that tracking errors are less than 1%. Additionally, the size of the tracer must be small so that it won't alter flow.

3.2. Experimental setup

The experiments to study the axial development of neutrally buoyant suspension pipe flows were conducted in a pipe setup at the Process and Energy department at TU Delft. The pipes used in the setup are made of Poly methyl methacrylate (PMMA), have an inner diameter of 30 mm and are 5 m in length. The schematic of the experimental setup is shown in figure 3.2. Each component is marked for better clarity. The upcoming sections elucidate the components of the experimental setup.

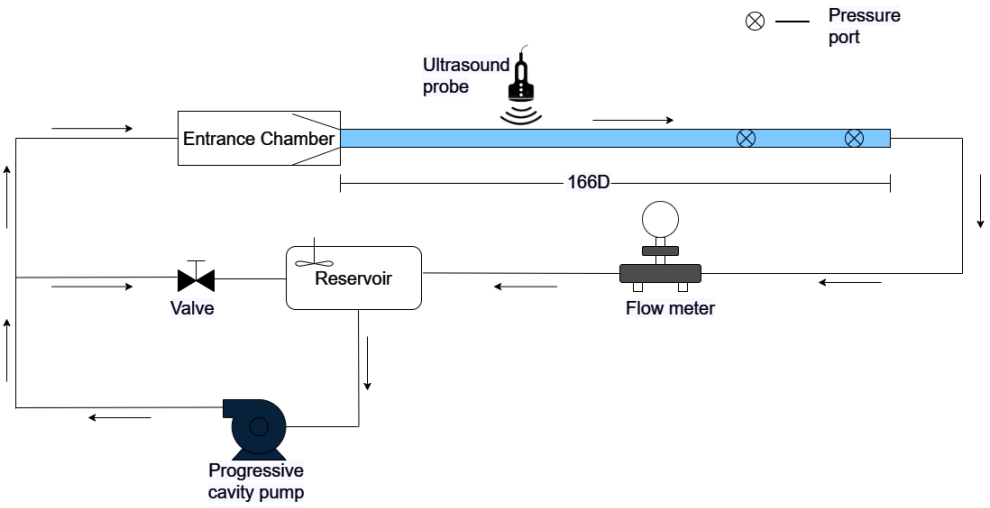

Figure 3.2: Schematic overview of the experimental setup. The arrow indicates the direction of flow.

3.2.1. Reservoir

Reservoir is a rectangular tank made from plastic, that functions as a containment vessel for the suspension or fluid. It serves as the primary source from which a pump extracts fluid or suspension. The reservoir allows for the addition or removal of particles, thereby facilitating the modification of volume fraction. Additionally, it also acts as a return tank for the fluid or suspension in the closed-loop setup. Within the reservoir, a mechanical stirrer is deployed to ensure the homogeneous dispersion of particles throughout the suspension thereby preventing settling.

3.2.2. Pump

A progressive cavity pump is used in the experimental campaign to transport the suspensions. The pump has a maximum capacity of 70 L/min and can sustain operations up to a pressure of 10 bar. Even though the pump can be operated at higher temperatures, up to $100°C$, the standard operating temperature range aligns with the experimental conditions, typically maintained between $20°C - 27°C$. The pump is coupled with a frequency controller to operate the system at different flow rates.

3.2.3. By-pass (Valve)

The By-pass loop serves the purpose of achieving reduced flow rates within the measurement section of the pipe by diverting a fraction of the volume (using the valve) back to the reservoir. By adjusting the valve, it is possible to divert a fractional portion of the fluid or suspension back to the return tank instead of directing it into the measuring pipe section. This adjustment of the valve facilitates the attainment of diminished flow rates in the measurement section of the pipe.

3.2.4. Entrance chamber

The entrance chamber as seen in figure 3.3 is used in the experimental setup to ensure a smooth profile when the flow enters the measuring pipe section. The functioning of the entrance chamber is as follows:

the entrance chamber's diameter significantly exceeds that of the pipe transporting the flow. This design induces a substantial reduction in velocity compared to the corresponding increase in the entrance chamber's diameter, thereby decreasing the Reynolds number. A decrease in Reynolds number implies the dominance of viscous forces over inertial forces. This increases the viscous dissipation of eddies, minimizing flow fluctuations. At the exit of the entrance chamber, a smooth contraction is present to prevent flow separation when the flow progresses into the measurement segment of the pipe.

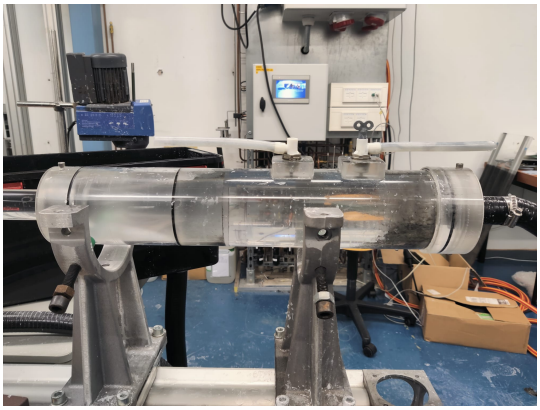

Figure 3.3: The entrance chamber (Flow is from right to left).

On the top of the entrance chamber, two air vents (see figure 3.3) are attached in order to remove the air bubbles that would be trapped inside the chamber. If not removed, air bubbles could potentially interfere with the experimental results.

3.2.5. Flow meter

An inline Coriolis mass flow meter is shown in Figure 3.4 (KROHNE OPTIMASS 7050c) is used in the return section of the flow loop to measure the volume flow rate. The measuring tube has an internal diameter of 15 mm and a total length of 450 mm. The flow meter is accurate up to 1% of the measured value, the repeatability is rated as 0.005% including hysteresis, linearity and zero stability. Additionally, the flow meter measures densities in the range of $500 - 2000\ kg/m^3$ with an accuracy of $\pm 2\ kg/m^3$. Furthermore, it provides temperature measurements for the fluid with an accuracy $\pm 1°C$. The flow meter is interfaced with a National Instruments (NI) USB-6212 BNC Bus-Powered M Series DAQ card to record the output via a Matlab program.

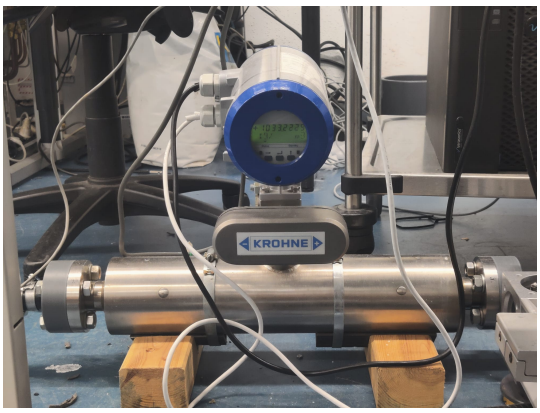

Figure 3.4: Coriolis flow meter used in the experimental campaign to measure the flow rate, density and temperature of the suspension. Flow is from left to right.

3.3. Equipment employed

The following subsections describe the equipment used for measurements in the experimental campaign.

3.3.1. Pressure sensor

The experimental setup uses a Validyne DP45 differential pressure transducer (see figure 3.5a) for pressure drop measurements across the pressure ports (see figure 3.2) which are 50 pipe diameters apart. The sensor uses a 20 diaphragm (see figure 3.5b) which can measure pressures up to 860 Pa with an accuracy of $\pm 0.5\%$ of the full-scale value. The pressure diaphragm is placed inside the pressure transducer and was calibrated for a maximum pressure of 539 Pa using a manometer. The pressure sensor is connected to a CD 15 carrier demodulator which is coupled with a USB-6212 BNC Bus-Powered M Series DAQ card to obtain the pressure drop measurements using a Matlab program. The calibration curve of the pressure sensor is shown Appendix A.

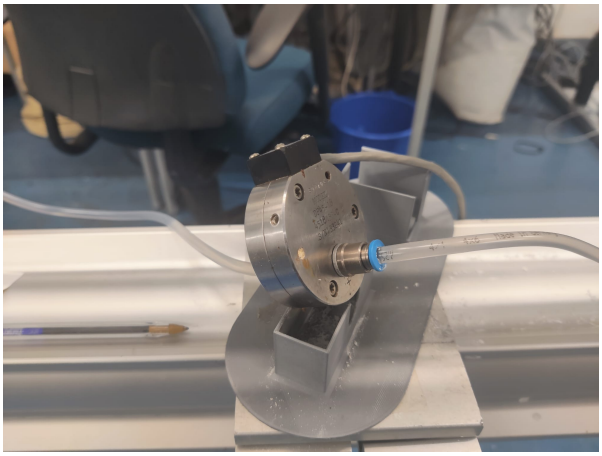

(a) Pressure transducer.

(b) Pressure diaphragm 20.

Figure 3.5: Pressure sensor

3.3.2. Ultrasound system

Data is acquired using a Verasonics Vantage 128 echography system in combination with L11-5v linear probe. The probe has an elevational focal depth of 18 mm and is operated at a frequency of 7.6 MHz. Furthermore, a bandwidth of 6-10 MHz is prescribed, as this gave a relatively good image quality after visual inspection. The probe consists of 128 single elements, each with a pitch of 0.3 mm. This results in a total length of 38.4 mm in the streamwise direction and this is the width of the field of view. Note that the resolution in radial and stream-wise directions is not equal. The depth of the field of view is set, such that the 80% pipe is visible.

Figure 3.6: Verasonics L11-5v linear probe used in the experimental campaign. Reproduced from Versasonics [56].

The ultrasound measurements are very sensitive and depends on the alignment of the ultrasound probe with the pipe. A fixed position of the ultrasound probe with respect to the pipe must be maintained at all downstream locations to get accurate measurements. In order to get consistent and reproducible measurements, a specialized probe holder was designed. Two distinct designs were conceptualized and manufactured through 3D printing. The initial design, illustrated in figure 3.7, had a limitation: once the ultrasound probe is inserted for measurements, it must remain within the holder. Improving on the design to circumvent this limitation, an improved probe holder design (refer to Figure 3.8) was devised. This final design not only overcomes the restriction of the probe remaining fixed within the holder but also ensures repeatability even when the ultrasound probe is removed and subsequently repositioned within the holder. The repeatability of both holders is shown in the Appendix B.

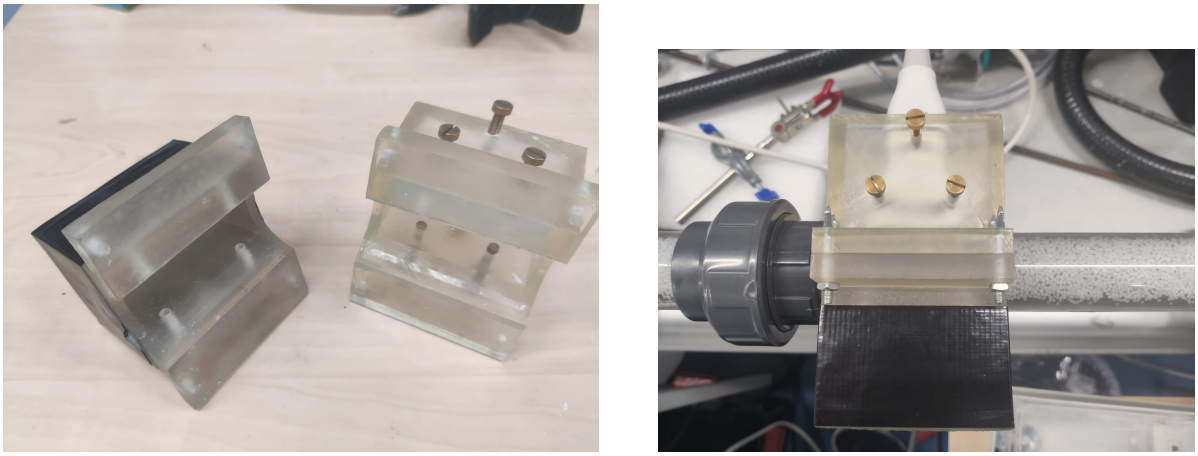

Figure 3.7: Preliminary design of probe holder.

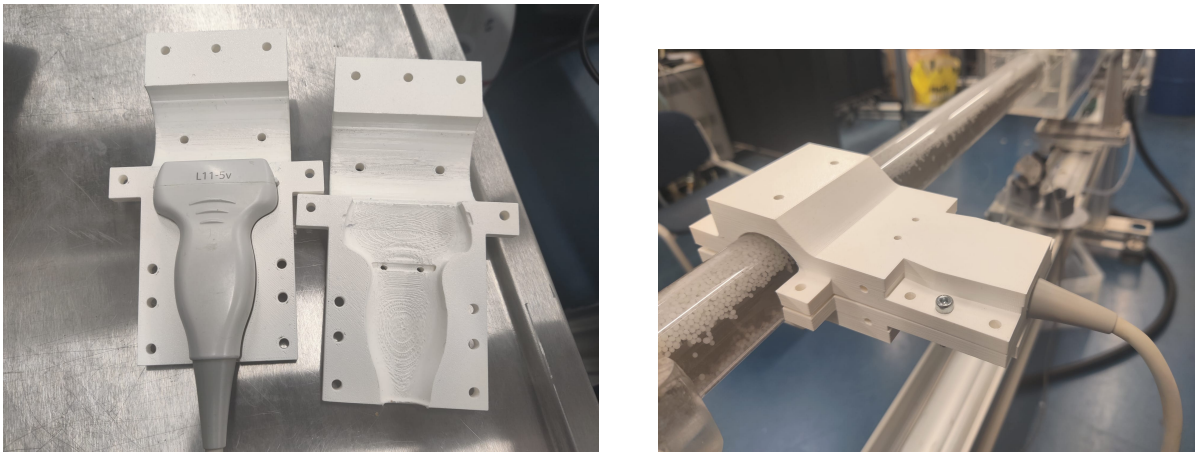

Figure 3.8: Final design of probe holder.

3.3.3. Flow seeding

For single-phase measurements, Vestosint particles were used as tracer particles. They have a mean diameter of 56 μm and a density of 1016 kg/m^3. These particles prove to be effective flow tracers as their particle response time (τ_p) is negligible thereby having a Stokes number less than 0.1. The particles not only faithfully follow the flow but also give good acoustic signals.

3.4. Experimental parameters

The following subsections look into the experimental parameters that were used to study the axial development of neutrally buoyant suspension pipe flows.

3.4.1. Field of view

In order to study the axial development, different locations along the streamwise direction along the pipe were considered. This was facilitated by the flexibility of the experimental setup, allowing for the ease of placement of the ultrasound probe at different locations. Figure 3.9 is an illustration of the field of views considered. It can be seen the particles are initially homogeneously distributed in the pipe (Field of view - 1). They migrate towards the core of the pipe so that the radial concentration profile gradually changes. This is observed in several downstream fields of view (Field of view - 3).

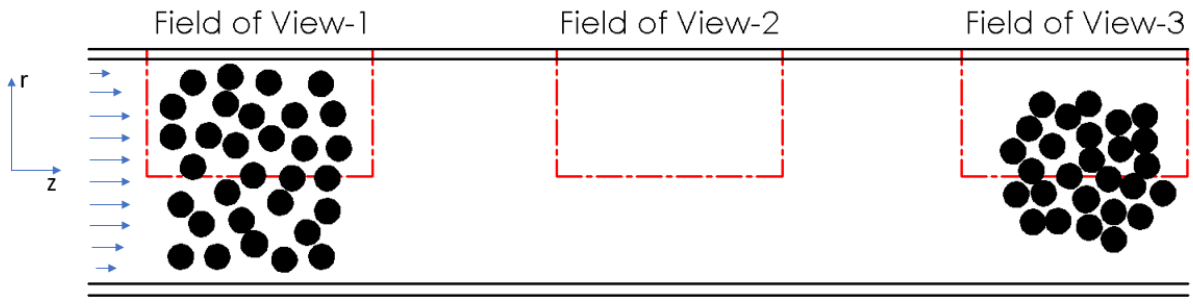

Figure 3.9: Illustration of the fields of view considered in the experimental campaign.

3.4.2. Parameters

Table 3.1 gives an overview of the parameters of the flow system of the experimental facility in this thesis study. Unexpanded polystyrene particles with particle diameter, d = 1.75 ± 0.12 mm are used as

the dispersed phase. The density of the continuous phase (water) is matched to the particles by adding Na_2SO_4. The addition of Na_2SO_4 increases the viscosity of the continuous phase and this corrected viscosity [1] is reported in the table 3.1. The ratio between particle and pipe diameter, a key parameter in suspension flows, is D/d = 17.1.

Parameter	Value
Pipe inside diameter (D)	30.35 mm
Total Length	5.0 m
Suspension Reynolds Number (Re_s)	$500 - 2000$
Fluid Density (ρ)	1034 kg/m^3
Working Temperature	$21 - 23\,^{\circ}$C
Fluid Viscosity	1.1×10^{-6} Pa.s

Table 3.1: An overview of parameters of the flow system.

The ultrasound probe captured a field of view of about 38.4mm × 29 mm in the streamwise (z) and radial (r) directions respectively. Imaging the entire pipe was not needed due to the axisymmetric nature of flow within the pipe. Only visualizing half of the pipe was sufficient for the measurement. Specifically, a region covering up to 80% of the pipe was taken into consideration.

The focus of this thesis is to study the effect of concentration and the suspension-based Reynolds number on the axial development of suspension pipe flows. The measurement matrix considered for the experimental campaign is shown in figure 3.10. All the points in the measurement matrix are measured at 8-9 locations along the pipe.

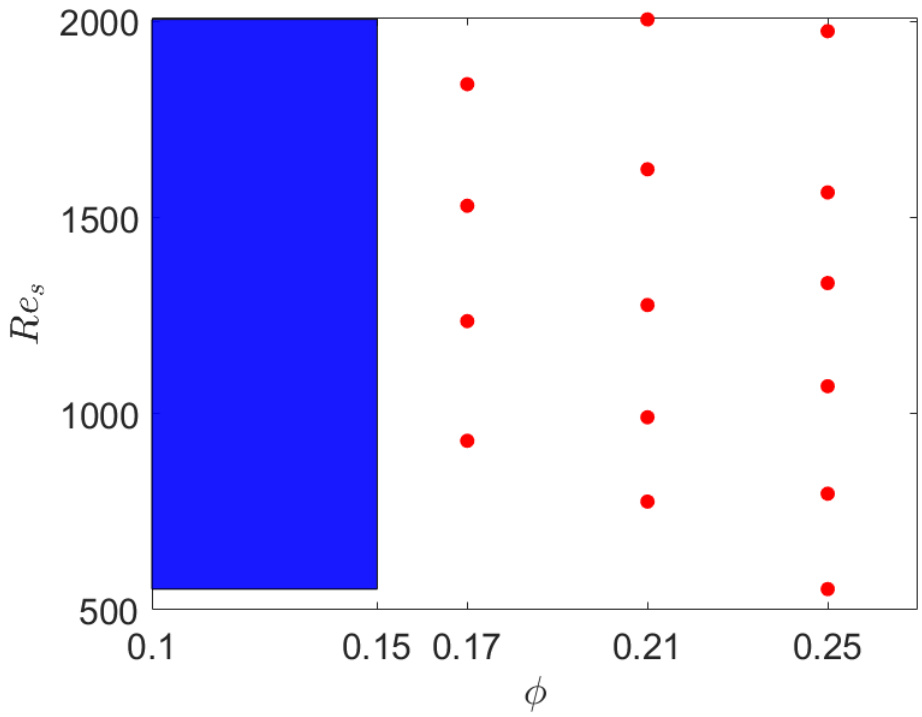

Figure 3.10: Measurement matrix considered in the experimental campaign.

As shown in figure 3.10, suspension Reynolds numbers below 931 and 776 were excluded from the experimental campaign for volume fractions of 0.17 and 0.21, respectively. The initial measurement matrix considered volume fractions 0.1 and 0.15 (blue shaded region in Figure 3.10), along with suspension Reynolds numbers ranging from 500 to 2000 for volume fraction 0.1 and 0.15. Subsequently, the measurement matrix was trimmed down to the one shown in figure 3.10 due to the prominence

of buoyancy effects, despite the closely matched densities of both phases especially at lower volume fractions and lower suspension Reynolds numbers. A detailed explanation is provided in section 5.1.1. Additionally, suspension Reynolds numbers exceeding 2000 were not considered, as the prominence of the particle core decrease for higher suspension Reynolds numbers.

3.5. Experimental procedure

To ensure the accuracy of measurements, a meticulous experimental protocol was carefully followed. Before operating the pump, a check of all connections was conducted to detect and rectify any potential leaks. The presence of air bubbles can affect the accuracy of measurements. A careful inspection was carried out, and any air bubbles present in the system were removed by either flushing them towards the reservoir or utilizing the air vents in the entrance chamber.

The pump was subsequently turned on at high flow rates for 2-3 minutes ensuring a homogeneous mixing of the suspension. Following this, the flow rate was adjusted to the required level, allowing 2 minutes for the flow to achieve a stable state. Each measurement at a specific position along the pipe involved a repetition of the experimental procedure. The particle concentration remained constant until measurements at all suspension Reynolds numbers were conducted for every position in the stream-wise direction.

For measurement, an echography system using a specialized probe holder attached to the pipe housing the L11-5v linear probe was utilized. Ultrasound gel was applied on the probe surface to prevent any air gaps between the sensors on the probe and the pipe. Concentration and velocity measurements were acquired at 10 fps (for uncorrelated images) and 200 fps using plane wave imaging ultrasound, respectively. Four sets of 2000 images at each location for a measurement point were acquired for both velocity and concentration. Simultaneously, the data from the flowmeter to measure flow parameters was obtained using a Matlab program which was interfaced with the DAQ card. The obtained data is further post-processed in Matlab to obtain the desired quantities.

3.6. Post processing

The raw image acquired using the ultrasound probe is shown in Figure 3.11. Even though the thickness of the pipe wall is 5 mm, it can be seen in the in the raw image that pipe wall thickness is around 3 mm. This is due to the fact that speed of sound is quicker in the pipe wall (made of plexiglass) compared to that of the suspension. The radial scaling is done with respect to the speed of sound in suspension which will be further explained below in the same section. Additionally, it can also be seen that the near wall region is corrupted with the reflections from the wall. The bright white spots in the raw image is the polystyrene particles (dispersed phase).

Spatial and temporal averaging of the acquired images yields an intensity profile, which correlates with concentration in a non-linear manner. The obtained intensity profile for the raw image is shown in figure 3.12 (a). The peaks shown in red circles in the figure 3.12 (a) correspond to reflections of the pipe wall.

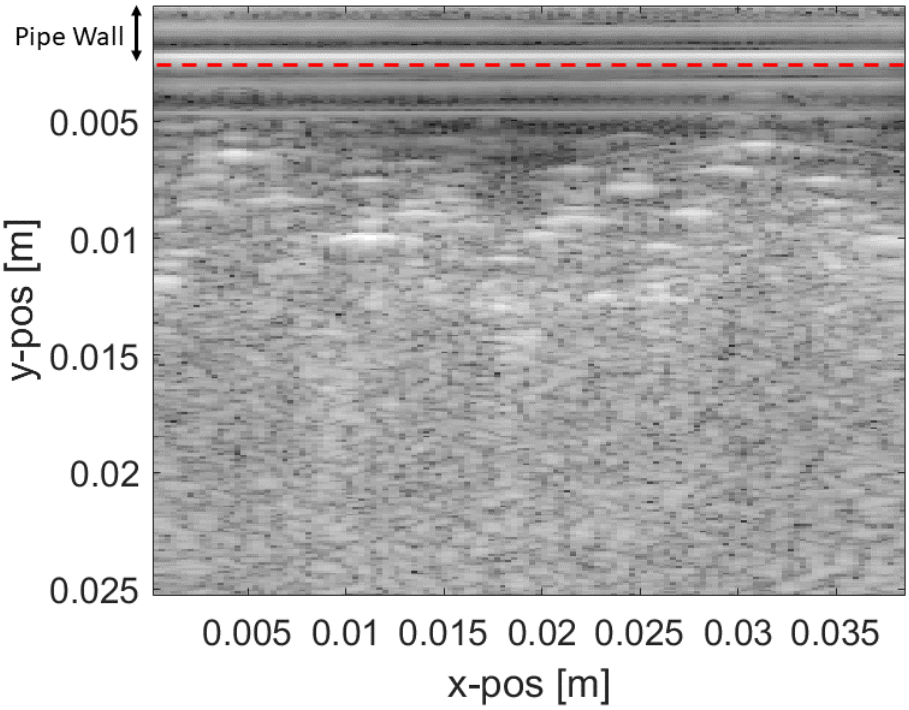

Figure 3.11: An example of a raw image acquired by the ultrasound probe. The red dotted line shows where the pipe wall ends.

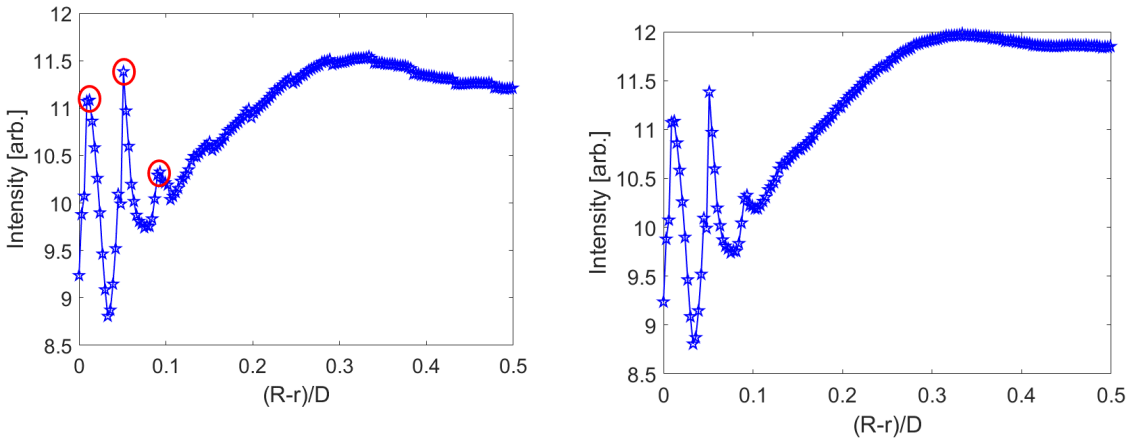

Figure 3.12: (a) Intensity profile obtained from the raw image (b) Intensity profile after TGC correction.

Additionally, small stepwise jumps are observable in the intensity profile, corresponding to the time gain compensation of the signal. To rectify this and ensure a smooth intensity profile, a correction process is implemented, as illustrated in figure 3.13. The point at which the intensity jump occurs is identified. The slope of the curve before the jump is computed using the preceding two points (point 1 and point 2 in Figure 3.13), and the signal intensity at the corresponding point where the jump initiates (point 4) is determined. The difference between the intensities at points 3 and 4 is then added to the rest of the segment of the signal. This procedure is repeated until every step-wise jump is corrected in the profile. This gives a smooth intensity profile as shown in figure 3.12 (b). This correction is same for all measurements.

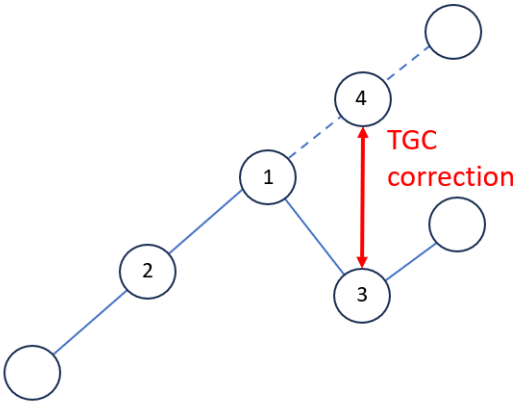

Figure 3.13: Illustration of time gain compensation (TGC) correction.

The images acquired using ultrasound were processed using an in-house PIV code written in MATLAB. The method of cross-correlation between image pairs is used to determine the instantaneous velocity fields. The image pairs are divided into small windows known as interrogation windows and are then cross-correlated to yield an average particle displacement per interrogation window. Using the displacement, time gap between the image pair and the magnification, the velocity of the dispersed phase is determined. For our experimental campaign, 32×32 interrogation windows were used with a single pass. The radial resolution in mm/pixel is calculated as

$$\text{radial scaling} = \frac{c_s}{2F}, \tag{3.4}$$

where c_s is the speed of sound in suspension and F is the frequency of the ultrasound emitted to capture the images. It can be seen that the radial resolution is dependent on the speed of sound and the relative speed of sound in suspension is given by Wood's equation [13]

$$\frac{c_s}{c_f} = \left[1 - \left(1 + \frac{\kappa_p}{\kappa_f}\right)\phi\right]\left[1 - \left(1 + \frac{\rho_p}{\rho}\right)\phi\right]^{-0.5}, \tag{3.5}$$

where c_f is the speed of sound in the fluid, κ_p (245 MPa^{-1} [7]) is the compressibility of the dispersed phase, and κ_f (459 MPa^{-1}) is the compressibility of the continuous phase. Table 3.2 gives an overview of the values obtained using Wood's equation,

S. No.	ϕ_b	c_s/c_f
1	0.17	0.91
2	0.21	0.89
3	0.25	0.87

Table 3.2: The speed of sound in suspension relative to the speed of fluid for all the volume fractions in the experimental study

It is to be noted that the Woods equation is valid for a uniform suspension. However, the occurrence of shear-induced migration results in the development of concentration gradients. In the field of views considered for the experiment, the speed of sound varies due to the concentration gradients formed as the Wood's equation depends on the volume fraction. Profiling concentration from intensity profiles is out of scope for the thesis and the thesis will rely on the assumption that the speed of sound remains constant within the field of view for a given volume fraction.

4

Results and Discussion

The chapter discusses the results obtained from the experiments conducted in the experimental setup. It commences by validating the setup and determining the entrance length for single-phase pipe flows. This is followed by a characterization of the inlet conditions for studying the entrance length in suspension pipe flows. Subsequently, the chapter dives into a discussion on intensity profiles and velocity profiles at different volume fractions. The final section attempts to understand the entrance length for suspension pipe flows and compares it with existing literature.

4.1. Single phase pipe flow

Before performing any experiments on a setup, the experimental setup has to be validated. Single phase pipe flow measurements were conducted using water as the fluid to validate the experimental setup by obtaining the Moody diagram as well as looking into the velocity profiles. The Moody diagram is a log-log plot illustrating the relationship between Reynolds number and Darcy friction factor. The Moody diagram obtained from the experimental setup along with analytical results are shown in Figure 4.1.

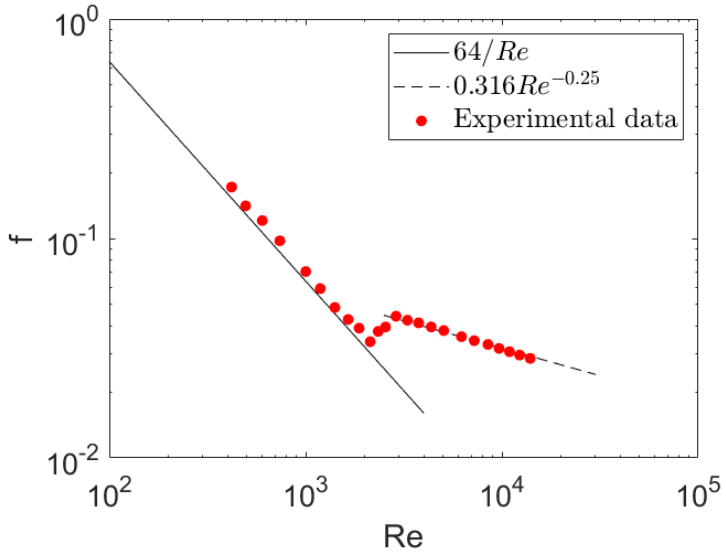

Figure 4.1: Moody diagram for single phase flow used to validate the experimental setup.

The relative error of f with the analytical result decreases as we go to higher Reynolds numbers and this can be attributed to the uncertainty with the pressure sensor whose accuracy corresponds to ± 4.3 Pa. The pressure drop is in $\mathcal{O}(1\text{ Pa})$ in the laminar region and this accuracy can have a huge significance on the Darcy friction factor calculated.

4.1.1. Velocity profiles

Velocity measurements at various positions downstream of the pipe were conducted to obtain the entrance length of single-phase pipe flows. Reynolds numbers of 550, 787, and 990 were considered, as illustrated in Figure 4.2. Furthermore, the volume flow rate was determined by integrating the velocity profile across the cross-section of the pipe ($Q = \int u_z \cdot 2\pi r dr$), and the results were compared with the readings from the flowmeter. The calculated volume flow rate values were found to be within 5% of the flowmeter reading.

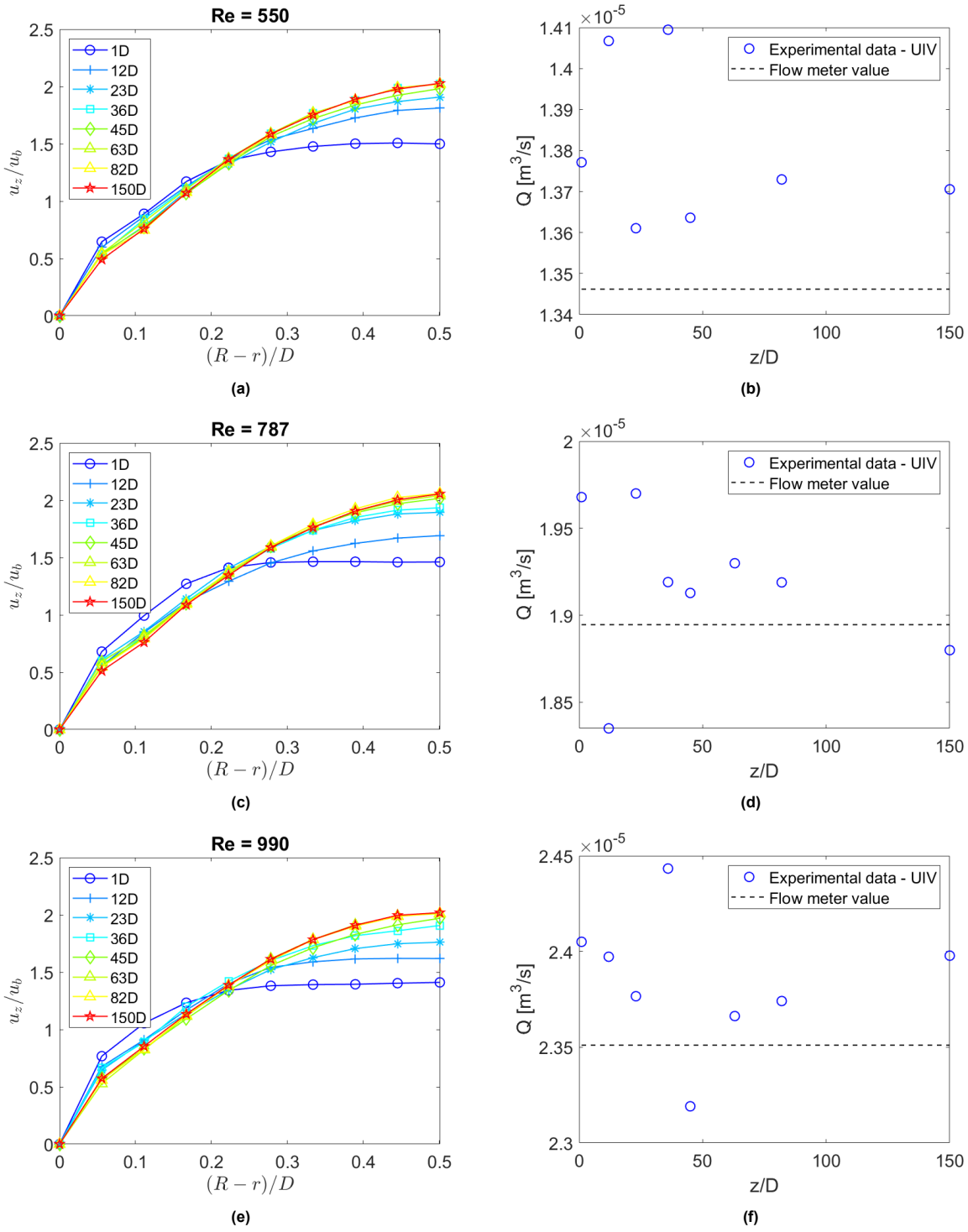

Figure 4.2: (a)Velocity profiles for Re = 550 (b) Volume flow rate comparison for Re = 550 (c) Velocity profiles for Re = 787 (d) Volume flow rate comparison for Re = 787 (e) Velocity profiles for Re = 990 (f) Volume flow rate comparison for Re = 990.

4.1.2. Entrance length

Understanding and accurately predicting the entrance length is essential for various engineering applications and the effective design of engineering systems. The main parameter of interest in this study, thus, is the entrance length or the development length which is defined as the length required for a uniform inlet to to develop into a fully developed flow. In practice, The entrance length is usually taken to be the distance from the pipe entrance to where the center line velocity (u_c) reaches within about 1 percent of the fully developed value.

The uniform inlet velocity profile undergoes a change towards a parabolic profile in incompressible laminar pipe flow due to the presence of the no-slip boundary condition at the wall which gives rise to the formation of the boundary layer. This is due to the viscous forces close to the wall which resists the fluid from flowing and starts forming gradient in velocities. As the inertial forces increases the prominence of the viscous forces in the boundary layer decreases. Since both inertia and viscous forces play a role in the development of the flow and Reynolds number being the ratio of inertial to viscous forces, the non-dimensional entrance length (L_v/D) is a function of the Reynolds number, where L_v is the entrance length for velocity and D is the pipe diameter. To obtain the entrance length, the centerline velocities at different positions are fitted with a curve of the form

$$U_c = \alpha_1 \left(1 - e^{\alpha_2 \cdot Z}\right) + \alpha_3 \tag{4.1}$$

where $Z = L/(D \cdot Re)$ is the non-dimensional axial distance from the exit of the entrance chamber (shown in Figure 4.3). The entrance length for velocity, L_v is defined as the point where U_c reaches 99% of the asymptotic value.

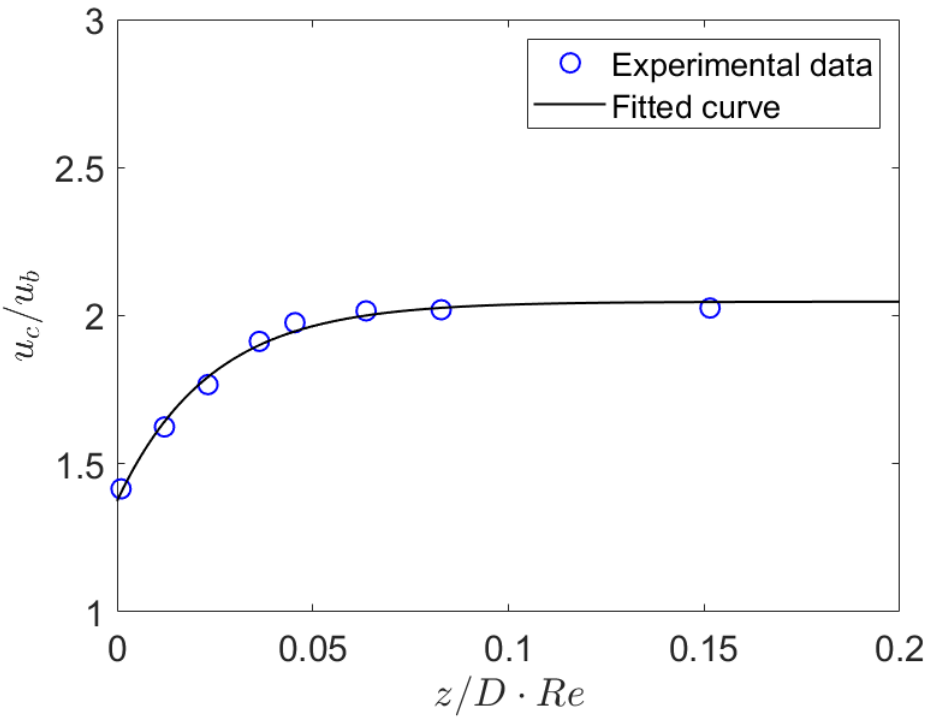

Figure 4.3: Illustration of the fitted curve on the centerline velocities for Re = 990.

The errorbars in Figure 4.3 refer to the standard deviation of all the measurements taken. The entrance lengths obtained for single phase pipe flow are summarised in table 4.1.

S. No.	Re	L_v/D
1	550	23
2	787	39
3	990	55

Table 4.1: Obtained entrance lengths for single-phase pipe flow experiments. These values are obtained based on the methods of Langhaar [31].

Upon comparing the obtained entrance lengths with the analytical result, as shown in Figure 4.4, it becomes evident that the entrance length obtained from our experiments is smaller in comparison to the analytical result. This discrepancy is anticipated since the entrance length calculated using the analytical results assumes a uniform inlet condition. However, our actual inlet condition has velocity gradients near the wall and is much more developed compared to a uniform inlet velocity profile, as seen from figure 4.2. In other words, our inlet condition is already in an intermediate stage in comparison with a uniform inlet condition and hence has a smaller entrance length.

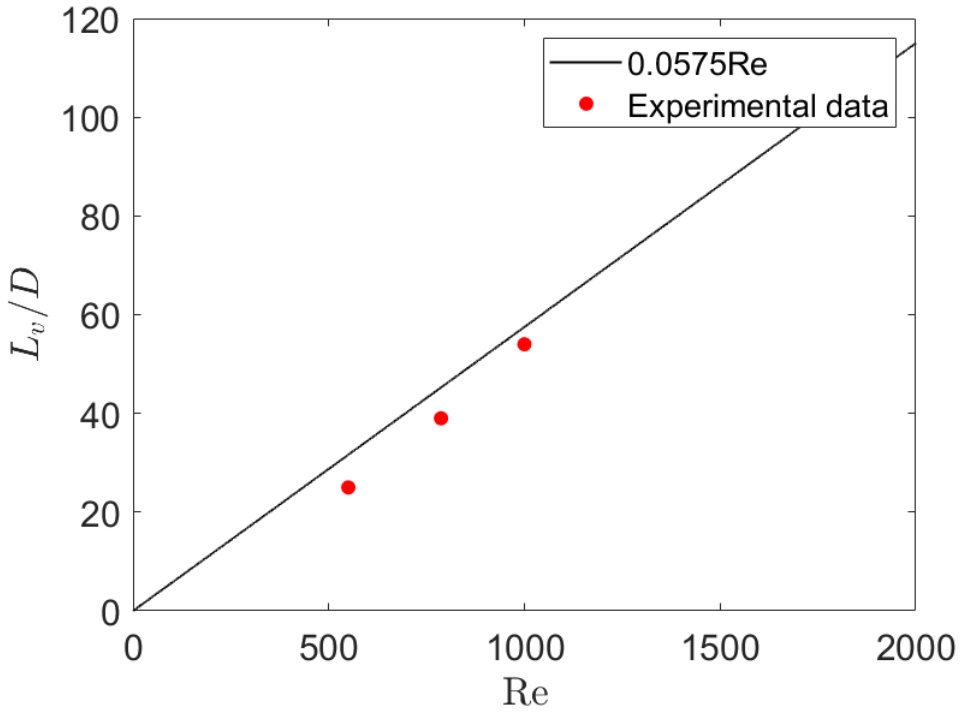

Figure 4.4: Comparison of the obtained entrance lengths with the analytical result.

These results for single-phase flows validate the experimental setup and the entrance length calculation acts as a baseline result to which multiphase flow results can be compared.

4.2. Entrance length in suspension pipe flows

Once the entrance length of single-phase flows is characterized, particles are added to study the entrance length of suspension pipe flows. The volume fractions of particles studied in this thesis range from 0.17-0.25. On adding particles, the viscosity of the suspension changes, and the change in effective viscosity of the suspension is accounted by the Eiler's viscosity model. Before moving on to

studying the axial development of suspension pipe flows, it is important to characterize the inlet conditions for both velocity and concentration.

4.2.1. Inlet condition

The inlet conditions for velocity are assumed to be the same as that of single-phase pipe flow which is shown in Figure 4.2. The velocity profile at 1D corresponds to the inlet conditions for velocity. To characterize the inlet conditions for concentration, particles are counted at the inlet and represented in a histogram. However, accurately counting particles within the volume fraction range of 0.17 to 0.25 becomes challenging due to excessive noise caused by multiple scattering surfaces in the images. Consequently, to characterize the inlet conditions, particles are counted at a volume fraction of 1% using MATLAB program. It is assumed that the observed trend at this lower volume fraction is representative of particle behavior across all volume fractions. The histograms are shown in Figure 4.5.

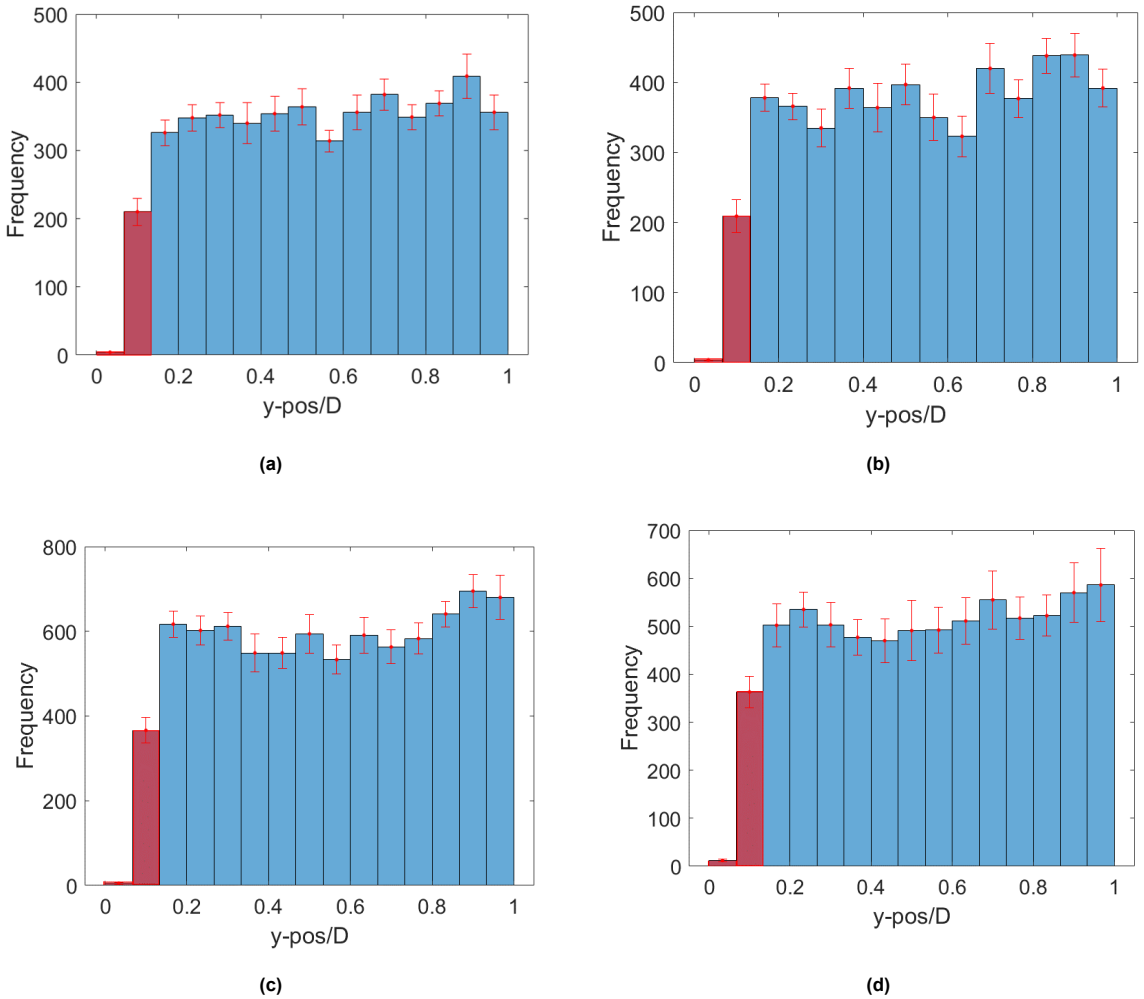

Figure 4.5: Inlet condtions for various suspension Reynolds numbers (a) $Re_s = 780$ (b) $Re_s = 1004$ (c) $Re_s = 1583$ (d) $Re_s = 2983$. The standard error for each bar is plotted at the top of each bar. y-pos/D = 0 corresponds to the top wall and y-pos/D = 1 corresponds to the bottom wall.

A bin size of 2 mm was selected to closely match the particle size of 1.75 mm. In Figure 4.5, the first two bars of the histograms are highlighted in red, indicating that these histogram bins are compromised by reflections from the wall, as illustrated in Figure 4.6. The errorbars shown in Figure 4.5 are calculated as follows.

$$\sigma_{SE} = \frac{\sigma}{\sqrt{n}}, \tag{4.2}$$

where σ_{SE} is the standard error in measurements, σ is the standard deviation and n is the number of measurements. The errorbars are reported at 99.7% confidence interval ($\pm 3\sigma_{SE}$). Additionally, it is evident from Figure 4.5 that particles closer to the bottom wall exhibit higher frequency. This phenomenon is attributed to the polydisperse nature of particle density. Despite matching densities of both phases, the bottom region contains a greater number of particles due to the inherent polydispersity in particle densities. To check for the convergence of the particle concentration histograms, Kullback-Liebler divergence was calculated between the histograms obtained from different measurements for a fixed Re_s and a value in the order of $\mathcal{O}(10^{-4})$ was achieved for all the suspension Reynolds numbers. Kullback-Liebler divergence is a statistical distance, a measure of how one distribution differs from another distribution. The detailed calculations of Kullback-Liebler divergence are shown in the Appendix C.

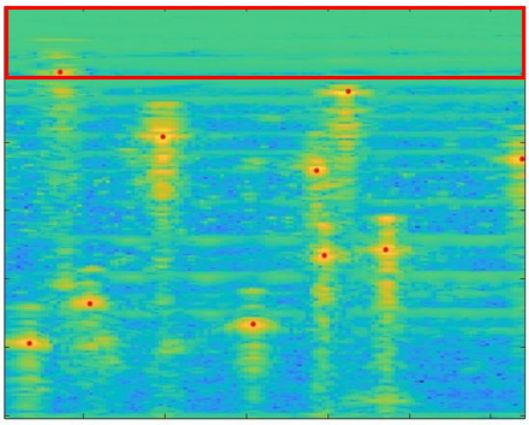

Figure 4.6: The reflections near the top wall. The region which corrupts the inlet conditions is shown in the rectangle. The red dots correspond to the particles which are counted.

The histograms in the Figure 4.6 are close to a uniform distribution. The deviation was calculated by plotting a uniform distribution line by excluding the red colored bars in the histograms as illustrated in Figure 4.7. All the histograms are close to uniform distribution with a mean error of 7%.

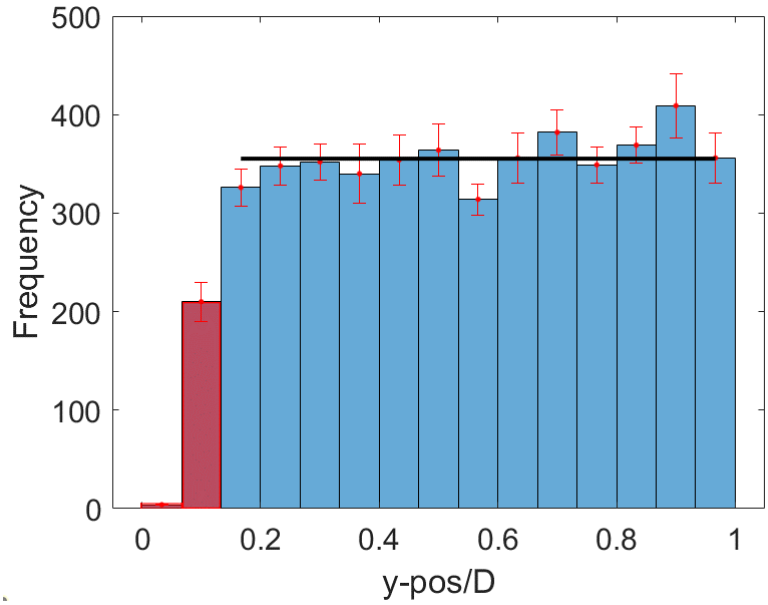

Figure 4.7: The histogram for $Re_s = 780$ plotted with a uniform distribution line.

In Figure 4.5, a minor discontinuity is observed between consecutive bins. For instance, consider

the case of $Re_s = 780$, the smallest bin (excluding the red ones) at the upper limit of the error bar has a frequency of 329. In comparison, the adjacent bins at their lower limit show frequencies of 342 and 330, indicating that the observed differences are not highly significant. These negligible jumps may be attributed to potential errors in precisely locating particles, possibly due to the vertical reflections of the particles. It is possible that the reflections from particles could lead to slight inaccuracies in position determination, and in some instances, particles might be missed altogether, contributing to these minor jumps in the histograms.

In summary, the inlet conditions for concentration have been characterized, obtaining a distribution that is very close to uniform distribution. With a clear understanding of the inlet conditions, we move on to understanding the axial development of neutrally buoyant suspension pipe flows. Volume fractions 0.17, 0.21, and 0.25 were chosen for the study.

4.2.2. Particle volume fraction - 17%

The image in Figure 4.8 displays snapshots of the raw ultrasound images at three distinct downstream locations. Notably, at the inlet, there is a uniform distribution of particles, with a lot of bright white spots near the wall. Moving downstream, there is a decrease in the number of these bright spots near the wall, indicating a decrease in the number of particles and suggesting migration. Interpreting the center of the pipe is difficult due to signal attenuation (even though it is compensated with time gain compensation) and the presence of multiple scattering surfaces, resulting in considerable noise. Given the axisymmetric nature of the neutrally buoyant pipe system, imaging only till $D/2$ is sufficient.

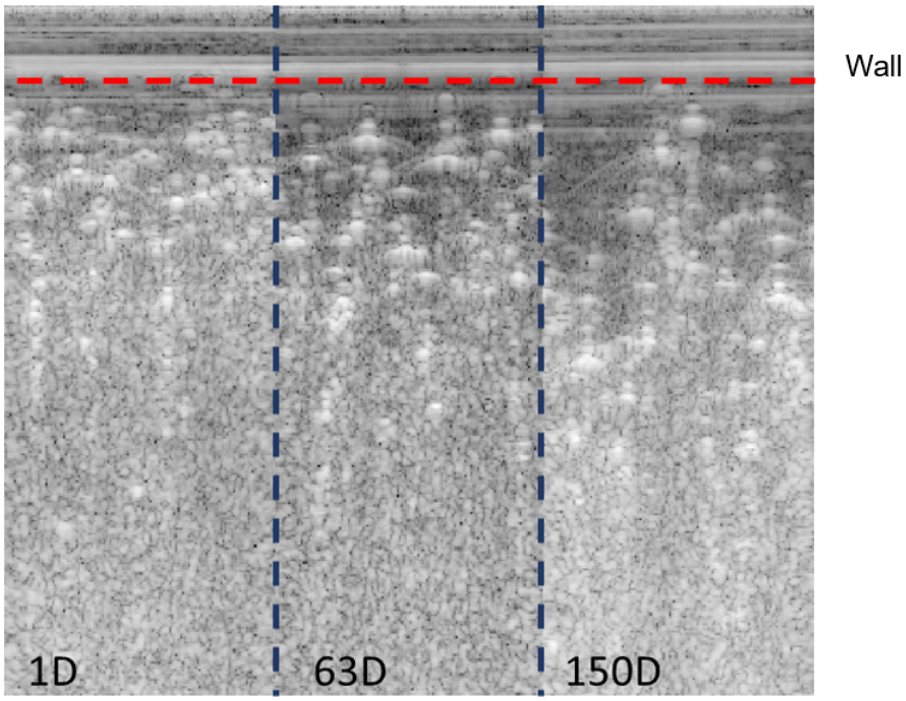

Figure 4.8: Three ultrasound images at three downstream locations (z = 1D (inlet), 63D, and 150D) illustrating the migration of particles. $Re_s = 931$ and $\phi_b = 0.17\%$. The red dashed lines indicate the location of the upper pipe wall.

Although directly correlating intensity to concentration is not trivial, the migration process can be assessed through consistent imaging using the ultrasound probe. This means that precise values or profile shapes are not that important; what matters is the ability to observe changes in the profiles at various positions along the pipe. The intensity plots at various locations downstream of the pipe for various suspension Reynolds numbers are illustrated in Figure 4.9. The peaks near the wall in the intensity profiles correspond to the reflections from the wall which corrupt the intensity values at the near wall region.

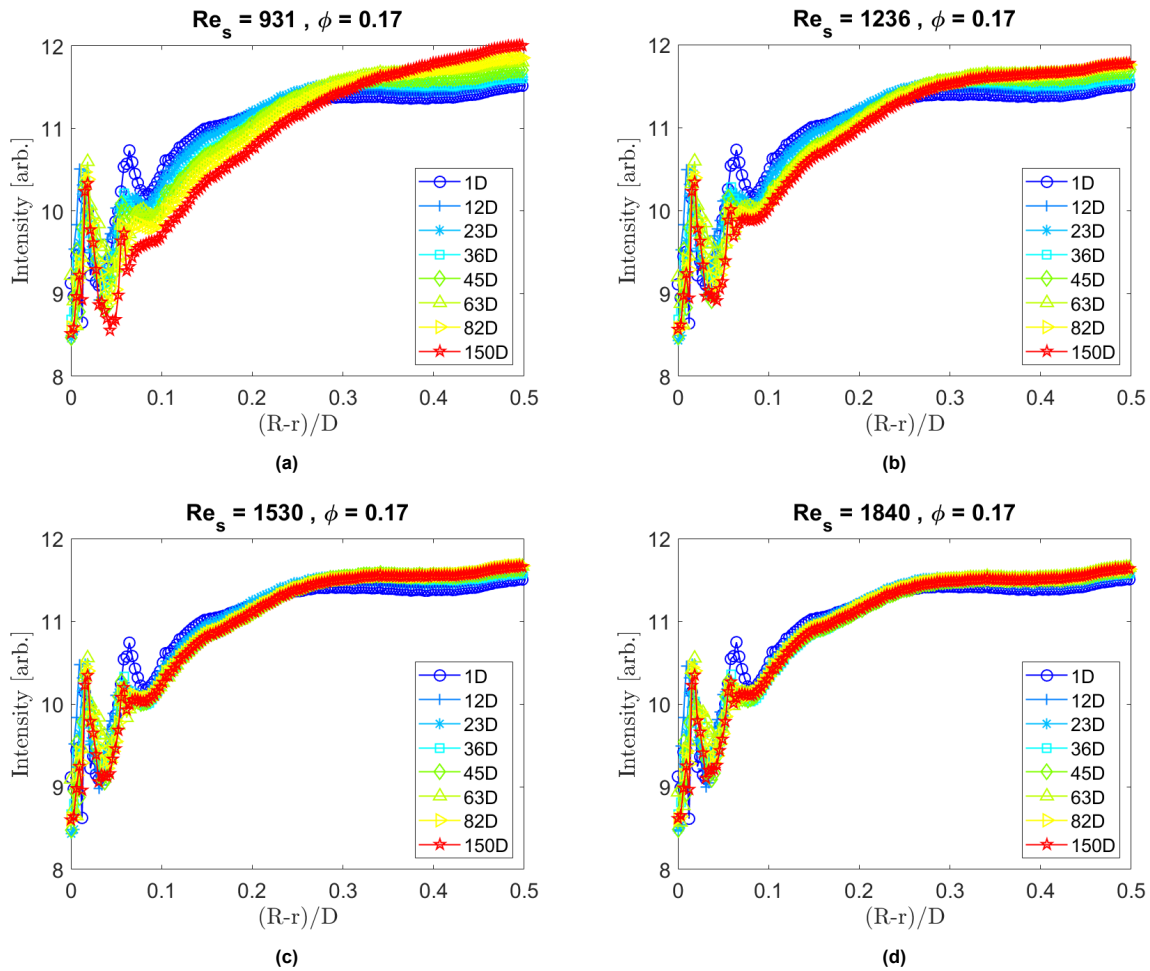

Figure 4.9: Intensity profiles for $\phi_b = 0.17$ (a) $Re_s = 931$ (b) $Re_s = 1236$ (c) $Re_s = 1530$ (d) $Re_s = 1840$.

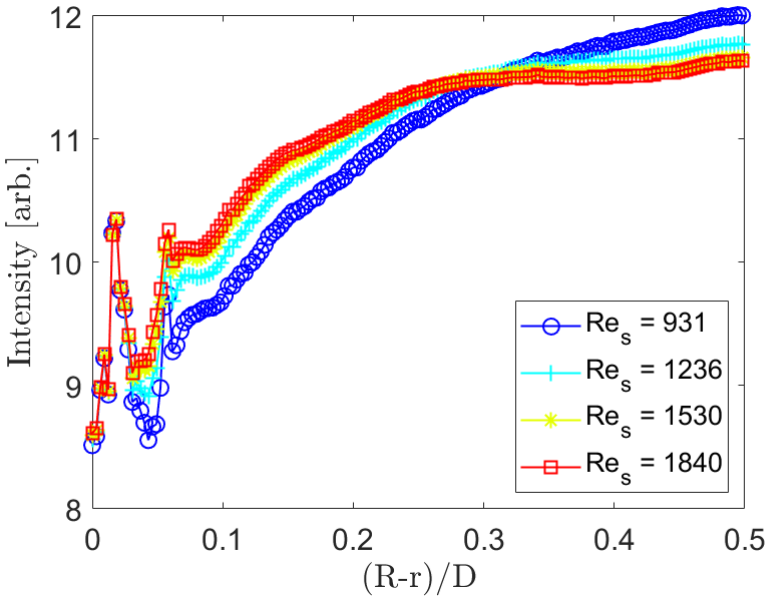

Figure 4.10: Intensity profiles for $\phi_b = 0.17$ for various Re_s at z = 150D. 'z' is the streamwise coordinate (see Figure 3.9)

Figure 4.9 illustrates the evolution of particle concentration through intensity plots along the tube length for $\phi_b = 0.17$ at various suspension Reynolds numbers. Across all Reynolds numbers, a consistent observation is found: as one moves along the tube length, intensity values near the pipe wall decrease while those in the center of pipe increase. This implies a decrease in particle concentration near the wall and an increase in particle concentration in the center of the pipe, suggesting particle migration and the presence of a particle core. This observation aligns with the findings of Hogendoorn [26], who predicted migration through MRI measurements for the same volume fraction.

Additionally, it is notable that for $Re_s = 931$ and $Re_s = 1236$, the profiles do not collapse, indicating a development length greater than 150D. Conversely, for $Re_s = 1530$ and $Re_s = 1840$, a collapse of intensity profiles is evident, suggesting a development length less than 150D. A collapse of intensity profiles indicate that the flow has developed. Moreover, an increase in suspension Reynolds number results in a quicker overlap, indicating a more rapid flow development.

To investigate the influence of inertia on shear-induced migration, intensity profiles at $z = 150D$ were plotted for $\phi_b = 0.17$ across the mentioned Reynolds numbers, as illustrated in Figure 4.10. The observation shows a decrease in intensities near the core with an increase in Re_s, indicating a reduced prominence of the particle core. Even though the the flow has not reached the fully developed state in case of $Re_s = 931$ and $Re_s = 1236$, this is a good comparison as the intensities would only increase at the core as the flow becomes fully developed. This phenomenon is likely attributed to mixing due to the increase in inertial forces, resulting in a more uniform distribution of concentration and diminishing the presence of the particle core. These findings are consistent with those reported by Hogendoorn [26].

To get an insight into how the migration affected the velocity profile and how the velocity profile developed for suspension pipe flows, velocity of dispersed phase was calculated using ultrasound imaging velocimetry. Since the densities of both phases are matched the Stokes number is $\mathcal{O}(10^{-3})$ suggesting that the particles should faithfully follow the flow. But due to the size of the polystyrene particles and particle-particle interactions being important at the volume fractions considered in the experimental campaign the particles need not faithfully follow the flow. The dispersed phase velocity was compared with that of fluid phase velocity obtained from MRI experiments of Hogendoorn [26] and is shown in Figure 4.11.

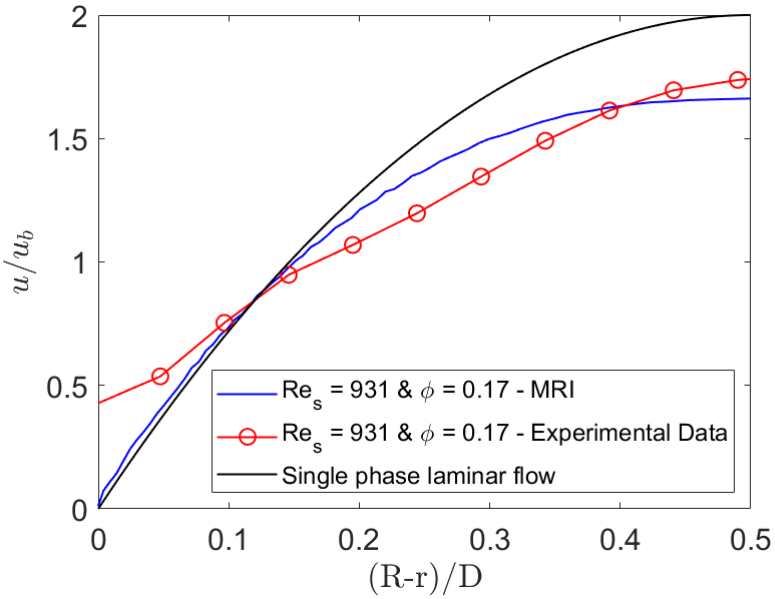

Figure 4.11: Illustration of velocity profiles of the dispersed phase obtained from experiments, fluid phase velocity data from MRI and velocity profile for laminar single phase pipe flow.

The observed deviation in velocity from the MRI data can be attributed to three factors. Firstly, the existence of a slip velocity near the wall implies a difference between particle velocity and fluid velocity. Secondly, the presence of particles settling on the top and bottom of the pipe (see Figure 4.12) due to difference in densities between both the phases contributes to this deviation. Measurements using the ultrasound probe are conducted from the sides to avoid capturing the settling effects. Settling reduces the effective area for the suspension to flow and consequently increasing particle velocity. This effect is more pronounced at lower Re_s values. Thirdly, reflections from the particles play a role, as seen in Figure 4.8, where particles detected near the wall exhibit vertical distortions. These reflections introduce discrepancies in radial resolutions, contributing to the inaccuracy in velocity values. The velocities obtained at the core of the pipe exhibit good agreement with the MRI data of Hogendoorn [26], with an error in centerline velocity of 4%. When compared to single-phase laminar pipe flow, a noticeable blunting in the velocity profile is observed. This is attributed to the presence of a particle core, which increases the viscosity at the center of the pipe, making it difficult for the suspension to flow smoothly. The slip velocity is defined as difference in velocities of the dispersed phase and the fluid phase. The obtained value for slip velocity at a distance of d/2 from the wall is calculated as

$$\frac{u_{\text{slip}}}{u_b} = 0.022. \tag{4.3}$$

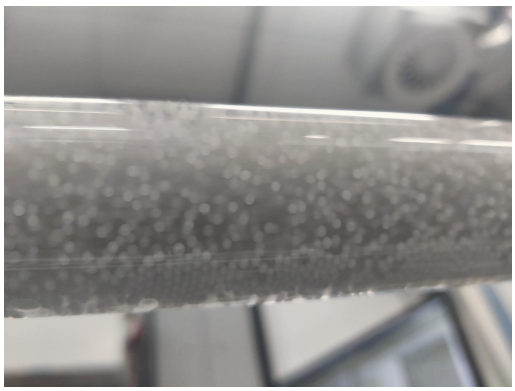

Figure 4.12: Buoyancy-induced settling of particles at both the top and bottom of the pipe, despite closely matched densities, highlighting the impact of polydispersity in particle densities. This was seen for all Re_s but prominently for lower values.

The velocity profiles of the dispersed phase at different downstream locations of the pipe for $Re_s = 931, 1236, 1530, 1840$ are shown in Figure 4.13. The collapse in velocity profiles indicates that the development length has been reached, and this is observed for all the Re_s.

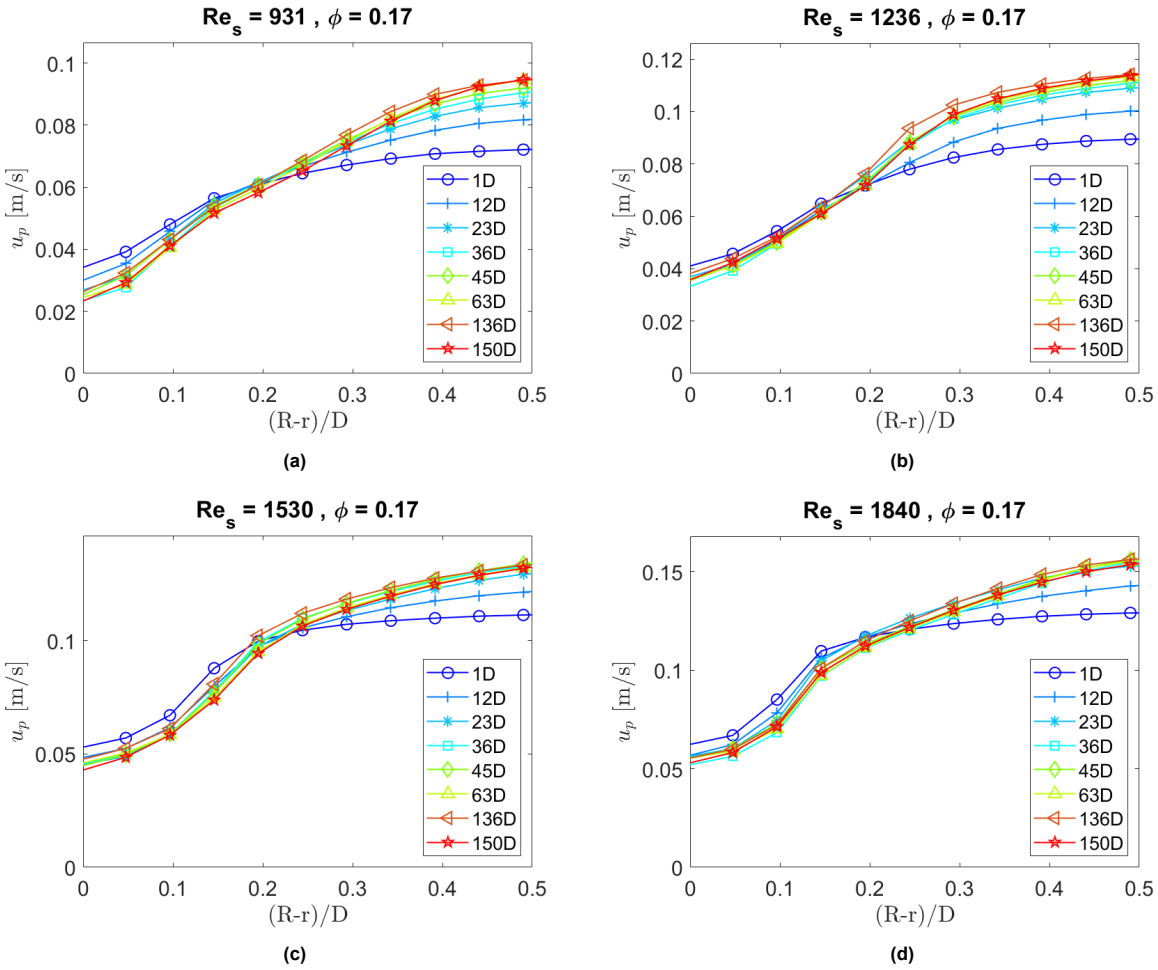

Figure 4.13: Velocity profiles of the dispersed phase for $\phi_b = 0.17$ (a) $Re_s = 931$ (b) $Re_s = 1236$ (c) $Re_s = 1530$ (d) $Re_s = 1840$.

Upon visual inspection of the velocity profiles of the dispersed phase, it appears that the volume flow rate increases as we progress downstream in the measurement pipe section. The volume flow rates were determined based on the dispersed phase velocities and are shown in Figure 4.14. It is notable that, with the exception of $Re_s = 1236$, there is no observable increasing trend in volume flow rates. This increase in volume flow rate as we progress to downstream locations of the pipe might be attributed to an effect in neutral buoyancy of the system during those measurements, causing particle settling at the top and bottom of the pipe. This settling could result in increased velocities at downstream locations due to reduced area for the suspension to flow, consequently leading to higher calculated volume flow rates.

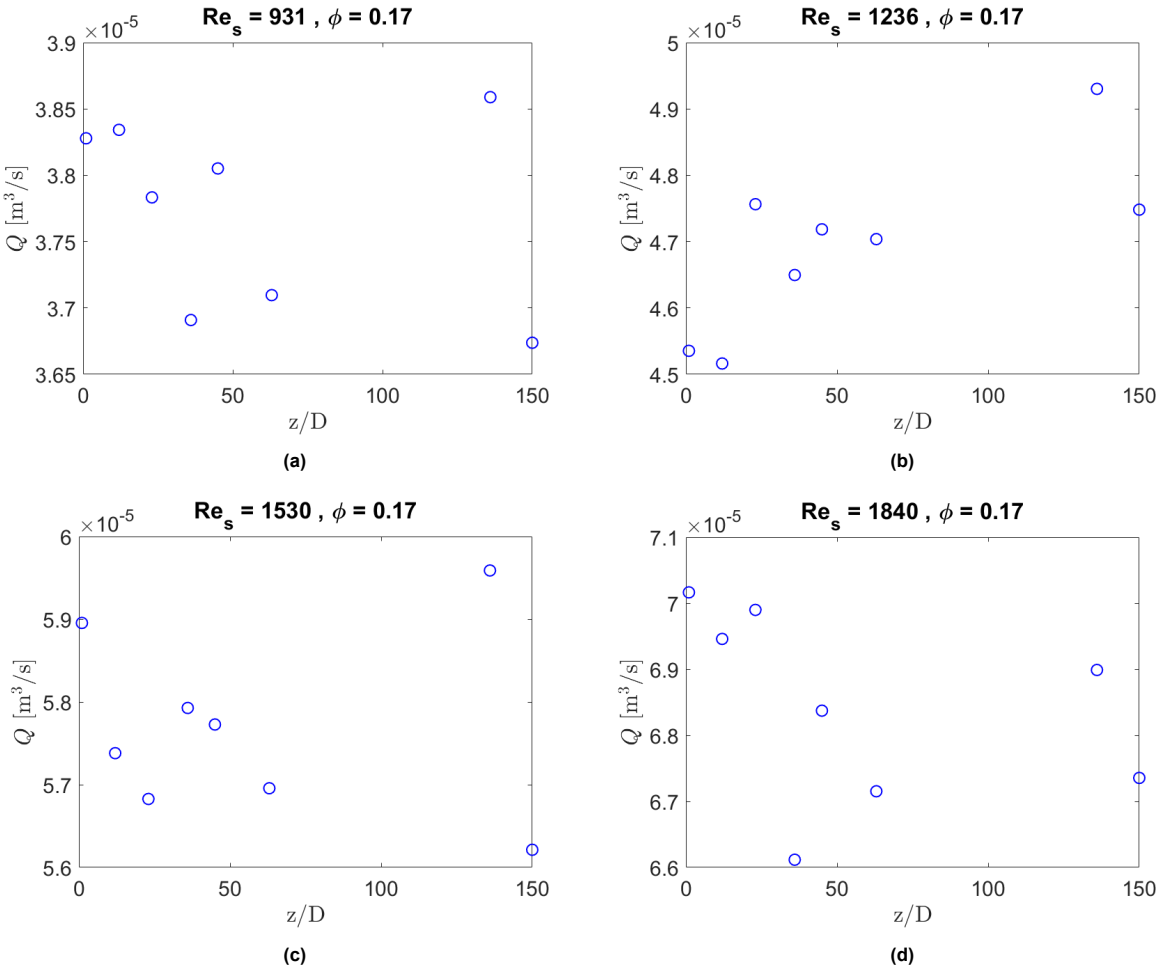

Figure 4.14: Volume flow rate calculated for $\phi_b = 0.17$ (a) $Re_s = 931$ (b) $Re_s = 1236$ (c) $Re_s = 1530$ (d) $Re_s = 1840$.

4.2.3. Particle volume fraction - 21%

Figure 4.15 illustrates intensity profiles for $\phi_b = 0.21$ at different suspension Reynolds numbers. Consistent with the findings for $\phi_b = 0.17$, a similar trend is observed across all Reynolds numbers. This involves a decrease in particle concentration near the wall and an increase in particle concentration in the center of the pipe, implying particle migration and the existence of a particle core. As Reynolds numbers increase, there is a quick collapse of the intensity profiles especially towards the end of the pipe, indicating rapid flow development. The peaks in intensity profiles closer to the wall are the reflections in the image acquired corrupting the intensity values closer to the wall.

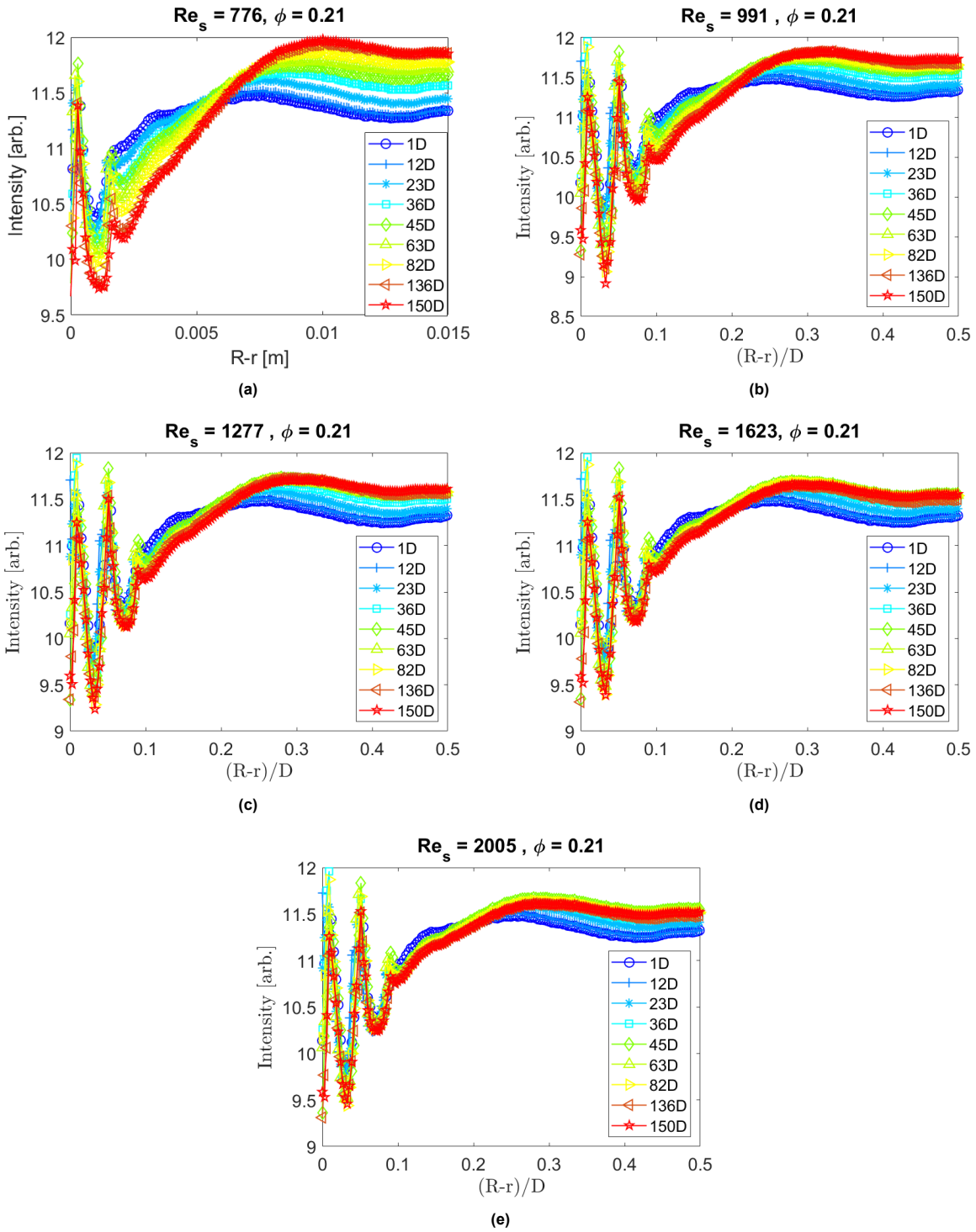

Figure 4.15: Intensity profiles for $\phi_b = 0.21$ (a) $Re_s = 776$ (b) $Re_s = 991$ (c) $Re_s = 1277$ (d) $Re_s = 1623$ (e) $Re_s = 2005$.

The velocity profiles of the dispersed phase and the corresponding volume flow rates, calculated at various downstream positions of the pipe for $Re_s = 776, 991, 1277, 1623, 2005$, are shown in Figure 4.16. The presence of a particle core results in a blunting effect on the velocity profiles. Notably, an increase in volume flow rates is observed at downstream locations for $Re_s = 776$ and $Re_s = 991$. In contrast, no trend is apparent for the other Re_s values. This discrepancy is attributed to particles settling at the top and bottom of the pipe in downstream regions, leading to a reduction in effective area. This phenomenon is more pronounced at lower Re_s, contributing to the observed increasing trend in volume flow rates as we move further downstream of the pipe.

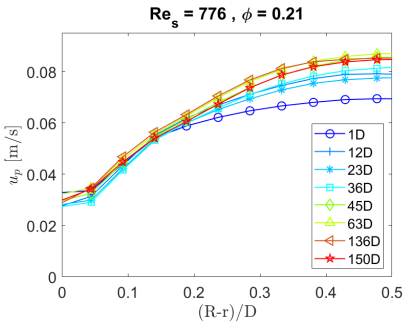

(a) Velocity profiles for $Re_s = 776$

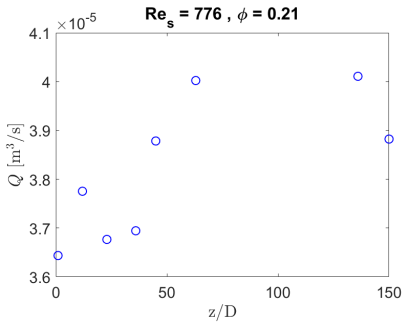

(b) Volume flow rates obtained at $Re_s = 776$

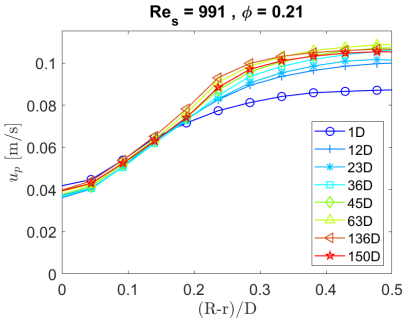

(c) Velocity profiles for $Re_s = 991$

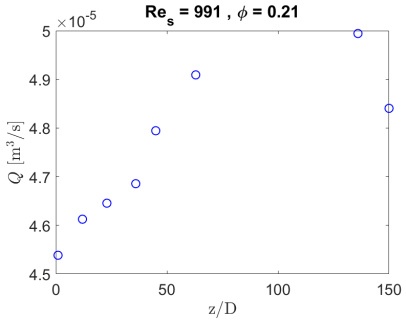

(d) Volume flow rates obtained at $Re_s = 991$

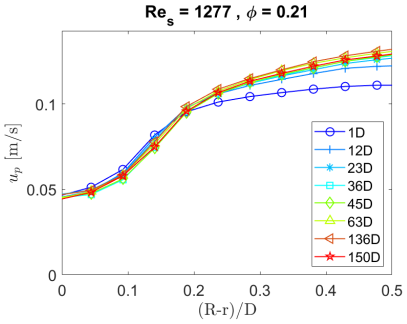

(e) Velocity profiles for $Re_s = 1277$

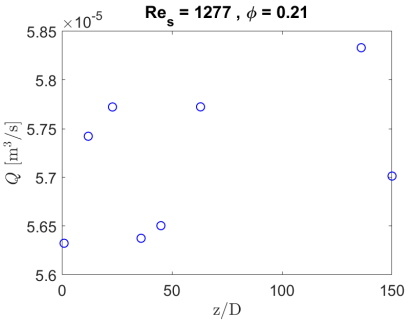

(f) Volume flow rates obtained at $Re_s = 1277$

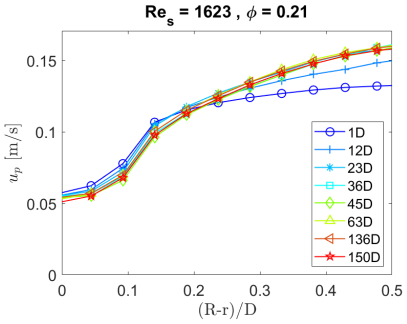

(g) Velocity profiles for $Re_s = 1623$

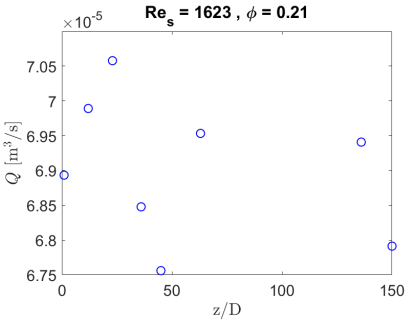

(h) Volume flow rates obtained at $Re_s = 1623$

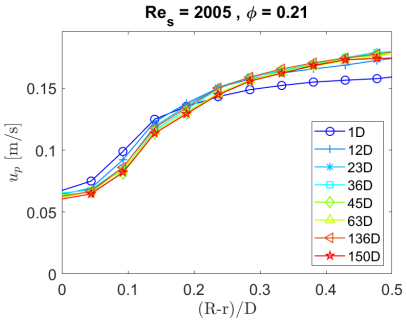

(i) Velocity profiles for $Re_s = 2005$

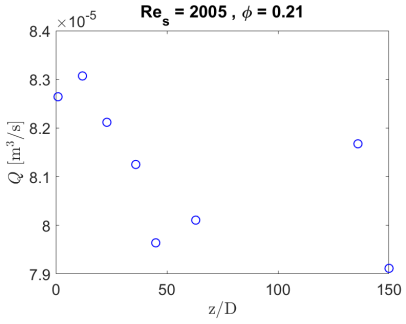

(j) Volume flow rates obtained at $Re_s = 2005$

Figure 4.16: Dispersed phase velocity profiles and volume flow rates for $\phi_b = 0.21$.

4.2.4. Particle volume fraction - 25%

Figure 4.17 illustrates intensity profiles for $\phi_b = 0.25$ at different suspension Reynolds numbers. Similar to the trend observed for $\phi_b = 0.17$ and $\phi_b = 0.21$, the same pattern is evident. With increasing Reynolds numbers, there is a more rapid collapse of the intensity profiles, indicating a quicker development of the flow. It can be observed that the there is huge jump from 1D for Re_s greater than 1070 and then a sudden collapse of intensity profiles, indicating that the flow develops very quickly from the inlet conditions and a quick collapse of profiles indicating a rapid development.

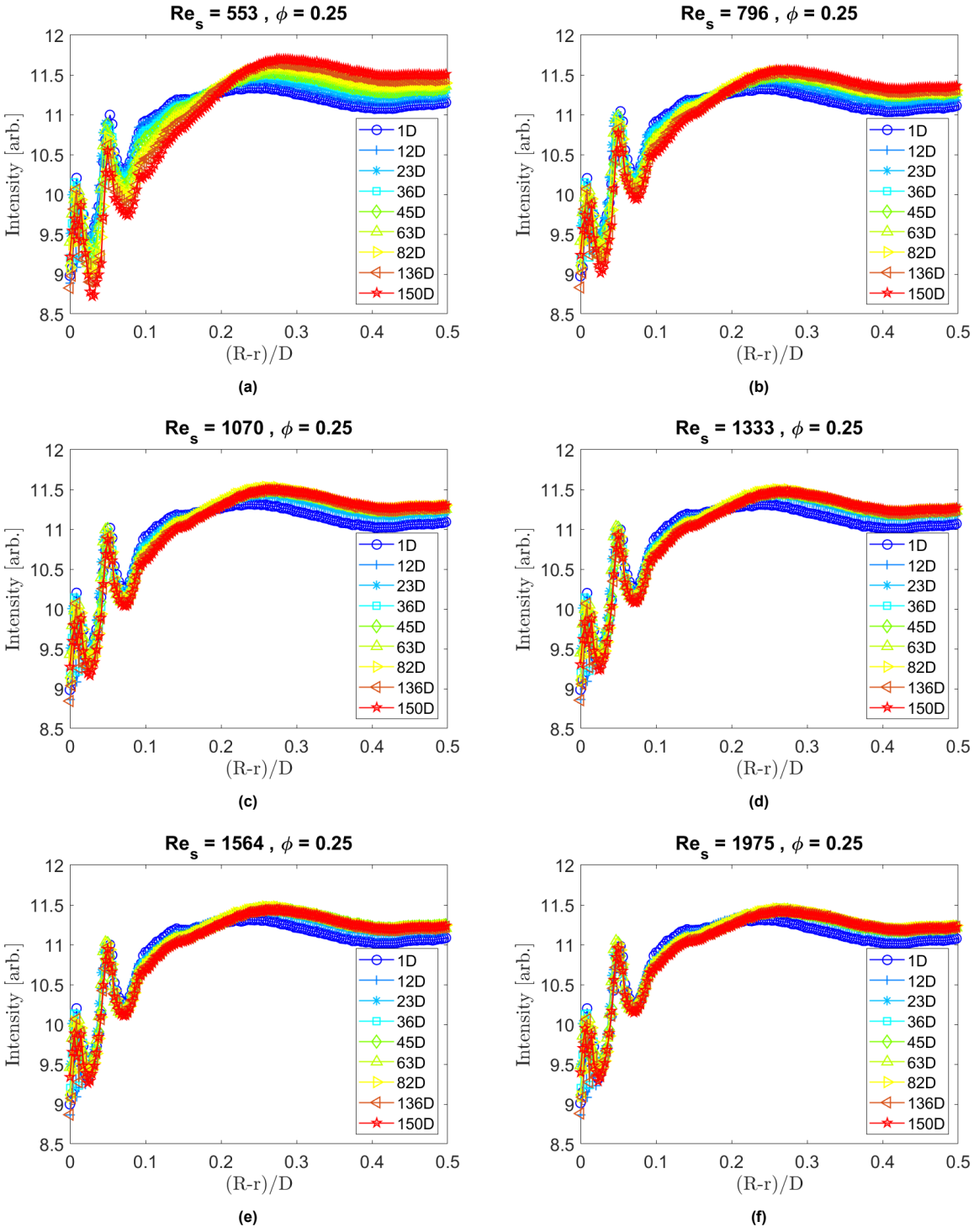

Figure 4.17: Intensity profiles for $\phi_b = 0.25$ (a) $Re_s = 553$ (b) $Re_s = 796$ (c) $Re_s = 1070$ (d) $Re_s = 1333$ (e) $Re_s = 1564$ (f) $Re_s = 1975$.

In the case of $Re_s = 1975$, an anomaly in the raw data was observed. The intensity profile at $z = 23D$ at the core was observed to smaller than that of the $z = 12D$. To correct for this a factor of 1.004 was multiplied to the intensity profile of $z = 23D$ so that it was inline with the fitted curve for calculating the entrance length as explained section 4.2.5. The intensity profiles and the evolution parameter (explained in section 4.2.5) is shown in Figure 4.18.

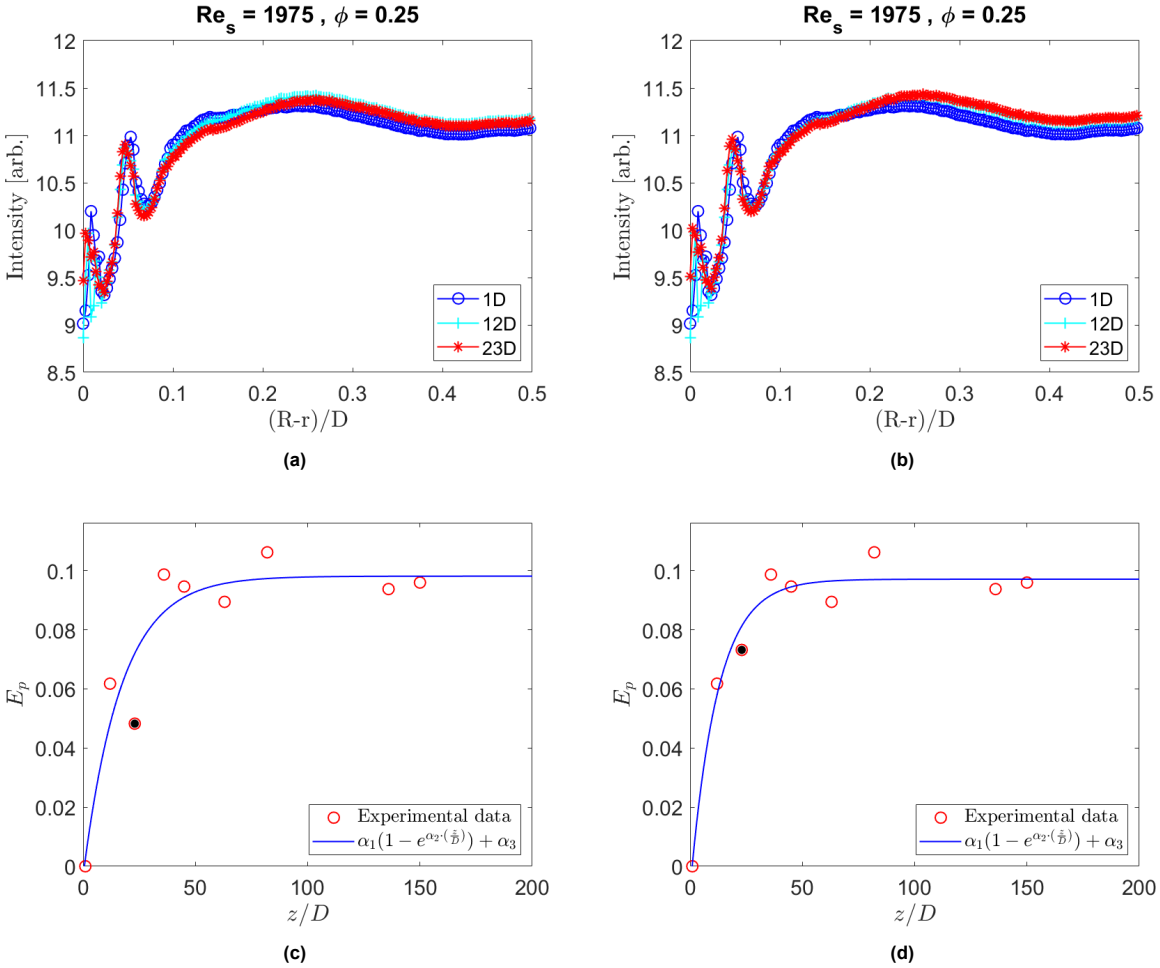

Figure 4.18: (a) Intensity profile obtained from the raw data (b) Corrected intensity profile (c) Evolution parameter for the profile obtained from the raw data. The black marker is the corresponding value of Ep obtained (d) Ep after correcting the intensity profile.

The velocity profiles of the dispersed phase at different downstream locations of the pipe for $Re_s = 553, 796, 1070, 1333, 1564$ are shown in Figure 4.16. A blunting in velocity profiles are observed which is due to the presence of a particle core and is more prominent due to higher bulk volume fraction.

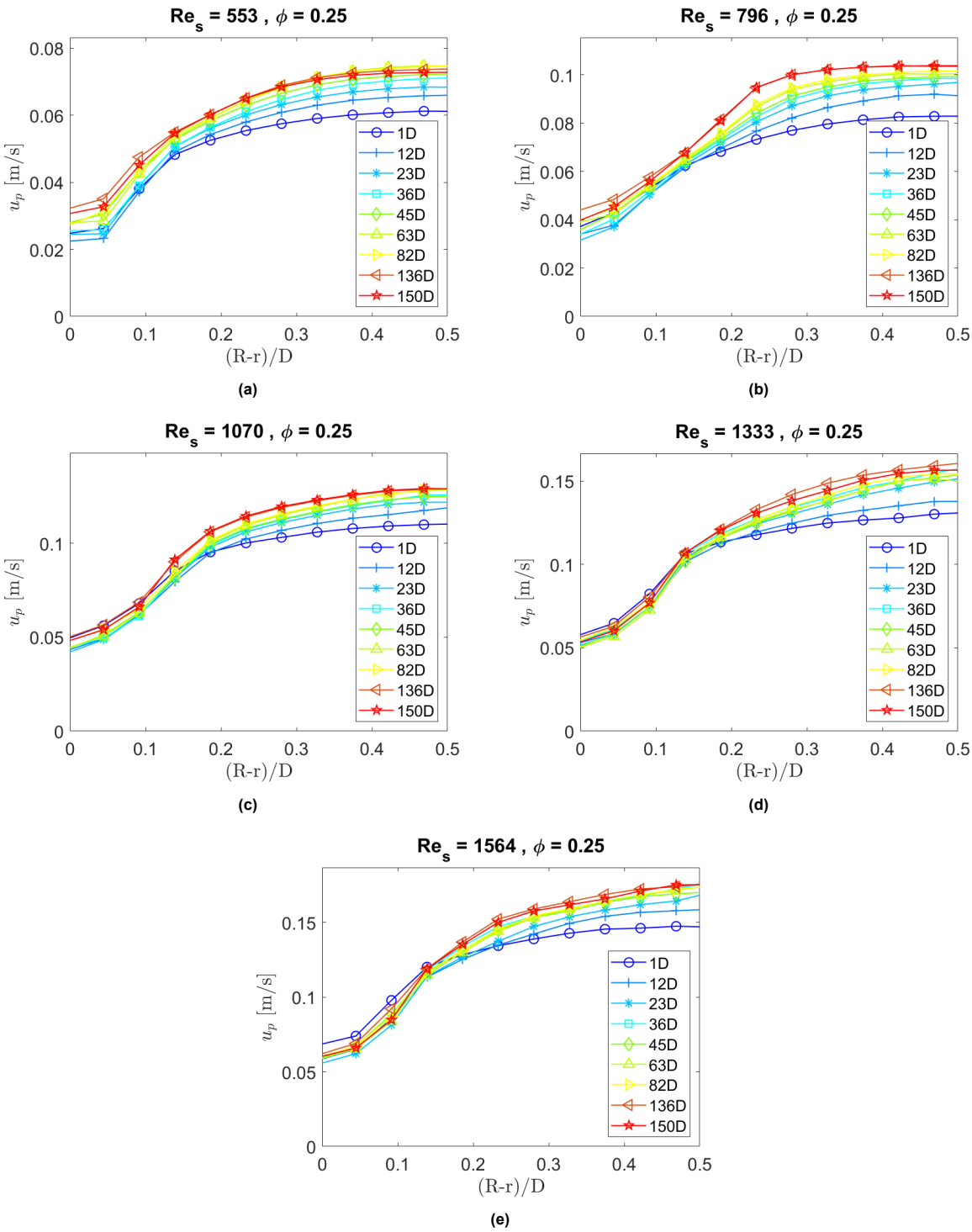

Figure 4.19: Velocity profiles for $\phi_b = 0.25$ (a) $Re_s = 553$ (b) $Re_s = 796$ (c) $Re_s = 1070$ (d) $Re_s = 1333$ (e) $Re_s = 1564$.

To study the effect of volume fraction on velocity profiles, the velocity of the dispersed phase at $Re_s \approx 1000$ was plotted for all the three volume fractions and is illustrated in the Figure 4.20 and are consistent with the results of Hogendoorn [26].

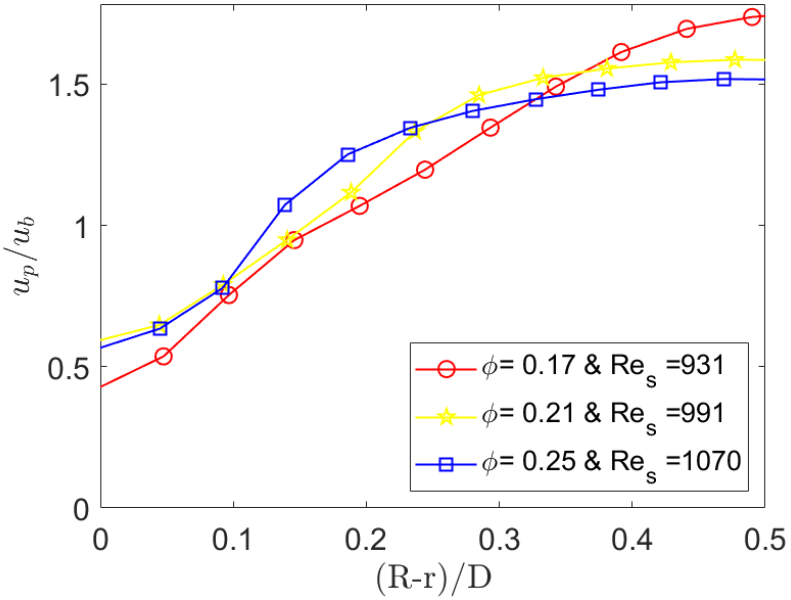

Figure 4.20: Effect of volume fractions on velocity profiles.

It is observed that the blunting of the velocity profile increases with an increase in volume fraction. This is expected, as the concentration at the core increases with the increase in bulk volume fraction (up to the jamming volume fraction), consequently increasing the viscosity at the core and leading to more prominent blunting of the velocity profile. The blunting of velocity profiles with increase in volume fractions has been reported by Hampton et al. [24], Karnis et al. [29] and Han et al. [25] in the Stokes regime suggesting that this is a volume fraction effect rather than an inertial effect.

Another important point to note is that in Figure 4.13, Figure 4.16, and Figure 4.19, it was observed that the volume flow rate is not conserved downstream of the pipe, especially for low suspension Reynolds numbers. This is attributed to buoyancy-induced settling of particles at both the top and bottom of the pipe, particularly in the downstream locations, despite closely matched densities of both phases as shown in Figure 4.12. A simple model was examined, as illustrated in Figure 4.21, with 5 particles at the top and bottom (based on Figure 4.12) to assess how the bulk velocity increased. The area available for the suspension to flow reduced by 7%, causing the bulk velocity to increase by 3.5%. It was observed that the centerline velocity was overpredicted by 4% when compared with the MRI data of Hogendoorn [26] for $\phi_b = 0.17$ and $Re_s = 931$ suggesting that this could be a possible reason. For smaller Re_s, it is possible that the particle layer could have more particles, further reducing the area and potentially increasing the bulk velocity even more.

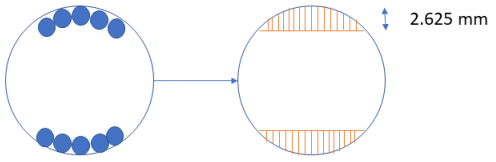

Figure 4.21: Effect of particle accumulation on top and bottom of the pipe. The black region is the area which is account for the particles in the top an bottom.

4.2.5. Entrance length

To study development length for concentration, we study two regions: one in the core of the pipe, extending from 0.01 m to 0.015 m (Region B), and another near the wall, which spans from 0.0035 m to 0.005 m (Region A), as illustrated in Figure 4.22. The region very close to the wall (R-r < 0.0035 m) is not considered as the intensity profiles in this area are corrupted due to the reflections from the wall.

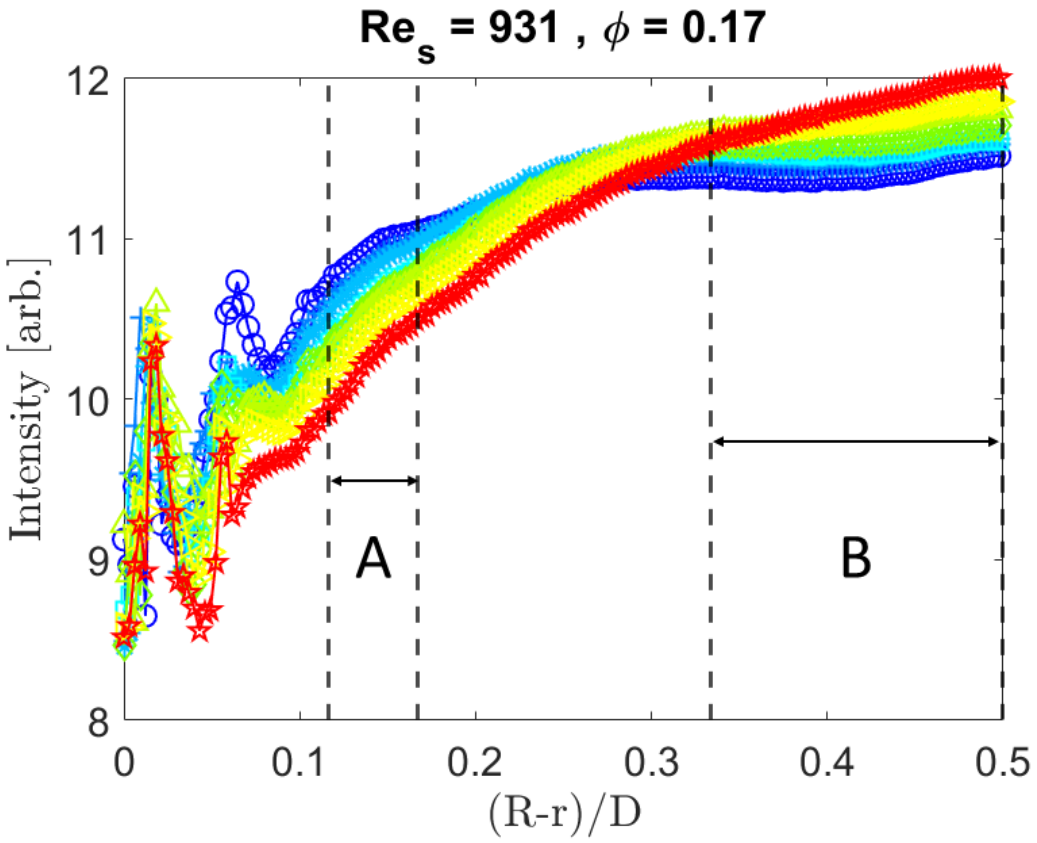

Figure 4.22: Illustrating the regions under consideration to study entrance lengths. Region B being the core of the pipe and A being the near wall region

Determination of the dependence of entrance length on Re_s and ϕ_b first requires that a definition of entrance length be given. This is done by defining a scalar parameter similar to that of Hampton et al.[24]. The evolution parameter E_p is defined as

$$E_p = \frac{1}{A}\int \left|\Phi - \Phi_{\text{ref}}\right| dA, \tag{4.4}$$

where Φ is the intensity profile at any give location and Φ_{ref} is the intensity profile at the inlet which corresponds to the intensity profile at 1D. E_p reaches an asymptotic value as the flow develops and the obtained profile is fitted with a curve of the form

$$E_p = \alpha_1 \left(1 - e^{\alpha_2 \cdot (z/D)}\right) + \alpha_3, \tag{4.5}$$

where z/D is the non dimensional length from the end of the entrance chamber. The most important parameter in the fit is α_2 as it governs how fast the curve approaches the asymptotic state. The entrance length for concentration (L_ϕ) is defined as the point where E_p reaches 99% of its asymptotic value. An illustration is shown in Figure 4.23,

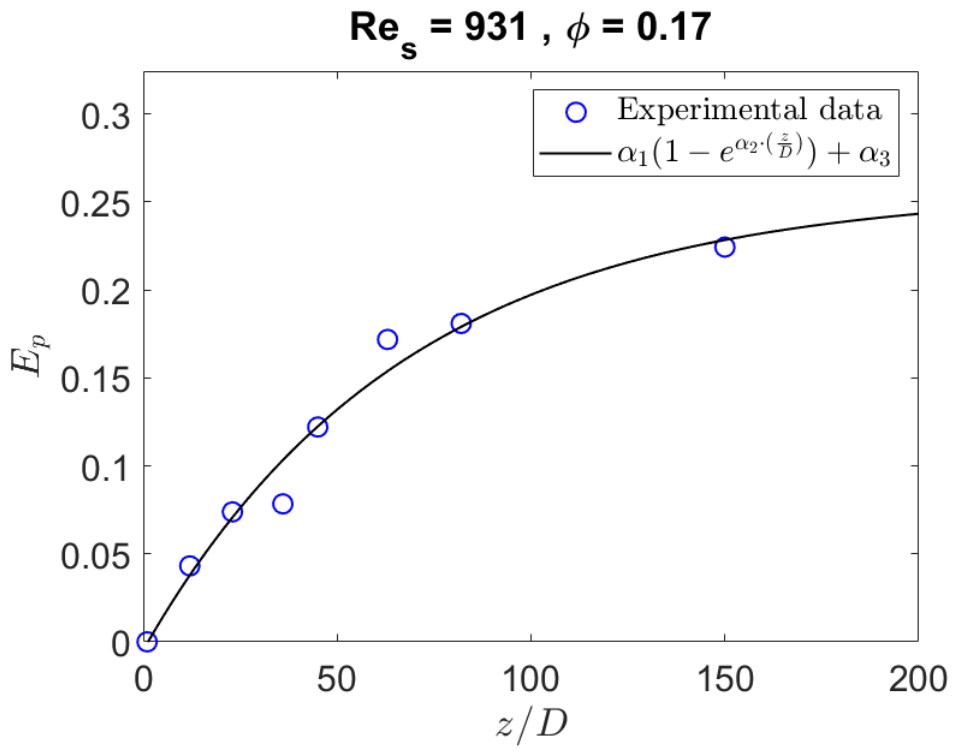

Figure 4.23: Illustration of fitting the values of E_p.

The development length for velocity is defined as the length at which the centerline velocity reaches 99% of its fully developed value, which is same as the entrance length in single-phase flow. To determine the entrance length for suspension pipe flows, the non-dimensional centerline velocity of the dispersed phase is fitted with a curve given by equation 4.3, as illustrated in Figure 4.24.

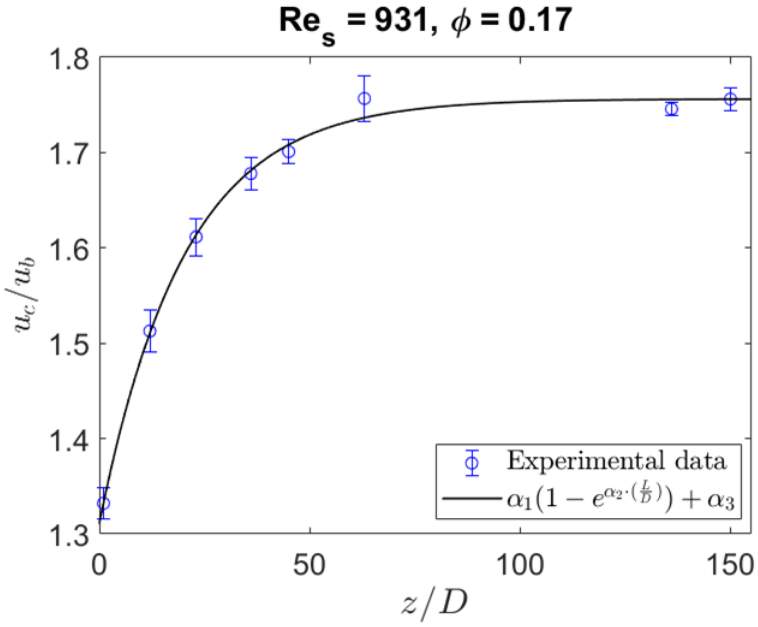

Figure 4.24: Illustration of fitting the values of non-dimensionless center-line velocity of the dispersed phase.

The obtained development lengths for both concentration and velocity are summarised in the table 4.2.

S.No	ϕ_b	Re_s	u_b (m/s)	L_ϕ/D (Region - B)	L_ϕ/D (Region - A)	L_v/D
1	0.17	931	0.0545	313	422	67
2		1236	0.0718	183	209	54
3		1530	0.089	105	118	43
4		1840	0.1072	86	93	38
1	0.21	776	0.0518	281	701	58
2		991	0.0664	211	398	40
3		1277	0.0854	156	203	38
4		1623	0.1082	86	150	31
4		2005	0.1332	77	89	27
1	0.25	553	0.044	317	1562	68
2		796	0.0633	147	513	65
3		1070	0.0851	90	211	59
4		1333	0.1059	70	158	49
5		1564	0.1240	64	156	45
6		1975	0.1564	58	145	-

Table 4.2: The obtained entrance lengths for both concentration and velocity.

From the results summarized in Table 4.2, it is seen that for all volume fractions and Re_s, the entrance length for the near-wall region is greater than that of the entrance length at the center of the pipe. This suggests that the core of the pipe forms first, and then the core builds up in size. Additionally, for the same, it is observed that the difference in entrance length between the two regions decreases with an increase in Reynolds numbers. This difference can be explained using the diffusive flux model proposed by Phillips et al. [44]. The model suggests that the diffusive flux results from the gradient in concentration and particle-particle interaction. As the flow progresses, the core of the pipe is formed, and the concentration near the wall decreases reducing the particle-particle interactions. The concentration gradient becomes minimal near the wall as the flow progresses, making the migration process slower near the wall resulting in a longer entrance length for the near wall region. The decrease in difference between the entrance lengths between the two regions is due to the inertial effect as the prominence of the particle core decreases resulting in a more uniform concentration profile thereby having almost equivalent entrance length for both.

A point to be noted is that, the elevational focal depth of the ultrasound probe is 18mm. This lack of focus could result in a slightly more scattered signal compared to the core of the pipe and could have an effect on the obtained entrance lengths in the near wall region. Additionally, only a small part of the near wall region could be considered as the reflections from the pipe wall corrupt the intensities of the near wall region. As a result, the comparison and further analysis will be done with the concentration entrance length obtained at the core of the pipe.

When comparing the entrance lengths of velocities across different volume fractions, a noteworthy trend emerges: the L_v/D initially decreases from $\phi_b = 0.17$ to $\phi_b = 0.21$ and then increases for $\phi_b = 0.25$ (see Figure 4.25). This anomaly could be attributed to the fact that, for $\phi_b = 0.17$ and $\phi_b = 0.21$, the center of the pipe never reaches the jamming volume fraction ($\phi_m = 0.64$), whereas for $\phi_b = 0.25$, the concentration at the center of the pipe approaches very close to the jamming volume fraction [26]. This could have an impact on the longer entrance length, as the effective Re_s at the core is significantly reduced, leading to a slower development of the profile. Additionally, there is effect of

settling at low Re_s which accelerates the flow at downstream locations which could give longer entrance lengths at low Re_s. Additionally, it should be noted that the trend is opposite compared to that of single phase pipe flows, where the the entrance length for velocity increases with increase in Reynolds number. To thoroughly understand if there is a regime change where concentrations reach the jamming volume fraction at the center, more data at higher concentrations and lower Re_s is required to comment more on the velocity entrance length.

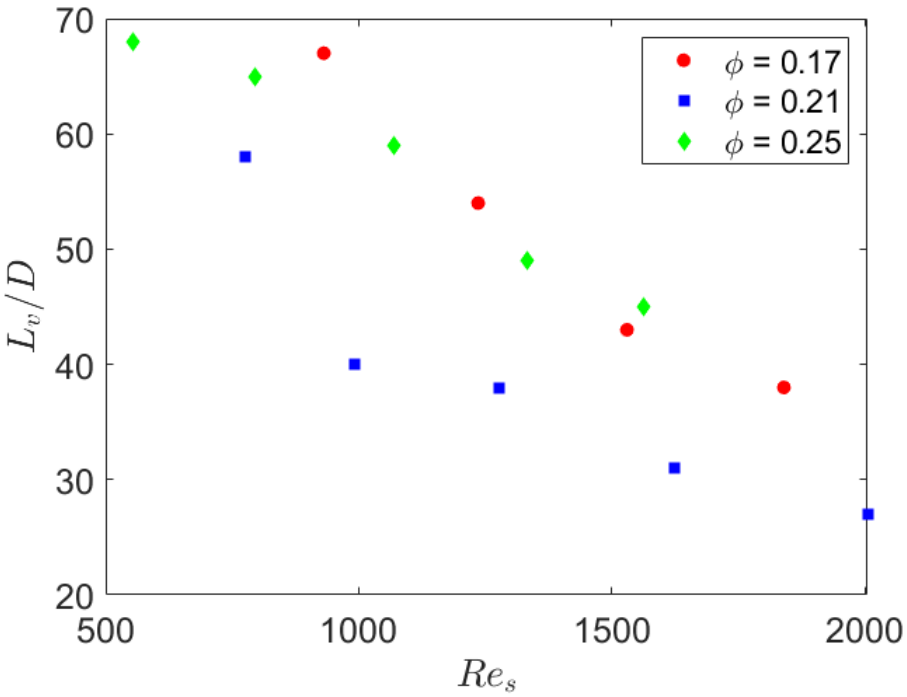

Figure 4.25: Illustration of velocity entrance length as a function Re_s. for different volume fractions.

Upon comparing the entrance lengths obtained for velocity and concentration, it is evident that the entrance length for concentration is greater than the entrance length for velocity for all volume fractions and Re_s considered in the study. This suggests that changes in velocity profile become smaller as the flow develops, whereas the effect on development of concentration profile is relatively larger. A similar observation was noted in the Stokes regime by Hampton et al. [24], N. Phan-Thien and Z. Fang [43], and Lecampion and Garagash [33]. However, Hampton et al. [24] and N. Phan-Thien and Z. Fang [43] observed that $L_\phi \approx 2.5L_v$, whereas Lecampion and Garagash [33] obtained $L_\phi \approx 1.136L_v$. No such trends were observed in the results obtained, and this difference could be due to the effect of inertia, as their studies were in the Stokes regime.

To study the effect of Re_s on the concentration entrance length, the concentration entrance length was plotted for all volume fractions and is illustrated in the Figure 4.26. It is observed that the concentration entrance length decreases with an increase in Re_s for all volume fractions. This phenomenon can be attributed to inertial effects, which cause increased interaction of particles at higher suspension Reynolds numbers, thereby initiating a rapid development of the concentration profile. As Re_s approaches 2000, it can be noted that the entrance lengths of concentration for all volume fractions are nearly the same. This suggests that at higher Re_s, the influence of inertial effects governs the entrance length more significantly compared to volume fraction effects. At smaller Re_s, when comparing entrance lengths for different volume fractions, it is apparent that the concentration profile develops more quickly with an increase in volume fraction, and this gap decreases with an increase in Re_s. A similar result was observed by Hampton et al. [24] for Re_s in the $\mathcal{O}(10)$, suggesting that the same trend is applicable for higher Re_s. It can be expected that at very high Re_s, the entrance lengths for all volume fractions will be more or less the same.

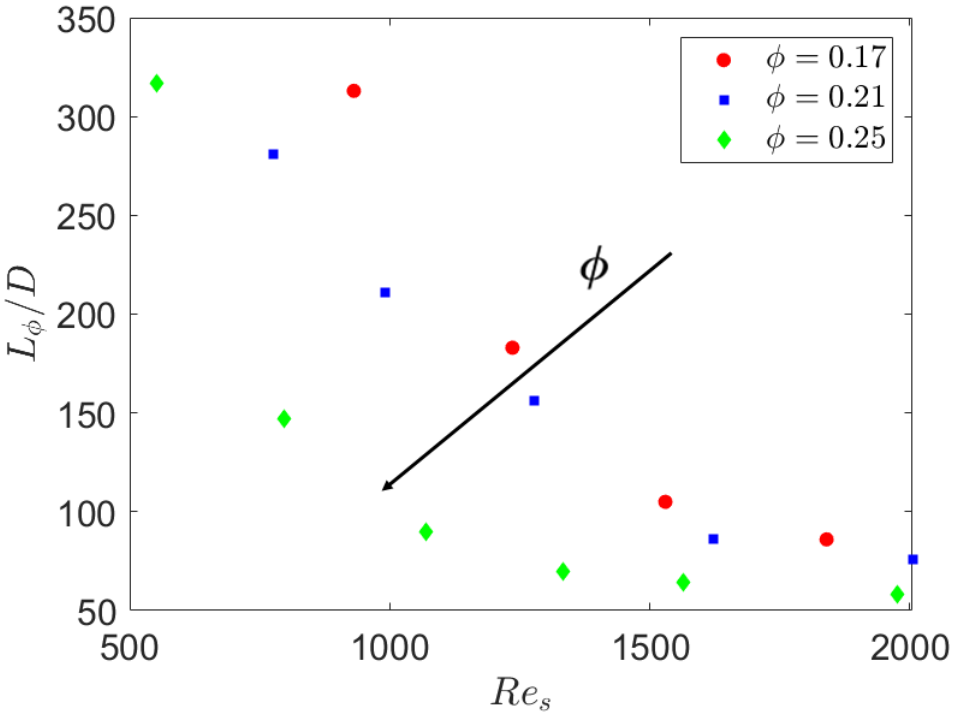

Figure 4.26: Illustration of concentration entrance length as a function Re_s. for different volume fractions.

To obtain how Re_s and ϕ_b scales with entrance lengths, the concentration entrance lengths obtained was fitted with a power law curve (see Figure 4.27), and the obtained result is given by

$$\frac{L_\phi}{D} = A \cdot Re_s^{-1.62} \phi_b^{-2.1}. \tag{4.6}$$

The obtained values indicate that Re_s scales with an exponent of -1.62 and ϕ_b scales with an exponent of -2.1. Here, the entrance length decreases with an increase in Re_s, suggesting a negative scaling. This observation is similar with an increase in bulk volume fraction as well. The scaling exponent obtained for volume fraction is closer to the one obtained by Nott and Brady [42]. The value of -2 (Leighton and Acrivos [34]) was used as the scaling exponent in the Stokes regime for $\phi_b < 0.3$. Leighton and Acrivos [34] explained that the migration of particles is due to the hydrodynamic interaction between the particles in the suspension. To have a net displacement, the presence of three or more particle interactions is needed and this interaction will no longer be symmetric and the particles will experience a net displacement. Since the scaling laws obtained are the same, it suggests that the particle-particle interactions affect the process of migration in a similar manner in the stokes regime as well as the inertial regime.

Despite starting with a uniform distribution of particles, the fully developed state shows gradients in concentration, with the highest particle concentration at the core of the pipe. Due to the concentration gradients in the flow, there is a corresponding viscosity gradient, with the maximum viscosity at the core due to the highest particle volume fraction at the center. The Eilers viscosity correction, however, does not account for the local viscosity distribution. Since Re_s is defined as the ratio of inertial to viscous forces, and a local viscosity distribution is necessary for accurately modeling the Reynolds number for suspensions, this discrepancy may be the reason why the scaling of Re_s deviates from 1 in the observed experimental results. Additionally, an increase in suspension Reynolds number implies that the inertial forces increase which could increase the interaction frequency between the particles thereby aiding quicker migration. The rate at which the interaction frequency is unknown and this could also be

a possible reason for the scaling exponent being different than 1. It is important to recognize that D/d influences both the entrance lengths of velocity and concentration (Hampton et al [24]). Therefore, it is necessary to analyze different D/d values to validate the scaling laws obtained. Additionally, more data is required at lower Re_s and smaller volume fractions to validate these scaling laws as there is quite a big interpolation at smaller Re_s and ϕ_b.

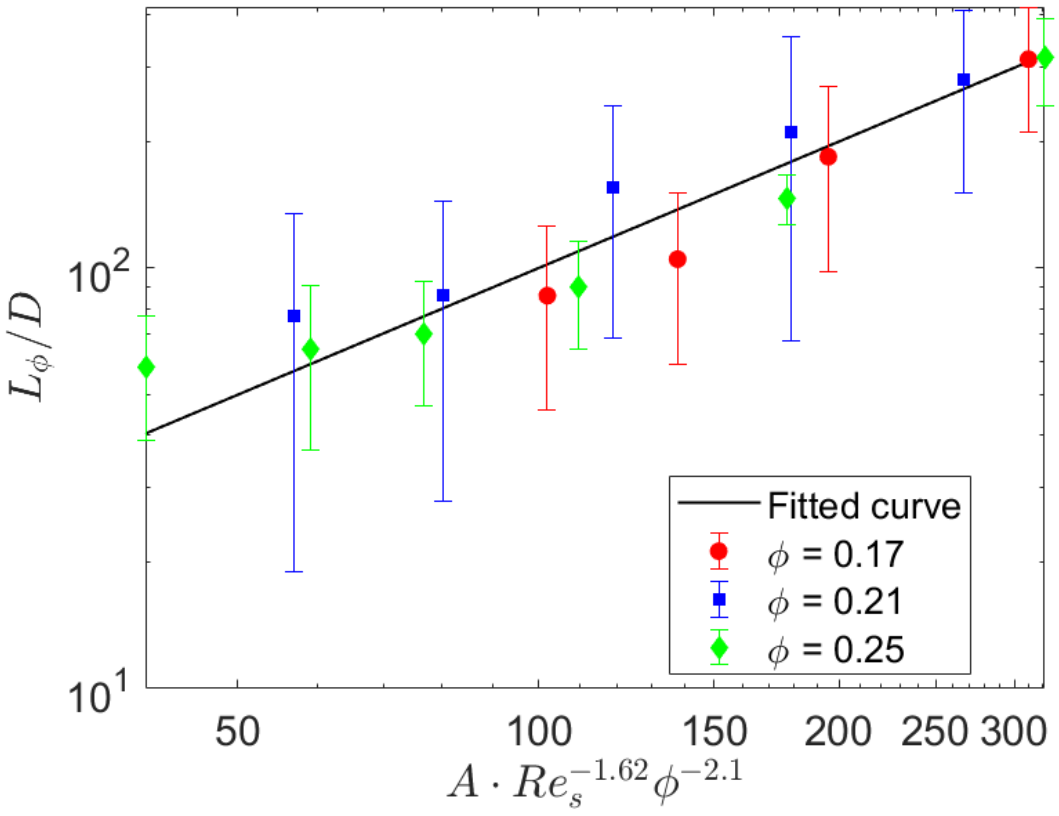

Figure 4.27: Illustration of concentration entrance length with the fitted power law curve.

The uncertainty analysis is described in detail in Appendix D.

5

Conclusion and Recommendations

The current chapter provides conclusions for the key results obtained from the experiments and concludes with recommendations for future research by addressing the challenges faced.

5.1. Conclusion

The present experimental study investigates the axial development of neutrally buoyant suspension pipe flows, studying the influence of suspension Reynolds number and volume fraction on the entrance length. Ultrasound measurements were conducted to circumvent the opacity of the suspension flows. The dispersed phase consisted of polystyrene particles with a mean diameter of 1.75 mm (D/d = 17), while water was used as the continuous phase. Densities of both the phases were matched by adding Na_2SO_4 to ensure a neutrally buoyant suspension. Velocity and concentration measurements (intensity plots) were conducted in this study to analyze the entrance lengths.

The experimental setup was validated using pressure drop measurements by plotting the Moody diagram for single phase pipe flow. Velocity measurements for single-phase pipe flow were conducted at various locations downstream of the pipe for $Re = 550, 787$, and 990 to study the entrance length. An exponential model was fitted to the centerline velocities to obtain the entrance length. The obtained entrance length was smaller compared to the analytical result, due to the inlet condition being more developed than a uniform inlet condition.

The inlet conditions for studying the entrance length of suspension flows were characterized by particle counting at 1% volume fractions, revealing a uniform distribution of particles at the inlet. Experiments for suspension flows were conducted for $\phi_b = 0.17, 0.21$, and 0.25. Although correlating concentration and intensities is not trivial, the development of suspension pipe flow was characterized by observing changes in the intensity profiles at various downstream locations. The effect of particle migration was evident in the intensity profiles, where intensity values decreased in the near-wall region and increased in the core of the pipe as the flow progressed. The velocity of the dispersed phase was also measured at locations downstream of the pipe using Ultrasound image velocimetry. Observations indicated that the velocity profile became blunted with an increase in volume fraction, consistent with findings from Hampton et al. [24], Karnis et al. [29] and Hogendoorn [26]. The effect of inertia on particle migration was studied, and the trend in intensity profiles suggested a decrease in the prominence of the particle core with an increase in Re_s. This aligns with the observations of Hogendoorn [26], suggesting that intensity profiles can serve as a valuable metric for examining how concentration profiles develop over the length of the pipe.

The concentration entrance length was derived from intensity profiles by defining a scalar, similar to the approach by Hampton et al [24]. Two distinct regions, the near-wall region and the core of the pipe, were analyzed, revealing that the entrance length obtained in the near-wall region was greater than the entrance length obtained for the core of the pipe. Concentration entrance lengths decrease with an increase in suspension Reynolds number, reaching a nearly same value for $Re = 2000$ for all the

volume fractions studied. The same trend was followed for an increase in bulk volume fraction which was similar to the trend observed by Hampton et al. [24] in the Stokes regime. For velocity entrance lengths, an increase in suspension Reynolds numbers led to a decrease, while no trend was observed with an increase in bulk volume fraction. A comparison between the entrance lengths for concentration and velocity indicated that the velocity entrance length was smaller than the concentration entrance length for all volume fractions and suspension Reynolds numbers in the study. A scaling analysis for the concentration entrance length revealed that suspension Reynolds number scales with an exponent of -1.62 and bulk volume fraction scaled an exponent of -2.1. It is crucial to revisit these claims with different particle sizes, as they also play a pivotal role in determining entrance lengths.

5.1.1. Recommendations for future studies

This section addresses some of the challenges faced and proposes improvements for the continuation of the study in this area. Additionally, it provides new aspects to explore for the research topic. One major challenge encountered was the polydispersity in the density of the particles used. Despite matching densities of particles, settling of particles occurred at lower volume fractions and lower suspension Reynolds numbers. An illustration of the intensity profiles for $\phi_b = 0.1$ and $Re_s = 1029$ at three locations is shown in Figure 5.1. It can be seen that the intensity values are smaller at all radial positions at z = 150D compared to z = 63D and z = 1D, suggesting fewer particles in the center of the pipe, implying the settling of particles at the top and bottom of the pipe. A similar problem was encountered for $\phi_b = 0.15$. Particles which are monodisperse in density can be used in the study so that lower suspension Reynolds number and lower volume fractions can be studied.

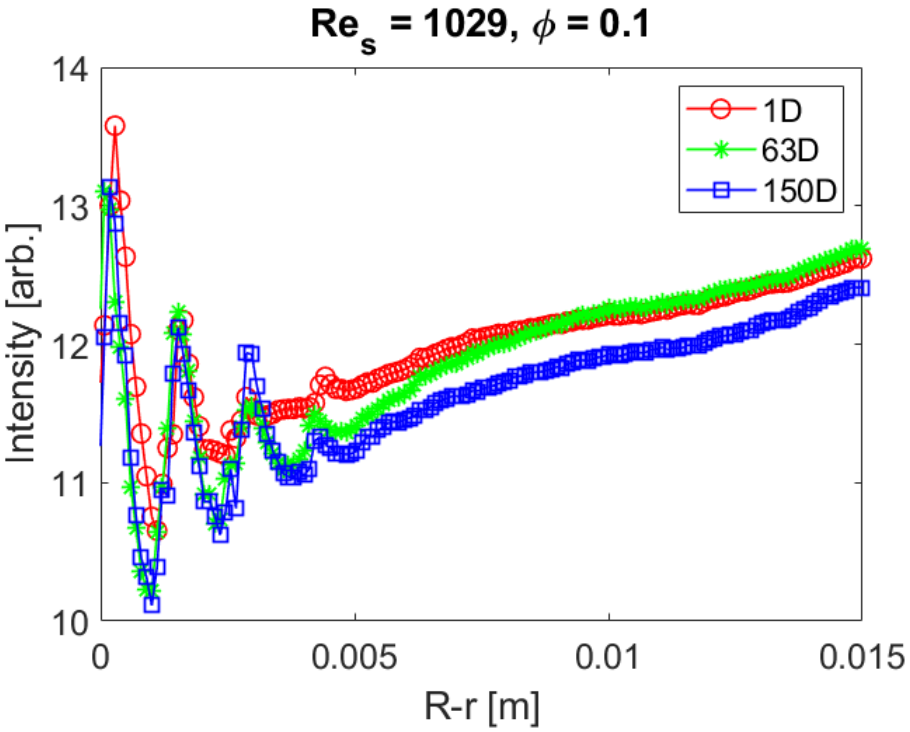

Figure 5.1: Intensity profiles at different locations $Re_s = 1029$ and $\phi_b = 0.1$.

Another challenge encountered was the issue with maintaining neutral buoyancy while conducting experiments over time which is illustrated in Figure 5.2. The particles rise onto the top wall of the pipe. To understand the cause, The temperature of the suspension was monitored and is illustrated in the Figure 5.3. A maximum difference of $1K$ was observed and this causes only a minor difference in density suggesting that the probable cause could be evaporation which happens during the day. A well controlled environment could be beneficial to mitigate this issue.

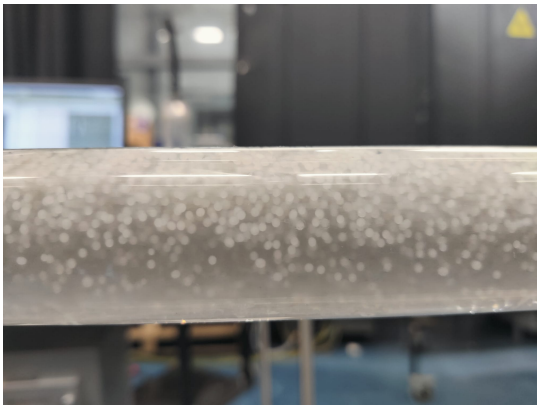

Figure 5.2: Particles rising while conducting experiments.

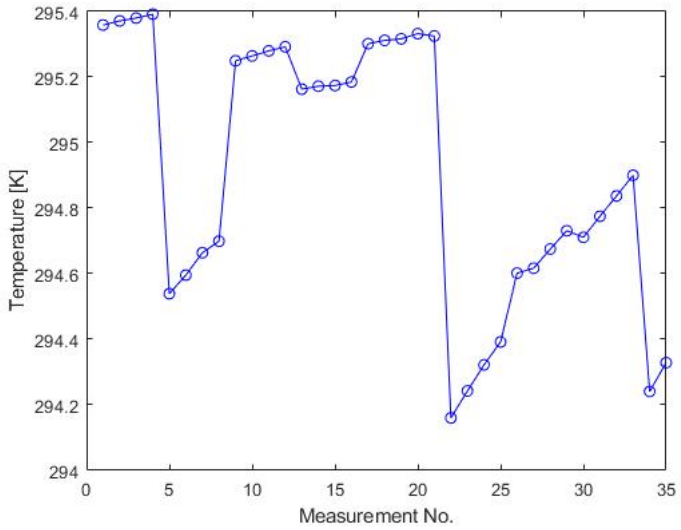

Figure 5.3: Temperature measurements as a function of number of experiments.

The present research is dedicated to investigating the entrance length for a single D/d ratio. Previous studies by Karnis et al. [29] and Hampton et al. [24] have noted that particle size influences both the entrance length and migration. Understanding how this relationship scales with the entrance length is crucial for gaining deeper insights into the underlying physics of the problem. Another interesting topic which can be considered is studying buoyant suspensions (ρ_p/ρ) since they have more practical applications. Ultrasound imaging was used in this investigation, and insights into concentration profiles were derived from intensity profiles. It is important to note that the conversion from intensity to concentration is not a straightforward process, and precise concentration values could not be determined in this study. To improve upon this, an MRI study could be conducted on the same topic to get concentration profiles and these could be analysed to get deeper insights.

A

Pressure calibration curve

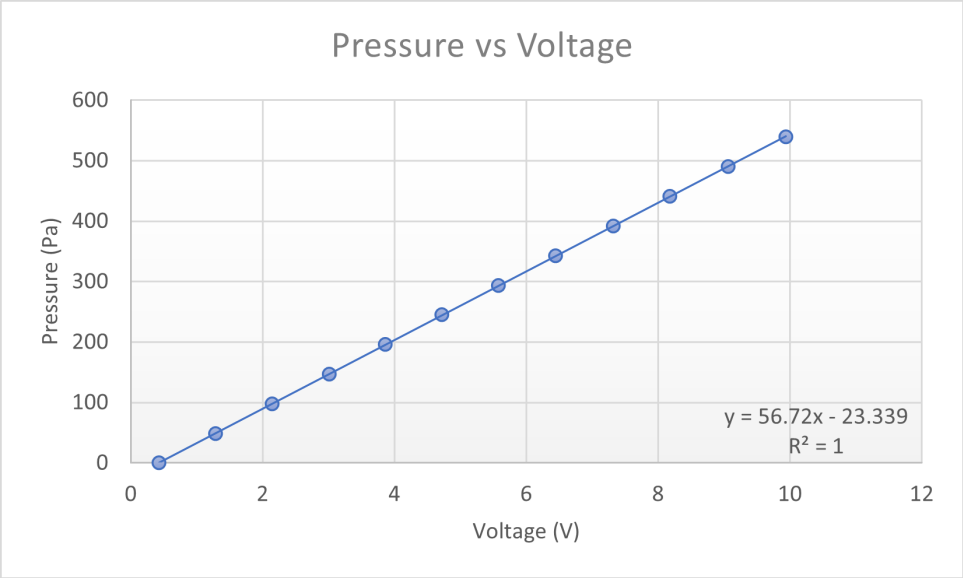

Figure A.1: Measured calibration curve fitted for Pressure drop vs Voltage output.

B

Holder Repeatability

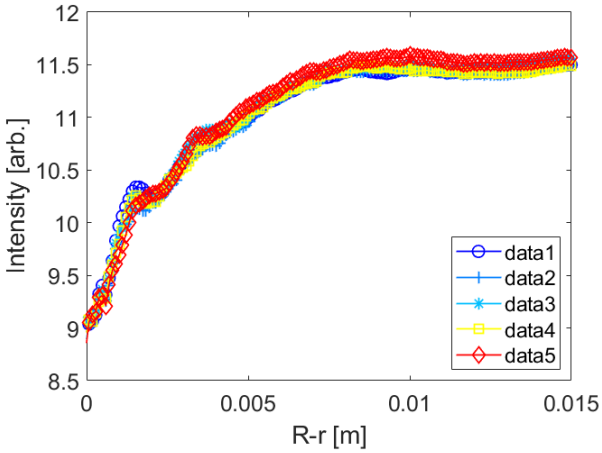

Figure B.1: Repeatability of the initial holder design.

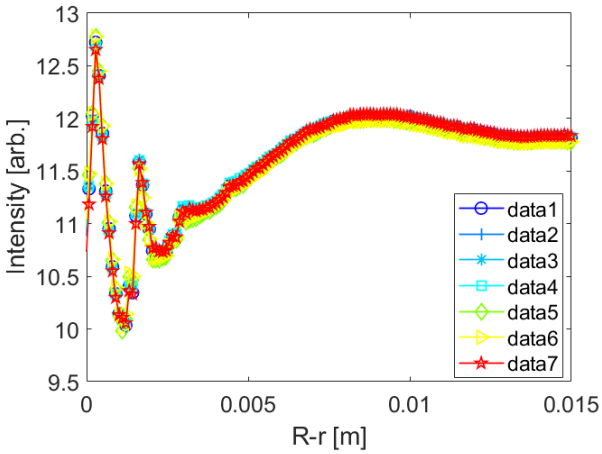

Figure B.2: Repeatability of the final holder design.

C

Kullback-Liebler Divergence

Kullback-Liebler divergence is a statistical distance, a measure of how one distribution differs from another distribution. For two discrete probability distributions P and Q defined on the same sample space Y, the Kullback-Liebler divergence from P to Q ($D_{\mathsf{KL}}(P \parallel Q)$) is defined as

$$D_{\mathsf{KL}}(P \parallel Q) = \sum_{x \in \mathcal{Y}} P(x) \log \left(\frac{P(x)}{Q(x)} \right). \tag{C.1}$$

The value of $D_{\mathsf{KL}}(P \parallel Q) = 0$ implies that the distributions are identical. The obtained data for inlet conditions were converted to discrete probability distributions and the convergence was checked using Kullback-Liebler divergence and the obtained convergence plots are shown in the Figure C.1. For all the suspension Reynolds numbers the KL divergence reach $\mathcal{O}(10^{-4})$ which is a good measure for convergence. The label 'iterations' on the x-axis corresponds to the number of data sets utilized until reaching convergence. For a given iteration 'i', the data sets up to (i-1) are aggregated, and the probability distribution is computed. This distribution is then compared with the probability distribution obtained from grouping the first 'i' data sets together.

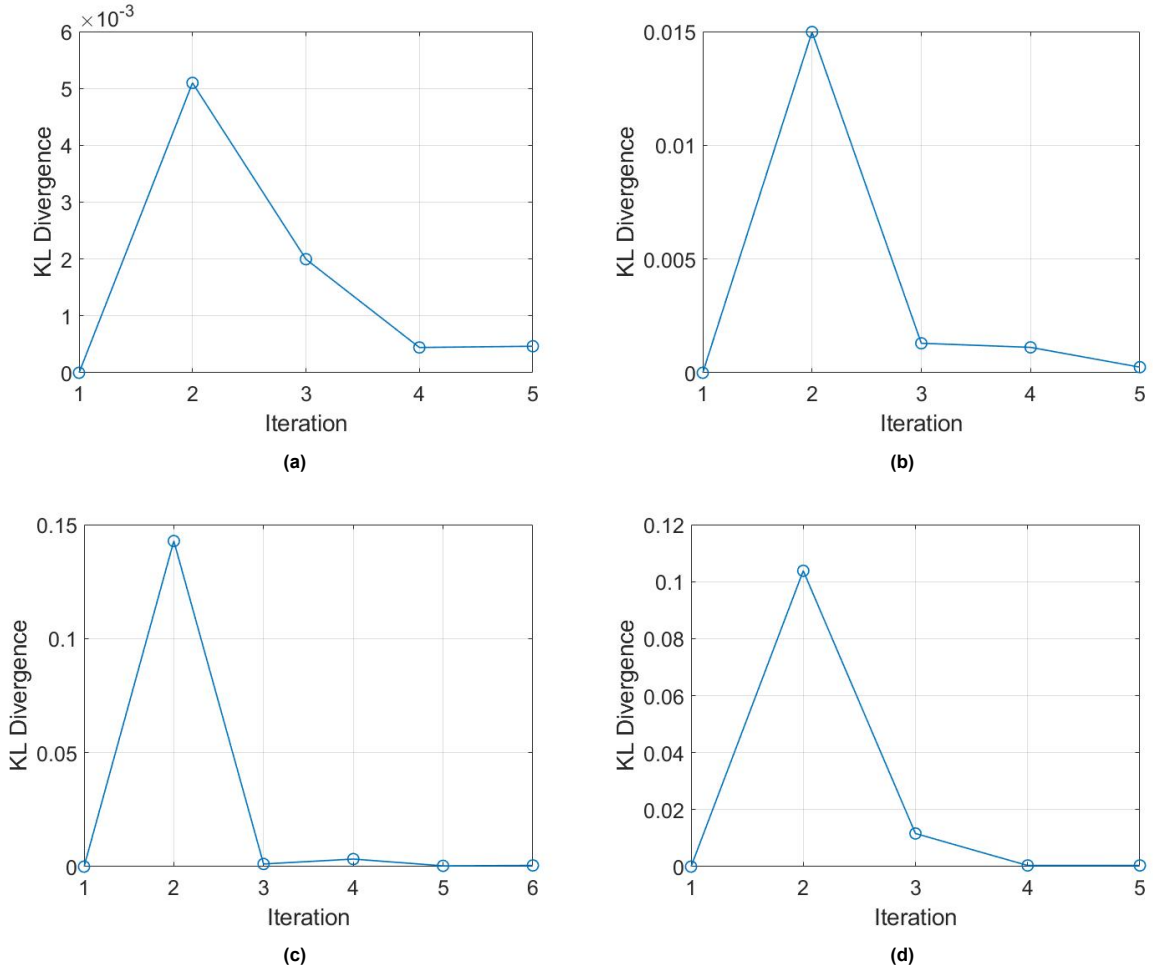

Figure C.1: Convergence analysis of inlet conditions using KL divergence. (a) $Re_s = 780$ (b) $Re_s = 1004$ (c) $Re_s = 1583$ (d) $Re_s = 2983$.

D

Uncertainty analysis

The uncertainty analysis was performed for friction factor and the entrance length obtained for concentration (L_ϕ/D).

- Uncertainty in Pressure:
  1. Zero error ($u_{0,\mathrm{p}}$) = ± 0.15 Pa
  2. Accuracy of sensor ($u_{1,\mathrm{p}}$) = ± 4.3 Pa
- Uncertainty in Density measurements (u_ρ) = ± 2 kg/m^3
- Uncertainty in Volume flow rate measurements (u_Q) = ± 0.1% of the measured value
- Uncertainty in bulk velocity (u_u) = u_Q/A

The total uncertainty in pressure drop is given by

$$u_{\Delta p} = \sqrt{u_{0,\mathrm{p}}^2 + u_{1,\mathrm{p}}^2}. \tag{D.1}$$

The friction factor is given by

$$f = \frac{\Delta p}{\frac{1}{2}\rho u^2 \frac{L}{D}}. \tag{D.2}$$

The propagation of uncertainty from each of the sources is given by

$$\text{Pressure drop: } \frac{\partial f}{\partial \Delta p} u_{\Delta p} = \frac{f}{\Delta p} u_{\Delta p}. \tag{D.3}$$

$$\text{Density: } \frac{\partial f}{\partial \rho} u_\rho = \frac{f}{\rho} u_\rho. \tag{D.4}$$

$$\text{Velocity: } \frac{\partial f}{\partial u} u_u = \frac{2f}{u} u_u. \tag{D.5}$$

The total uncertainty in f is given by

$$u_f = f\sqrt{\left[\left(\frac{u_{\Delta p}}{\Delta p}\right)^2 + \left(\frac{u_\rho}{\rho}\right)^2 + \left(\frac{2u_u}{u}\right)^2\right]}. \tag{D.6}$$

A similar analysis was done for the concentration lengths obtained at the core region.
The obtained length is given by

$$\frac{L_\phi}{D} = \frac{-1}{\alpha_2} ln(\frac{\alpha_1 - E_{p,val} - \alpha_3}{\alpha_1}). \tag{D.7}$$

The propagation of uncertainty from each of the sources is given by

$$\frac{\partial\left(\frac{L_\phi}{D}\right)}{\partial\alpha_1}u_{\alpha_1} = \frac{E_{p,val}+\alpha_3}{\alpha_1\alpha_2(\alpha_1-E_{p,val}-\alpha_3)}u_{\alpha_1} \tag{D.8}$$

$$\frac{\partial\left(\frac{L_\phi}{D}\right)}{\partial\alpha_2}u_{\alpha_2} = \frac{1}{\alpha_2^2}ln(\frac{\alpha_1-E_{p,val}-\alpha_3}{\alpha_1})u_{\alpha_2} \tag{D.9}$$

$$\frac{\partial\left(\frac{L_\phi}{D}\right)}{\partial\alpha_3}u_{\alpha_3} = \frac{1}{\alpha_1\alpha_2(\alpha_1-E_{p,val}-\alpha_3)}u_{\alpha_3}, \tag{D.10}$$

where u_{α_1}, u_{α_2} and u_{α_3} are the uncertainties in α_1,α_2 and α_3 respectively. The total uncertainty in the length obtained is given by

$$u_{L_{\phi/D}} = \sqrt{\left(\frac{\partial\left(\frac{L_\phi}{D}\right)}{\partial\alpha_1}u_{\alpha_1}\right)^2+\left(\frac{\partial\left(\frac{L_\phi}{D}\right)}{\partial\alpha_2}u_{\alpha_2}\right)^2+\left(\frac{\partial\left(\frac{L_\phi}{D}\right)}{\partial\alpha_3}u_{\alpha_3}\right)^2} \tag{D.11}$$

References

[1] IM Abdulagatov, A Zeinalova, and ND Azizov. “Viscosity of aqueous Na2SO4 solutions at temperatures from 298 to 573 K and at pressures up to 40 MPa”. In: *Fluid Phase Equilibria* 227.1 (2005), pp. 57–70.

[2] Fabien Anselmet, Fabien Ternat, Muriel Amielh, Olivier Boiron, Patrick Boyer, and Laurence Pietri. “Axial development of the mean flow in the entrance region of turbulent pipe and duct flows”. In: *Comptes Rendus Mécanique* 337.8 (2009), pp. 573–584.

[3] Mehdi Niazi Ardekani, Léa Al Asmar, Francesco Picano, and Luca Brandt. “Numerical study of heat transfer in laminar and turbulent pipe flow with finite-size spherical particles”. In: *International Journal of Heat and Fluid Flow* 71 (2018), pp. 189–199.

[4] Rubén D Arias-Pérez, Natalia A Taborda, Diana M Gómez, Jhon Fredy Narvaez, Jazmín Porras, and Juan C Hernandez. “Inflammatory effects of particulate matter air pollution”. In: *Environmental Science and Pollution Research* 27.34 (2020), pp. 42390–42404.

[5] Bernard Atkinson, MP Brocklebank, CCH Card, and JM Smith. “Low Reynolds number developing flows”. In: *AIChE Journal* 15.4 (1969), pp. 548–553.

[6] Kerstin Avila, David Moxey, Alberto De Lozar, Marc Avila, Dwight Barkley, and Björn Hof. “The onset of turbulence in pipe flow”. In: *Science* 333.6039 (2011), pp. 192–196.

[7] Bangslabs. *Material properties of polystyrene and poly(methyl methacrylate) (PMMA)*. Nov. 2023. URL: https://www.bangslabs.com/sites/default/files/imce/docs/TSD%200021%20Material%20Properties%20Web.pdf.

[8] DC Bogue. “Entrance effects and prediction of turbulence in non-Newtonian flow”. In: *Industrial & Engineering Chemistry* 51.7 (1959), pp. 874–878.

[9] Jason E Butler and Roger T Bonnecaze. “Imaging of particle shear migration with electrical impedance tomography”. In: *Physics of fluids* 11.8 (1999), pp. 1982–1994.

[10] Andrea W Chow, Steven W Sinton, Joseph H Iwamiya, and Thomas S Stephens. “Shear-induced particle migration in Couette and parallel-plate viscometers: NMR imaging and stress measurements”. In: *Physics of Fluids* 6.8 (1994), pp. 2561–2576.

[11] EB Christiansen and HE Lemmon. “Entrance region flow”. In: *AIChE Journal* 11.6 (1965), pp. 995–999.

[12] John M Cimbala and Yunus A Cengel. *Fluid mechanics: fundamentals and applications*. McGraw-Hill Higher Education, 2006.

[13] Kevin W Cushing, Fabio Garofalo, Cecilia Magnusson, Lars Ekblad, Henrik Bruus, and Thomas Laurell. “Ultrasound characterization of microbead and cell suspensions by speed of sound measurements of neutrally buoyant samples”. In: *Analytical chemistry* 89.17 (2017), pp. 8917–8923.

[14] F. Durst, S. Ray, B. Ãœnsal, and O. A. Bayoumi. “The Development Lengths of Laminar Pipe and Channel Flows”. In: *Journal of Fluids Engineering* 127.6 (June 2005), pp. 1154–1160. ISSN: 0098-2202. DOI: 10.1115/1.2063088. eprint: https://asmedigitalcollection.asme.org/fluidsengineering/article-pdf/127/6/1154/6697501/1154_1.pdf. URL: https://doi.org/10.1115/1.2063088.

[15] Engineeringtoolbox. *Slurry transport*. 2020. URL: https://www.engineeringtoolbox.com/slurry-transport-velocity-d_236.html.

[16] Amir Eshghinejadfard, Seyed Ali Hosseini, and Dominique Thévenin. “Fully-resolved prolate spheroids in turbulent channel flows: a lattice Boltzmann study”. In: *AIP Advances* 7.9 (2017), p. 095007.

[17] D Fargie and BW Martin. “Developing laminar flow in a pipe of circular cross-section”. In: *Proceedings of the Royal Society of London. A. Mathematical and Physical Sciences* 321.1547 (1971), pp. 461–476.

[18] James Feng, Howard H Hu, and Daniel D Joseph. “Direct simulation of initial value problems for the motion of solid bodies in a Newtonian fluid. Part 2. Couette and Poiseuille flows”. In: *Journal of fluid mechanics* 277 (1994), pp. 271–301.

[19] Walter Fornari, Francesco Picano, and Luca Brandt. “The effect of polydispersity in a turbulent channel flow laden with finite-size particles”. In: *European Journal of Mechanics-B/Fluids* 67 (2018), pp. 54–64.

[20] M Friedmann, J Gillis, and N Liron. “Laminar flow in a pipe at low and moderate Reynolds numbers”. In: *Applied Scientific Research* 19 (1968), pp. 426–438.

[21] F Gadala-Maria and Andreas Acrivos. “Shear-induced structure in a concentrated suspension of solid spheres”. In: *Journal of rheology* 24.6 (1980), pp. 799–814.

[22] Élisabeth Guazzelli and Olivier Pouliquen. “Rheology of dense granular suspensions”. In: *Journal of Fluid Mechanics* 852 (2018), P1.

[23] RC Gupta. “Laminar flow in the entrance of a tube”. In: *Applied Scientific Research* 33 (1977), pp. 1–10.

[24] RE Hampton, AA Mammoli, AL Graham, N Tetlow, and SA Altobelli. “Migration of particles undergoing pressure-driven flow in a circular conduit”. In: *Journal of Rheology* 41.3 (1997), pp. 621–640.

[25] Minsoo Han, Chongyoup Kim, Minchul Kim, and Soonchil Lee. “Particle migration in tube flow of suspensions”. In: *Journal of rheology* 43.5 (1999), pp. 1157–1174.

[26] Willian Hogendoorn. “Suspension dynamics in transitional pipe flow”. In: (2021). URL: `https://doi.org/10.4233/uuid:e3f9d78b-8ff0-49a7-8018-142b351ea4de`.

[27] Philip Alan Hookham. *Concentration and velocity measurements in suspensions flowing through a recatngular channel (Laser-Doppler Anemometry)*. 1986.

[28] Robert W Hornbeck. “Laminar flow in the entrance region of a pipe”. In: *Applied Scientific Research, Section A* 13 (1964), pp. 224–232.

[29] Karnis, HL Goldsmith, and SG Mason. “The kinetics of flowing dispersions: I. Concentrated suspensions of rigid particles”. In: *Journal of colloid and interface science* 22.6 (1966), pp. 531–553.

[30] Christopher J Koh, Philip Hookham, and L Gary Leal. “An experimental investigation of concentrated suspension flows in a rectangular channel”. In: *Journal of Fluid Mechanics* 266 (1994), pp. 1–32.

[31] Henry L Langhaar. “Steady flow in the transition length of a straight tube”. In: (1942).

[32] Iman Lashgari, Francesco Picano, Pedro Costa, Wim-Paul Breugem, and Luca Brandt. “Turbulent channel flow of a dense binary mixture of rigid particles”. In: *Journal of Fluid Mechanics* 818 (2017), pp. 623–645.

[33] Brice Lecampion and Dmitry I Garagash. “Confined flow of suspensions modelled by a frictional rheology”. In: *Journal of Fluid Mechanics* 759 (2014), pp. 197–235.

[34] David Leighton and Andreas Acrivos. “Measurement of shear-induced self-diffusion in concentrated suspensions of spheres”. In: *Journal of Fluid Mechanics* 177 (1987), pp. 109–131.

[35] David Leighton and Andreas Acrivos. “The shear-induced migration of particles in concentrated suspensions”. In: *Journal of Fluid Mechanics* 181 (1987), pp. 415–439.

[36] King CP Li, Roger P Tart, Jeffrey R Fitzsimmons, Brett L Storm, Jintong Mao, and Richard J Rolfes. “Barium sulfate suspension as a negative oral MRI contrast agent: in vitro and human optimization studies”. In: *Magnetic resonance imaging* 9.2 (1991), pp. 141–150.

[37] Ryan M Miller and Jeffrey F Morris. “Normal stress-driven migration and axial development in pressure-driven flow of concentrated suspensions”. In: *Journal of non-newtonian fluid mechanics* 135.2-3 (2006), pp. 149–165.

[38] Lewis F Moody. “Friction factors for pipe flow”. In: *Transactions of the American Society of Mechanical Engineers* 66.8 (1944), pp. 671–678.

[39] Saki Nakayama, Hiroshi Yamashita, Takuya Yabu, Tomoaki Itano, and Masako Sugihara-Seki. “Three regimes of inertial focusing for spherical particles suspended in circular tube flows”. In: *Journal of Fluid Mechanics* 871 (2019), pp. 952–969.

[40] Charles P Newcombe and D Donald MacDonald. “Effects of suspended sediments on aquatic ecosystems”. In: *North American journal of fisheries management* 11.1 (1991), pp. 72–82.

[41] Jay T Norman, Hebri V Nayak, and Roger T Bonnecaze. “Migration of buoyant particles in low-Reynolds-number pressure-driven flows”. In: *Journal of Fluid Mechanics* 523 (2005), pp. 1–35.

[42] Prabhu R Nott and John F Brady. “Pressure-driven flow of suspensions: simulation and theory”. In: *Journal of Fluid Mechanics* 275 (1994), pp. 157–199.

[43] N Phan-Thien and Z Fang. “Entrance length and pulsatile flows of a model concentrated suspension”. In: *Journal of Rheology* 40.4 (1996), pp. 521–548.

[44] Ronald J Phillips, Robert C Armstrong, Robert A Brown, Alan L Graham, and James R Abbott. “A constitutive equation for concentrated suspensions that accounts for shear-induced particle migration”. In: *Physics of Fluids A: Fluid Dynamics* 4.1 (1992), pp. 30–40.

[45] Christian Poelma. “Ultrasound imaging velocimetry: a review”. In: *Experiments in Fluids* 58 (2017), pp. 1–28.

[46] Ahmadreza Rashedi, Mohammad Sarabian, Mohammadhossein Firouznia, Dallas Roberts, Guillaume Ovarlez, and Sarah Hormozi. “Shear-induced migration and axial development of particles in channel flows of non-Brownian suspensions”. In: *AIChE Journal* 66.12 (2020), e17100.

[47] Ludwig Schiller. “Die Entwicklung der laminaren Geschwindigkeitsverteilung und ihre Bedeutung für Zähigkeitsmessungen,(Mit einem Anhang über den Druckverlust turbulenter Strömung beim Eintritt in ein Rohr.)” In: *ZAMM-Journal of Applied Mathematics and Mechanics/Zeitschrift für Angewandte Mathematik und Mechanik* 2.2 (1922), pp. 96–106.

[48] G Segre and A Silberberg. “Radial particle displacements in Poiseuille flow of suspensions”. In: *Nature* 189 (1961), pp. 209–210.

[49] Steven W Sinton and Andrea W Chow. “NMR flow imaging of fluids and solid suspensions in Poiseuille flow”. In: *Journal of Rheology* 35.5 (1991), pp. 735–772.

[50] Braden Snook, Jason E Butler, and Élisabeth Guazzelli. “Dynamics of shear-induced migration of spherical particles in oscillatory pipe flow”. In: *Journal of Fluid Mechanics* 786 (2016), pp. 128–153.

[51] EM Sparrow, SH Lin, and TS Lundgren. “Flow development in the hydrodynamic entrance region of tubes and ducts”. In: *The Physics of Fluids* 7.3 (1964), pp. 338–347.

[52] Jonathan J Stickel and Robert L Powell. “Fluid mechanics and rheology of dense suspensions”. In: *Annu. Rev. Fluid Mech.* 37 (2005), pp. 129–149.

[53] Salvatore P Sutera and Richard Skalak. “The history of Poiseuille’s law”. In: *Annual review of fluid mechanics* 25.1 (1993), pp. 1–20.

[54] Kuwait times. *Indonesian volcano erupts again, spewing ash cloud*. 2021. URL: `https://www.kuwaittimes.com/indonesian-volcano-erupts-again-spewing-ash-cloud/`.

[55] Vectorstock. *Red blood cells flow inside a capillary vein*. 2023. URL: `https://www.vectorstock.com/royalty-free-vector/red-blood-cells-flow-inside-in-artery-medical-vector-41947953`.

[56] Verasonics. *Verasonics transducers*. Aug. 2023. URL: `https://verasonics.com/verasonics-transducers/`.

[57] JS Vrentas, JL Duda, and KG Bargeron. “Effect of axial diffusion of vorticity on flow development in circular conduits: Part I. Numerical solutions”. In: *AIChE Journal* 12.5 (1966), pp. 837–844.

[58] Andrew Wickert. *Sediment transported by the Connecticut river into Long Island Sound*. 2020. URL: `https://geomorphonline.github.io/fluvial/sediment_and_transport_modes/`.

[59] Kyongmin Yeo and Martin R. Maxey. “Numerical simulations of concentrated suspensions of monodisperse particles in a Poiseuille flow”. In: *Journal of Fluid Mechanics* 682 (2011), pp. 491–518. DOI: 10.1017/jfm.2011.241.

[60] Wenchao Yu, Ivana Vinkovic, and Marc Buffat. “Finite-size particles in turbulent channel flow: quadrant analysis and acceleration statistics”. In: *Journal of Turbulence* 17.11 (2016), pp. 1048–1071.